Spring 1984

An Investigation of Refractive Index of Solutions of Ammonia and Water at Various Concentrations and Temperatures

Effendy Arif
Old Dominion University

AN INVESTIGATION OF REFRACTIVE INDEX OF SOLUTIONS OF AMMONIA AND WATER AT VARIOUS CONCENTRATIONS AND TEMPERATURES

by

Effendy Arif
Ir., June 1976, Universitas Hasanuddin (Indonesia)
M.E., July 1980, Old Dominion University

A Dissertation Submitted to the Faculty of
Old Dominion University in Partial Fulfillment of the
Requirements for the degree of

DOCTOR OF PHILOSOPHY

MECHANICAL ENGINEERING

OLD DOMINION UNIVERSITY
April 1984

Approved by:

Robert L. Ash (Director)

Surendra N. Tiwari

Gennaro L. Goglia

Sushil K. Chaturvedi

John J. Swetits

ABSTRACT

AN INVESTIGATION OF REFRACTIVE INDEX OF
SOLUTIONS OF AMMONIA AND WATER
AT VARIOUS CONCENTRATIONS AND TEMPERATURES

Effendy Arif
Old Dominion University, 1984
Director: Dr. Robert L. Ash

Refractive index of ammonia-water solutions is investigated experimentally (for λ = 632.8 nm) and semi-empirically (for λ = 589.3 and 632.8 nm) in ammonia-weight concentration of up to 30%, over a temperature range of 20 to 60°C. The experiment employs a specially designed and built refractometer that measures the displacement of a laser beam due to refraction in the test solution. The refractive index is then deduced from the beam displacement. Based on the experimental data, the refractive index is correlated empirically with the concentration and temperature. A semi-empirical investigation is developed based on the Lorentz-Lorenz equation and the additive rule of mixtures with an empirical correction function. Both the experimental and semi-empirical results indicate that the refractive index increases with the concentration and they confirm qualitatively the general behavior of refractive indices of liquids, i.e.; they decrease with increases in either temperature or wave length of light. Quantitatively, both sets of results are in reasonably good agreement, especially, for moderate concentrations (up to 15%).

DEDICATION

The author wishes to dedicate this report to his wife Riny and his son Ronald who have been constant supports and sources of inspiration during his study in the USA.

ACKNOWLEDGEMENTS

The author wishes to express his sincere appreciation to his advisor, Dr. Robert L. Ash, for his invaluable guidance and encouragement throughout the course of this work. He wishes to express his gratitude to the members of the advisory committee, Dr. Gennaro L. Goglia, Dr. Surendra N. Tiwari, Dr. John J. Swetits, and Dr. Sushil K. Chaturvedi, for their help and useful suggestions. He is indebted to Messrs. Edward W. Cronce, Kent B. Ferguson, Jerry B. Robertson, and John F. Schmitt of the ODU Instrumentation Laboratory for their contribution in manufacturing and setting-up the experimentation used in this work. He is grateful to the government of the Republic of Indonesia and to the MUCIA-AID-Indonesian Higher Education Project that have made his study in the USA possible. He also wishes to thank Mrs. Rowena B. Pierce for typing the final draft of the dissertation and Mrs. Jean C. Seacrist for proofreading the manuscript. Last and most importantly, he wishes to thank his dearly beloved mother, Mrs. Murniaty Rachmat, who has constantly supported and encouraged him to pursue better and higher education.

TABLE OF CONTENTS

LIST OF TABLES

LIST OF FIGURES

LIST OF SYMBOLS

A	molecular refractivity
a	distance between the scale and the focal point of the spherical mirror
$B(T)$	second virial coefficient
B_j	constants in Eq. (5.9) ($j = 1,2, \ldots, 5$)
b	magnified displacement
C_j	constants in Eq. (5.10) ($j = 1,2, \ldots, 6$)
d_m	molecular density
Er	error sum defined in Eq. (5.11)
f	focal length of the spherical mirror
h	specific enthalpy
k	number of data points/observations
k_B	Boltzmann's constant
l	distance between two reflected beams near the laser aperture (Fig. 4.4)
M	molecular weight
m	mass
$\dot{m}$	mass flow rate
N	number of molecules perunit volume
n	refractive index
N_A	Avogrado's number
P	pressure
q_c	energy loss from the condenser
q_{in}	energy input into the generator

q_{out}	energy loss from the dephlegmator
q_s	low grade thermal energy input
q_u	recover useful energy in the absorber
R	gas constant
r	effective radius of a molecule
s	length of light-path (Fig. 2.3)
SR	specific refractivity
T	temperature
t	thickness
V	volume
v	specific volume
W	weight concentration
w	energy required by pump
X	molecular concentration
x	measured value in Eq. (5.1)

Greek letter

α	refraction angle (Fig. 2.3)
β	isothermal compressibility
γ	angle in Eq. (2.1)
Δ	designates measurement uncertainty
δ	displacement due to light refraction
ε	designates discrepancy or deviation
η	angle (Fig. 2.2)
θ	angle (Fig. 2.2)
λ	wave length of light
μ	angle (Fig. 2.2)
ρ	density

σ	designates standard deviation
ϕ	tilted angle of the test chamber
Ψ	small tilted angle

Subscript

a	air
cor	denotes corrected value
data	denotes data value
G	glass
L	liquid
mix	ammonia-water solution
o	denotes observed value
tot	total
1	ammonia
2	water

Superscript

-	denotes mean value or absolute value

Chapter 1

INTRODUCTION

The purpose of this work is to investigate the refractive index of ammonia-water solutions at different temperatures and concentrations. These data are required to enable interpretation of measurements of the diffusion (absorption) of ammonia vapor into water when holographic interferometric techniques are used.

The refractive index of a substance is defined as the ratio of the standard velocity of light, at a given wavelength, in air (or vacuum) to the corresponding velocity in the substance. This ratio is different for different wavelengths (colors), and also depends on the temperature, pressure, chemical composition, homogeneity, etc. of the substance. Since the refractive indices of gases and vapors (including air) are very nearly equal to unity, it is customary to refer their refractive indices to vacuum. Such refractive indices are called absolute refractive indices, $\bar{n}$. Air, for convenient measurement, is generally accepted as the standard with respect to which refractive indices of solids and liquids are expressed. Whenever refractive indices are referred to air as the standard, they are called relative refractive indices, n. The relation between absolute and relative refractive indices is $\bar{n} = \bar{n}_a \, n$, where $\bar{n}_a$ is the absolute refractive index of air.

Knowledge of refractive index data is the most important requirement in all interferometry investigations. The refractive index

data, in such investigations, are used to deduce the investigated properties such as temperature, density, concentration, etc. The refractive index data obtained in this investigation could be employed eventually in experimental investigations of diffusion of ammonia vapor into water using holographic interferometry. The importance of such diffusivity data for engineering applications will be discussed in the following paragraphs. This was the original motivation for the work reported herein.

Many terrestial processes (solar, geothermal, biomass, industrial waste heat for example) can provide large quantities of low grade thermal energy. This energy has a typical temperature of under 100°C and low availability. Availability is defined as the maximum possible work that can be produced by a system when it is brought into equilibrium with its surroundings. The prospect of utilizing low grade thermal energy directly to produce useful work or cooling for environmental control is too ambiguous for two reasons: First, only low thermodynamic efficiencies are possible and second, significant losses in availability occur even for very small temperature drops which occur normally in any conventional thermal system.

A step-up temperature device would be useful to increase the temperature as well as the availability of low grade thermal energy before it can be used more effectively. One possible approach to raising the temperature is to use a modified ammonia-water absorption cycle [1,2]*. A schematic and theoretical thermodynamic analysis of a

---

*The numbers in brackets indicate references.

possible modified cycle is presented in Appendix A. This cycle is based on the chemical separation and recombination of ammonia-water solutions which can produce useful energy at higher temperatures and availabilities (in the absorber). Rather than using chemical separation alone as a means of storage, the analysis has shown that it may be desirable to store thermal energy conveniently at around 50°C, then use chemical recombination of ammonia and water to recover and use the stored energy at temperature near 90°C. The estimates have shown that approximately half of the thermal energy stored at 50°C can be recovered at a temperature of 85°C (since the availability of energy is doubled at the same time, 50% recovery is consistent and satisfactory). Theoretically, this system has proven to be a step-up device for elevating the temperature continuously from a low grade thermal energy source.

The success of the modified system and other absorption systems depends mainly on the capability of the absorber to produce ammonia-water solution at controlled concentrations and flow rates. Since the modified system also requires controlled release of thermal energy at specified temperatures and pressures, the basic thermophysical data are essential.

Macriss et al. [3] have presented an extensive review of the thermodynamic data for ammonia-water solutions which includes: solution vapor pressure, saturated composition, and enthalpies of saturated liquid and vapor phases. Data in the form of a Mollier chart extend up to a pressure of 3.4 MPa. In addition, Shultz [4] has developed a computerized approach using Gibbs free energy of the components (ammonia and water in this case) and the thermodynamic fundamental equations to

calculate the other thermodynamic variables of the solution. However, there is a serious lack of diffusion coefficient data and absorption rate data which are required to design controlled absorption devices. These data are, for the most part, unavailable for the absorption of ammonia vapor into water or into weak concentrations ammonia-water solutions. The limited available data are essentially for dilute ammonia-water solutions at atmospheric pressure and temperatures around ambient [5,6,7]. Furthermore, all of these data were taken in the last century and variations of up to 60% were reported [8].

Several empirical models have been developed to correlate diffusivity of other fluids with chemical composition [9,10,11] but those correlations were limited to specific kinds of mixtures (i.e ideal, non-associated with similar composition). Solutions of ammonia and water cannot be included in such simple mixtures, since the heat of mixing and volume changes during the mixing process are so large that they cannot be ignored. The mixing process is further complicated by the presence of chemical reactions. Therefore, it is necessary to have more reliable experimental diffusivity data over a much wider range of temperature, pressure, and concentration for ammonia-water solutions before any theoretical or empirical approaches can be validated.

Previous experimental methods were reviewed in order to determine an appropriate approach to measure the diffusivity of ammonia vapor in water. Even though no diffusion experiments were developed as part of this investigation the review summary by Himmelblau [12] is noted as good future starting point. In general, all methods are initially used to determine the concentration distribution in the diffusion coefficient. It was found that optical or interferometric methods have

several advantages over other methods for measuring concentration distributions. The interference pattern that they produce can enable accurate resolution of continuous concentration profiles either instantaneously or averaged with respect to time [13]. Both incoherent (for conventional interferometry) and coherent (for holographic interferometry) light sources can be used [14,15], however, the coherent light technique is preferred here.

Absorption of ammonia vapor into water not only involves mass transfer but also heat transfer due to the heat of mixing. For such a phenomenon, a special double exposure holographic interferometry technique which produces interference patterns due to changes in refractive index resulting from variations in concentration and temperature has been proposed by Mayinger and Panknin [16]. This technique employs two different light sources (two lasers with different wavelengths) to resolve simultaneously the concentration and temperature distributions. However, its application is limited to ideal gas absorption where simple P-V-T and mixing rules are available. For ammonia absorption, no such simplicity is available. It is proposed here, as a possible alternative, that simultanenous resolution of temperature and concentration effects require independent measurement of the local temperature distribution using thermocouples. At this point the importance of refractive index data for ammonia-water solutions becomes evident.

The future diffusion experiment would employ double exposure holographic interferometry to provide refractive index distributions in a diffusion cell. Simultaneously, thermocouple readings could provide the temperature distribution. Thus, refractive index and temperature at

each point/location in the diffusion cell could be deduced. Obviously if the refractive index data of ammonia-water solutions at various temperatures and concentrations were available then the concentration distribution in the diffusion cell can be determined. Unfortunately such important data for ammonia-water solutions are extremely limited.

The only available refractive index data of ammonia-water solutions [17] are for sodium-D light (λ=589.3 nm) at 20°C, 1 atm, and concentrations up to 30% (by weight) of ammonia. Therefore, it is necessary to perform semi-empirical predictions along with experimental measurements of the refractive indices at various temperatures and concentrations for the Helium-Neon laser (λ=632.8 nm) , since this coherent light source is the one most commonly used in holographic interferometry investigations.

A theoretical background of refractive index predictions which includes various expressions of molecular refractivity is presented in Appendix B. The decision to employ the Lorentz-Lorenz equation in this investigation is based on the discussion in this appendix. Furthermore, the Lorentz-Lorenz equation is simple, it consists of only four parameters (refractive index, density, refractivity, and molecular weight) and it has a sound theoretical foundation. The Lorentz-Lorenz equation has also been accepted as a relation to correlate the temperatures and the refractive indices in most interferometric investigations [13].

Having discussed the bases and types of the theoretical and empirical models for predicting refractive index, the attention is now directed toward aspects of the experimental measurements. A rigorous

review of refractive index measurements has been presented by Tilton and Taylor [18], and it will not be repeated here, but in summary, the refractive index measurement techniques can be classified into the four methods listed below:

1. Absolute method of (relative) refractive index measurement.
2. Standard comparison method.
3. Substitution method.
4. Interferometric method.

The absolute method uses air as the reference standard and one or more light refraction in the substance being measured. The refraction angles and their equivalents are directly measured and the refractive indices are deduced according to Snell's law.

The standard comparison method utilizes a homogeneous block of transparent medium as a comparison standard for which refractive indices have been carefully measured with respect to air. The refractive indices of the sample are measured by comparing the sample and the comparison standards. The Abbe and Dipping refractometers [18] are examples of instruments based on this principle.

The substitution method is an improvement of the standard comparison method which can produce better accuracy and higher precision measurements. The unknown and the standard samples are compared, either simultaneously or in rapid succession, at test conditons which are nearly identical.

The interferometric method is based on the interference phenomena produced by two different optical media-one is the unknown and the other is the standard medium (either air or a vacuum) which has a lower

refractive index than that of the unknown sample. This method provides the most accurate and convenient measurements for gases and vapors with refractive indices which are very nearly equal to unity. This method, however, is not recommended for measurements with large differences in refractive indices because of the limitations in total index range that can be covered with a single interferometer configuration. Another disadvantage of this method is that it requires expensive optical instrumentation such as optical flats, an optical table, vibration isolators, etc.

The nature of the substances being investigated and the intended application of the data so obtained enforce the following limitations on the refractometer relevant to this work:

1. Ammonia-water solutions, especially at high concentrations are hazardous, since significant amounts of ammonia can be released as the temperature is increased. The recommended maximum ammonia concentration in air is 100 ppm. Breathing air containing more than 5000 ppm can cause instant death [19]. Therefore ammonia-water solutions have to be mixed and investigated in a closed test chamber.
2. The type of light source of the refractometer used should be identical to the light source used in the future interferometric investigations (which is assumed to be a Helium-Neon laser with wavelength of 632.8 nm).
3. Based on previous experimental data, it is expected that the range of variation of the refractive index will be large.

The first and the second limitations preclude the use of commercially available refractometers such as Abbe and Dipping refractometers. In these refractometers, the sample is not confined in

a closed chamber and the light source is typically the sodium-D light with wavelength of 589.3 nm. The last limitation prevents the application of interferometers. As has been mentioned earlier, interferometers are costly and recommended only for measurements with a small range of refractive index variation. As an alternative, a special and simple refractometer based on an idea of Stong [20] has been designed and built for the present investigation. According to the earlier classification, this refractometer falls into the first category which is the absolute type. The refractive indices are deduced from the measurements of the displacements of light due to refraction in the test chamber (containing the ammonia-water solutions). The test chamber was also designed to function as a mixing chamber where ammonia-water solutions were mixed to various desired concentrations. This will make transfer of solutions to different containers unnecessary and also ensure that the investigated solution concentration is equal to the mixed value.

Chapter 2

EXPERIMENTAL METHOD

2.1 Introduction

Based on the limitations and justifications discussed in the introductory chapter, the absolute method of refractive index measurement has been employed in this work. Instead of direct measurement of the refraction angle, the displacement of light due to refraction in the test chamber has been used to deduce refractive index.

To increase the resolution of the experiment, a concave spherical mirror has been used to magnify the displacement. The so magnified displacement was the experimentally observed quantity from which the refractive index was calculated. The formulas used in the calculation were derived based on Snell's law and geometric relations.

This chapter is divided into four sections. Following the introduction, details of the experimental principle are discussed. The formulas used to calculate the sample refractive index have been derived in Sec. 3, and Sec. 4 describes the main elements of the experiment.

2.2 Experimental Principle

A schematic diagram of the experimental set-up (in the horizontal plane) is shown in Fig. 2.1. The set-up consists of six main components: A helium-neon laser (light source), a test chamber, a spherical mirror, a scale, a laser power meter equipped with a

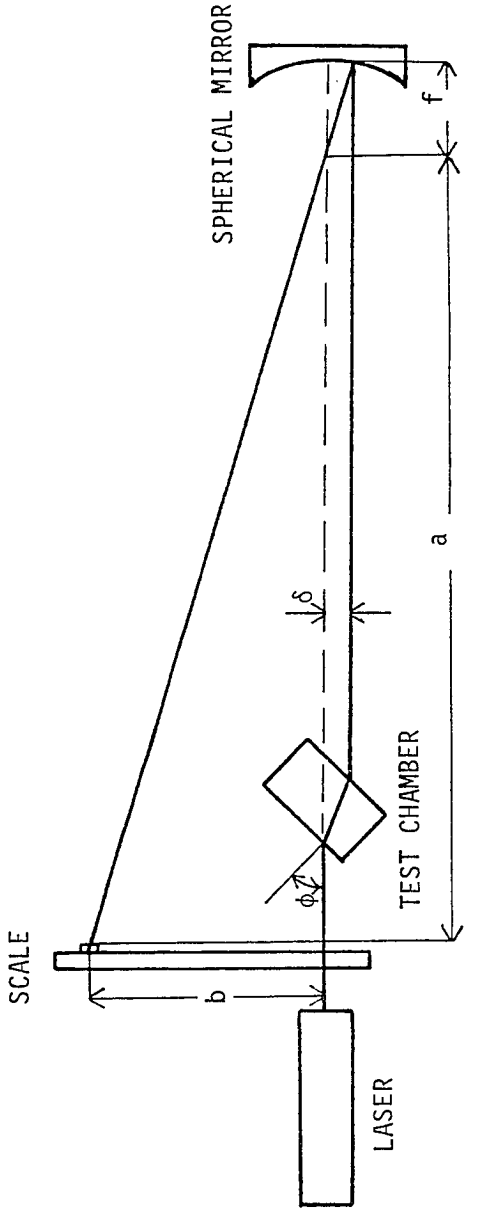

Fig. 2.1 Schematic diagram of the experimental set-up.

photodetector, and an optical bench. In this configuration, a beam of light falls obliquely (with angle ϕ) on the front glass window of the test chamber (containing the test ammonia-water sample solution in this case). Due to the refraction of light, the beam is bent in the horizontal plane at the interface of the air and the test chamber. It then propagates through the front glass window, the liquid sample, and then emerges into the air through the opposite glass window. At each interface, there is additional bending of the beam due to refractive index differences. Since the glass windows are optically flat the light beam is deflected by exactly the same angle leaving the glass as it was entering the glass, but in the opposite direction. This occurs because when the beam enters the chamber, it proceeds from a medium of relatively low refractive index (air) into a medium of higher refractive index. At the exit interface the beam proceeds in the reverse succession. Therefore the path of the beam leaving the test chamber should be parallel to its path prior to entering the chamber, but offset. Obviously, the displacement between the two parallel paths, δ, is the total sum of the displacements due to the light refractions in the test sample and both glass windows. This total displacement increases with the refractive index of the test sample. However, the gradients are too small to detect--even for large differences in refractive index. The spherical mirror, which was aligned to be perpendicular to the original beam (before entering the chamber), is used to magnify this displacement by reflecting the beam back through the focal point with an angle that increases with the displacement. Theoretically, the displacement, b, so magnified can be measured on the scale (shown schematically in Fig. 2.1) and then used to deduce the

refractive index of the test sample. However, since the original beam has a finite cross section, and even laser light has a spreading angle, the reflected beam has a cross section that increases with the distance away from the focal point. This unavoidable optical behavior makes the accurate measurement of the magnified displacement, b, very difficult without the use of a detector to determine the center of the beam cross section. By assuming that the center of the beam possesses the maximum light intensity, a digital laser power meter was used to scan the incident beam pattern to determine the point of maximum intensity. Subsequently, the magnified displacement, b, on the scale was measured.

2.3 Refractive Index Formulation

The path displacement, δ, can be related to the magnified displacement, b, according to the formula described below: In the horizontal plane consider the path travelled by the beam (not drawn to scale in Fig. 2.2). The values of a, b, and f are known--either chosen or observed--and the radius of curvature of the mirror, AC, is twice the value of f. Therefore,

$$\delta = AC \sin\eta = 2 f \sin\eta \qquad (2.1)$$

where: $\eta = \theta - \gamma$

$\theta = \tan^{-1} (\frac{b}{a})$

$\mu = 180° - \theta$

$\gamma = \sin^{-1}(\frac{1}{2} \sin\mu)$

Once the displacement, δ, is known, the refractive index of the liquid sample can be calculated according to the formula that can be derived as follows: Consider the details of the light path in the test

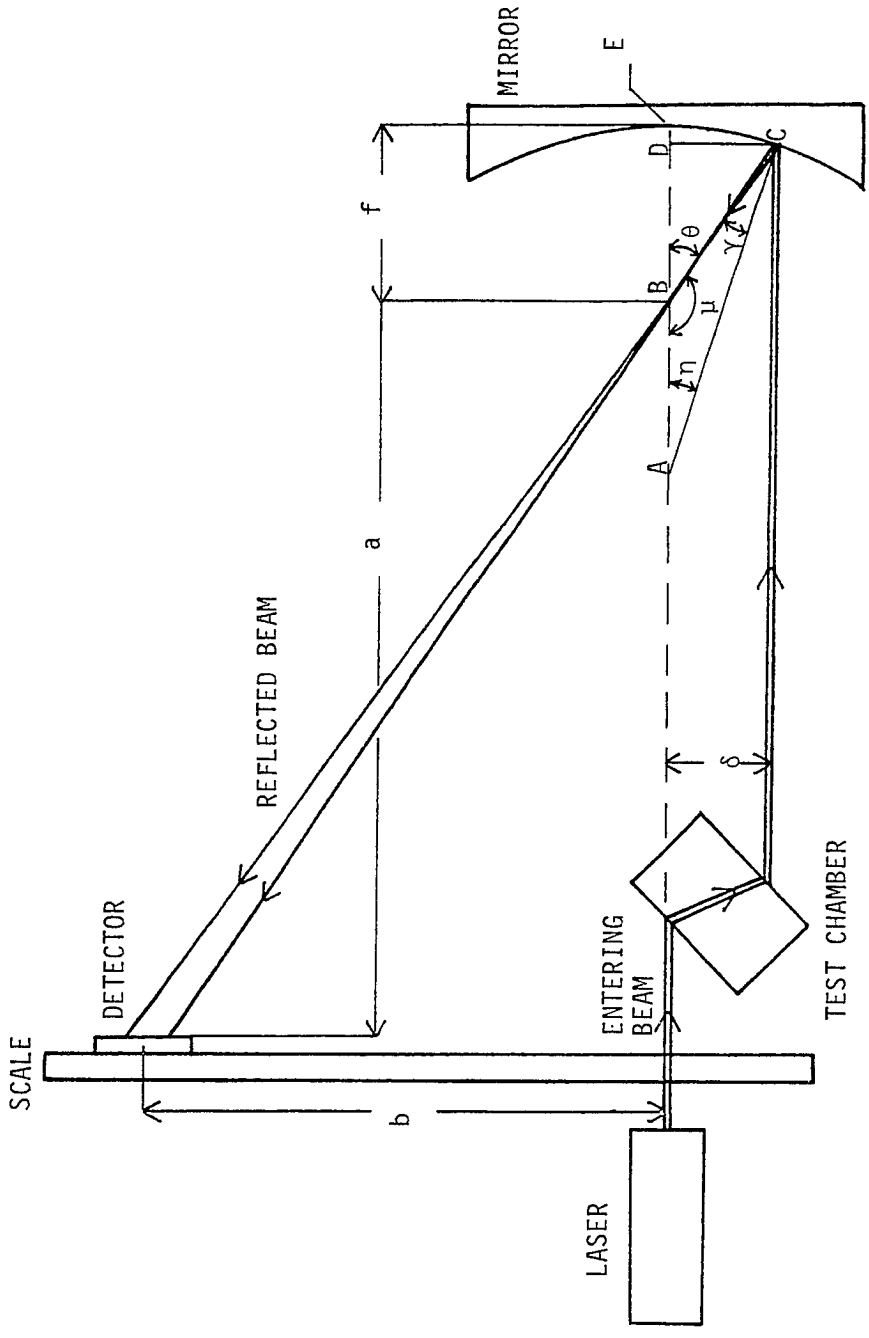

Fig. 2.2 Light path in the experimental set-up.

chamber, as shown in Fig. 2.3. The total displacement, δ, is the sum of the displacements in the glass windows, δ_1, and δ_3, and the displacement due to the test sample refractions, δ_2.

In the front glass window, Snell's law yields

$$n_a \sin\phi = n_G \sin\alpha \tag{2.2}$$

since $n_a \cong 1.00000$, Eq. (2.2) can be rewritten as

$$\sin\alpha = \frac{\sin\phi}{n_G} \tag{2.3}$$

The other geometric correlations are

$$s_1 = t_1/\cos\alpha \tag{2.4}$$

and

$$\delta_1/s_1 = \sin(\phi - \alpha) = \sin\phi\cos\alpha - \sin\alpha\cos\phi \tag{2.5}$$

The last two equations can be combined to yield

$$\sin^2\alpha = \frac{\sin^2\phi \left[1 - \frac{\delta_1}{t_1 \sin\phi}\right]^2}{\cos^2\phi + \sin^2\phi \left[1 - \frac{\delta_1}{t_1 \sin\phi}\right]} \tag{2.6}$$

The square of Eq. (2.3) can then be substituted into Eq. (2.6) to obtain

$$n_G^2 = \left[\frac{\cos\phi}{1 - \delta_1/t_1 \sin\phi}\right]^2 + \sin^2\phi \tag{2.7}$$

$$\delta_1 = t_1 \sin\phi \left[1 - \frac{\cos\phi}{(n_G^2 - \sin^2\phi)^{1/2}}\right] \tag{2.8}$$

Similiarly, the displacement, δ_3, of the opposite glass window can be written as

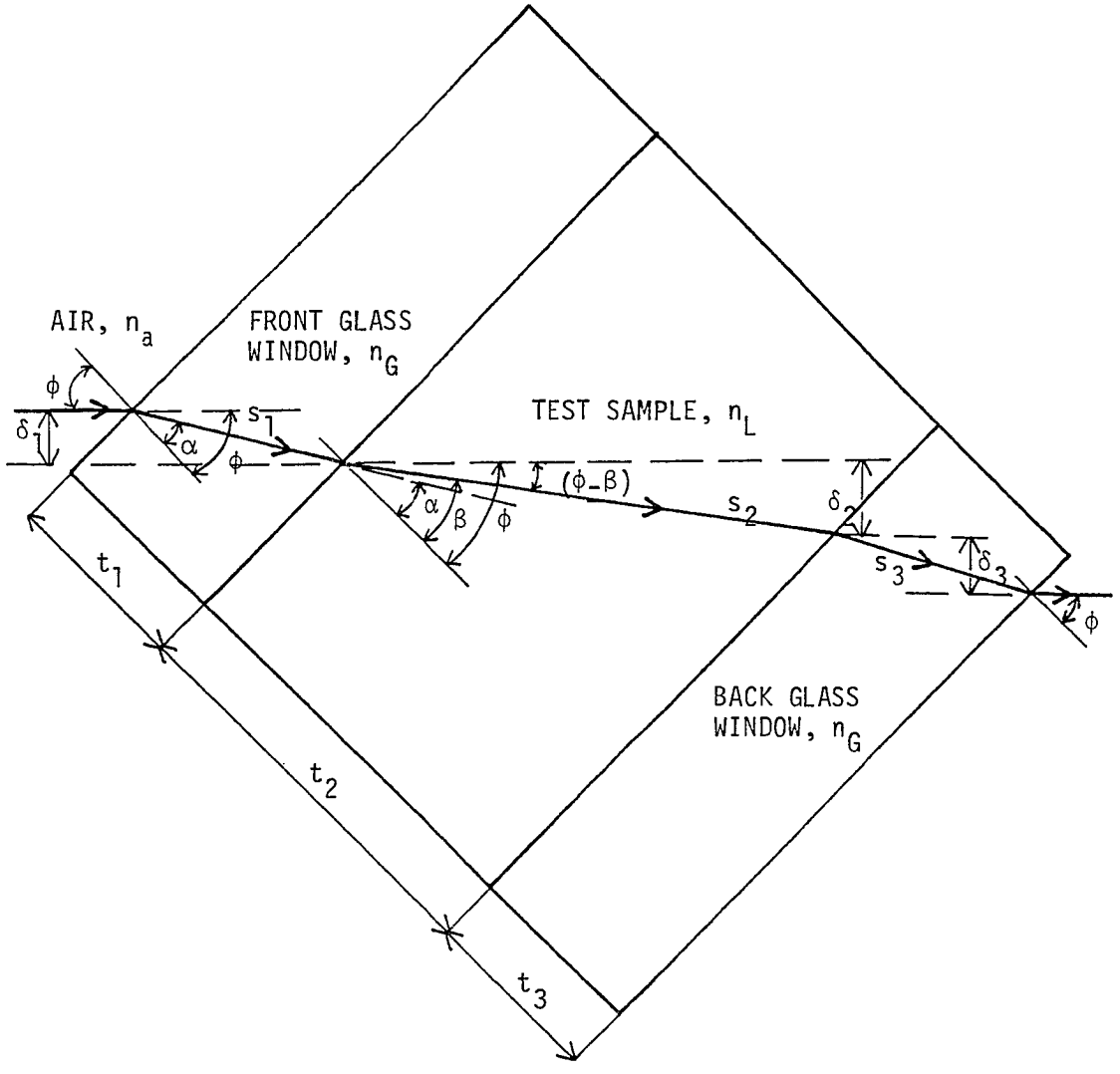

Fig. 2.3 Light path in the test chamber.

$$\delta_3 = t_3 \sin\phi \left[1 - \frac{\cos\phi}{(n_G^2 - \sin^2\phi)^{1/2}} \right] \tag{2.9}$$

For the refraction in a liquid sample, Snell's law gives

$$n_G \sin\alpha = n_L \sin\beta \tag{2.10}$$

The left term of Eq. (2.10) is equal to $\sin\phi$ [see Eq. (2.3)]. Therefore, the equation can be rewritten as

$$n_L = \frac{\sin\phi}{\sin\beta} \tag{2.11}$$

And the other geometric correlations are

$$s_2 = t_2/\cos\beta \tag{2.12}$$

$$\delta_2/s_2 = \sin(\phi - \beta) \tag{2.13}$$

With similar procedures as for the front glass window, Eqs. (2.10) - (2.12) can be combined to obtain

$$\delta_2 = t_2 \sin\phi \left[1 - \frac{\cos\phi}{(n_L^2 - \sin^2\phi)^{1/2}} \right] \tag{2.14}$$

and

$$n_L = \left[\left\{ \frac{\cos\phi}{1 - \delta_2/t_2 \sin\phi} \right\}^2 + \sin^2\phi \right]^{1/2} \tag{2.15}$$

In summary, calculation of the refractive index of the test sample should proceed as follows:

1. Obtain the scale magnified displacement, b, by observation.
2. Calculate the total displacement, δ, using Eq. (2.1).
3. Calculate the displacements due to the glass windows, δ_1 and δ_3, according to Eqs. (2.8) and (2.9) respectively.
4. Calculate the displacements in the test sample, $\delta_2 = \delta - \delta_1 - \delta_3$.

5. And finally, calculate the refractive index according to Eq. (2.15).

The sensitivity of this experiment is determined by the magnitude of the magnified displacement, b. A more careful look at Fig. 2.2 reveals that this displacement can be approximated as

$$b \cong a \frac{\delta}{f} \tag{2.16}$$

Therefore, the magnified displacement, b, and subsequently the sensitivity of the experiment can be increased theoretically by the following procedures:

1. Increasing distance, a, which is distance between the focal point and the scale.
2. Increasing the total displacement, δ.
3. Minimizing the focal length, f.

However, there were some constraints in the implementation of the aforementioned procedures. The distance, a, besides having a geometrical limitation (such as the optical bench dimension), was limited by the size of the incident beam cross section that could be scanned effectively by the detector. As has been mentioned earlier this cross section increases with the distance, a. A larger total displacement, δ, for a certain test sample could be obtained by enlarging the liquid thickness, t_2 (see Fig. 2.3). But this enlargement also required a larger test chamber depth; Otherwise the beam entering the test chamber could not pass through the cell without striking a solid boundary. As for the focal length, f, the choice for this work was limited to manufactured mirrors that were readily available and

inexpensive.

Compromises between sensitivity and repeatability influenced the overall geometrical dimensions and the design of the experimental set-up and its components significantly.

2.4 Description of the Experimental Components

The experimental measurements were performed in Duckworth Engineering Laboratory at Old Dominion University. A photograph of the experimental set-up is shown in Fig. 2.4. The main components such as the laser light source, the mirror assembly, the test chamber, the scale, and the detector were placed and secured on a wide flange shape I-beam (W14 x 53), eight feet in length which was used as an optical bench. The bench was placed (on its flanges) on a laboratory bench which was equipped with four heavy duty casters to enable some degree of portability. This arrangement successfully minimized vibrations and prevented unnecessary individual movements of the components.

The test chamber was built by the ODU Engineering Machine Shop, and the other components and materials were purchased with funds from the ODU Mechanical Engineering and Mechanics Department and the MUCIA-AID Indonesian Higher Education Project. The accessory equipment such as the digital multimeter, the voltage regulator, and the vacuum pump were supplied by the ODU Instrument Laboratory.

2.4.1 Laser Light Source

A Spectra-Physics, Model 155 helium-neon laser was used to provide the required laser beam. The laser was secured to a mini type optical bench equipped with a level-adjusting screw on each of its four legs.

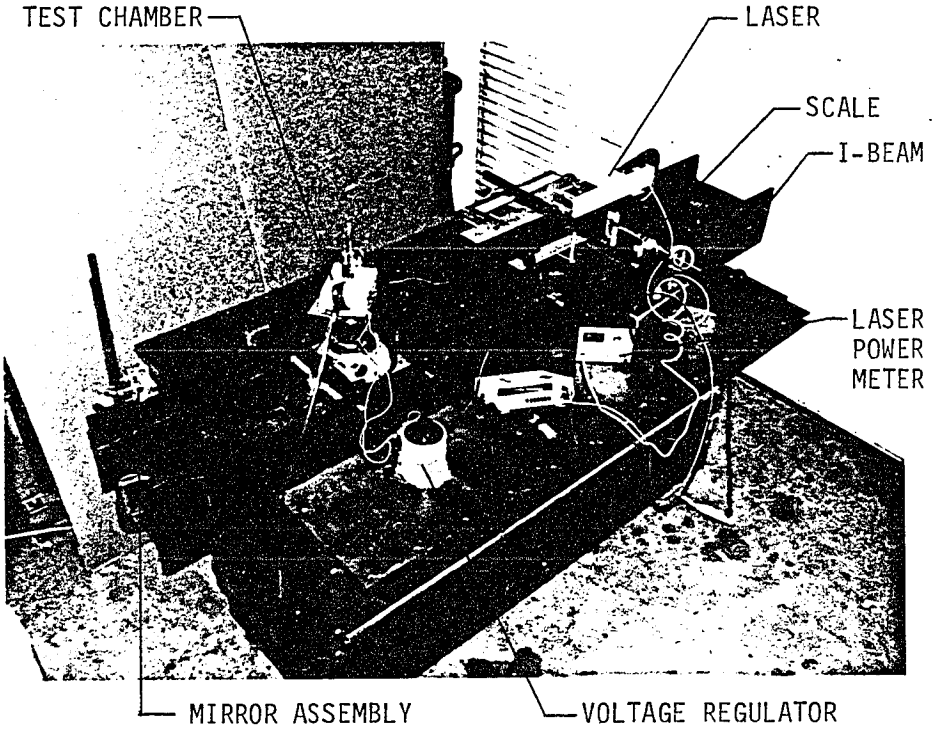

Fig. 2.4 Photograph of the experimental set-up.

Specifications for the Model 155 are given in Appendix C.

2.4.2 Mirror Assembly

A thin concave spherical mirror, manufactured by the Ealing Corporation, has been employed to magnify the beam displacement. This front surfaced mirror had a focal length of 103.9 mm and a diameter of 75 mm. It was selected because it was the mirror with the shortest focal length available. The reflecting (front) surface was produced by aluminizing.

The mirror was attached to a mounting, forming an adjustable mirror assembly as shown in Fig. 2.5. By using RTV, the mirror and the circular metal base were bonded to the ends of the connecting rubber cylinder. The springs, bolts, and adjusting nuts (three of each) provided the means for adjusting the mirror orientation. The assembly was then attached to a small metal pole which in turn was secured to the I-beam. Its position on the pole was also adjustable in the vertical direction and angular orientation could be varied.

2.4.3 Test Chamber

A photograph of the test chamber which also functioned as the mixing chamber in the test sample preparation is shown in Fig. 2.6. The chamber consisted of six principle parts: a body, two glass windows, two window retainers, and a base. In addition, the test chamber was equipped with several valves/connectors, a thermocouple assembly, a pressure gage, and an electric heater. The parts and the valves/connectors that were in direct contact with the corrosive ammonia-water solution were made from stainless steel.

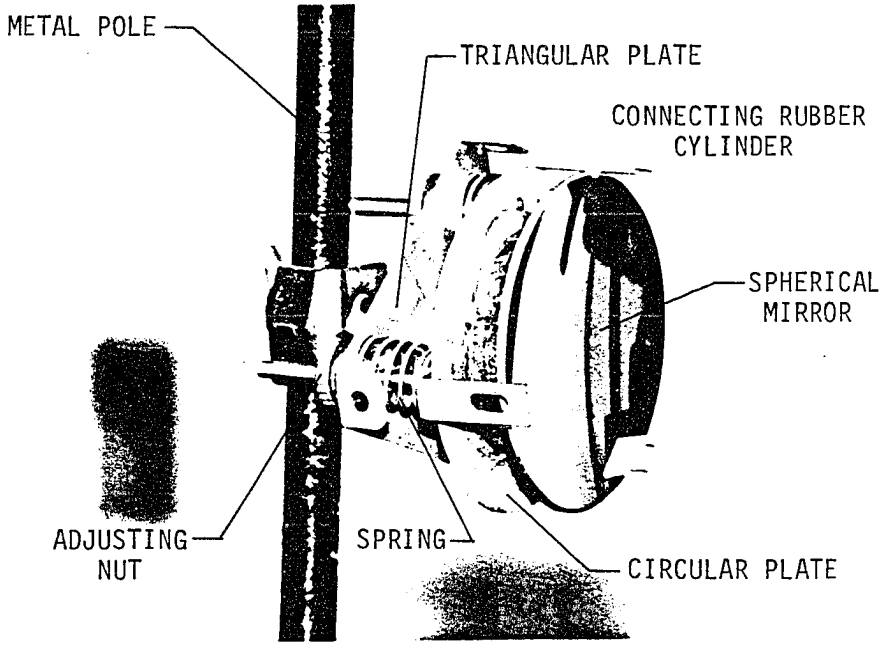

Fig. 2.5 Photograph of the mirror assembly.

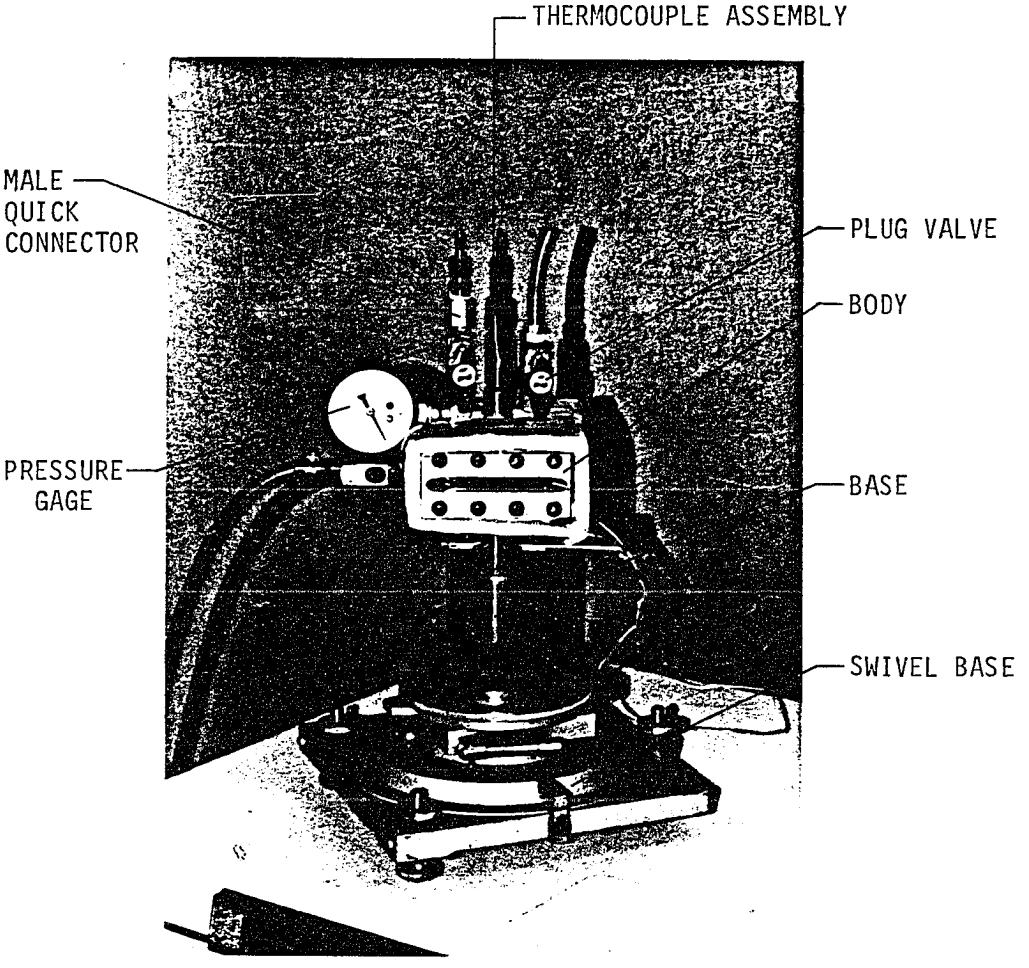

Fig. 2.6 Photograph of the test chamber.

The temperature of the test samples inside the test chamber was controlled using the electric heater. The heater tape was wrapped around the test chamber surfaces. Using a voltage regulator, the electrical input to the heating tape, and thus the supplied heat were varied according to prescribed conditions. To reduce the necessary heat requirement, which in turn minimized the temperature variation and the possible free convection motion in the test sample, the heating tape and the remaining test chamber surfaces were insulated from the ambient using 12.5 mm thick styrofoam insulation.

2.4.3.1 Test chamber body. Details and physical dimensions of the test chamber body are shown in Fig. 2.7. It was made from two stainless steel blocks, machined and bolted together to form a shallow tunnel through which the laser beam propagated in the test sample. Five threaded holes were drilled at various locations on the body to provide connection ports for other devices/parts. The 1/2" NPT hole on the bottom was used to connect the body to the base. A stainless steel plug valve with a quick open and close feature was placed in the 1/4" NPT hole on one side of the body. The other end of the valve was connected by a flexible tube to a sink and was used for discharging the test chamber and also could be connected to a vacuum pump--for evacuation purposes--prior to the introduction of the test sample into the chamber.

A second identical valve was placed on one of the three holes on the top of the body, to provide an access connection for either a water flush or a burret which was used in the test sample preparation. An Omega thermocouple assembly, Model NB1 CPSS-18G-1 with a one inch long stainless steel probe, was bolted into the middle (1/2" NPT) hole on the

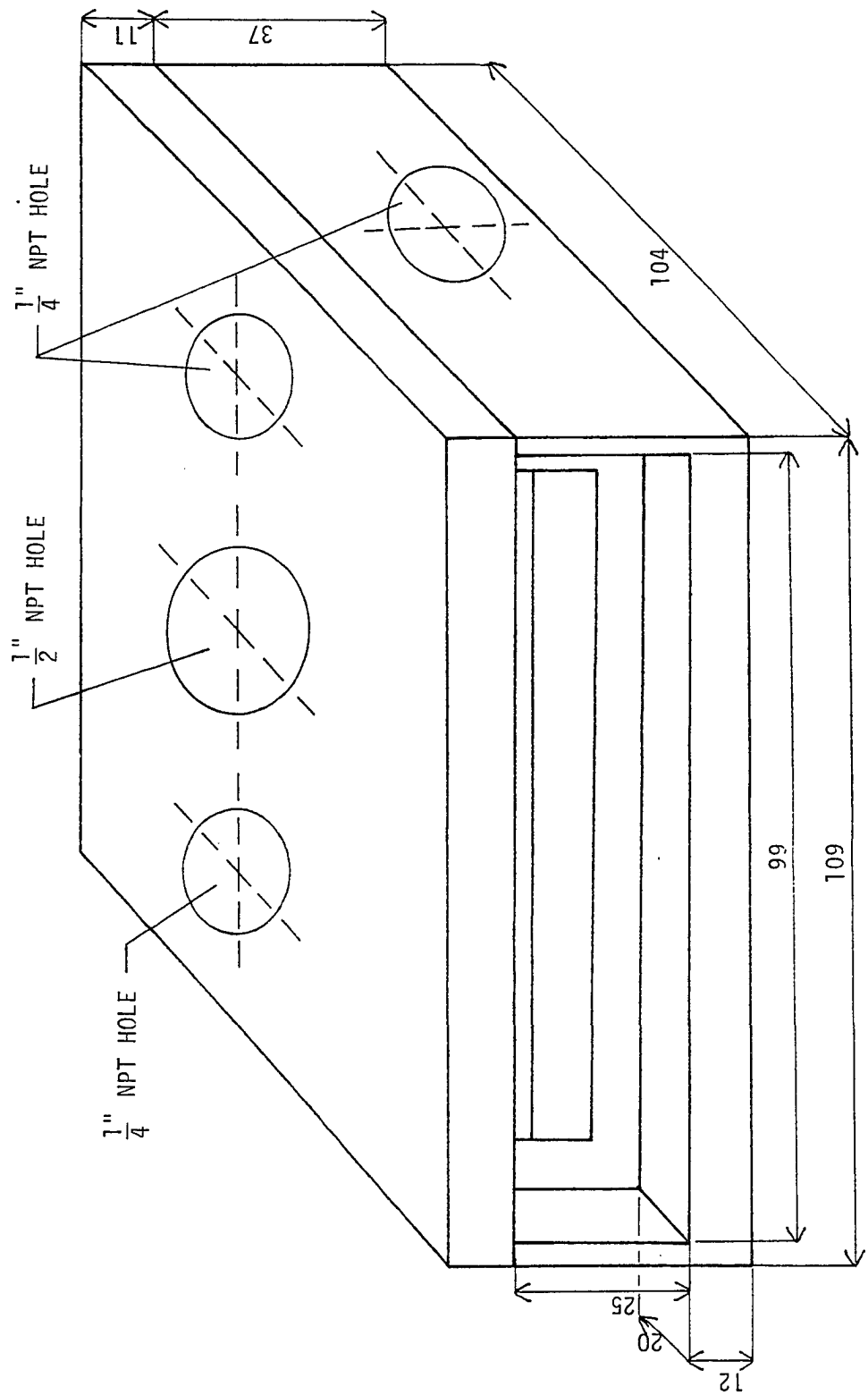

Fig. 2.7 Details and physical dimension of the test chamber body.

top of the body. This type T (copper-constantan) thermocouple has been used to monitor the test sample temperature. The last 1/4" NPT hole on the top accommodated a Cajon female branch tee connector, one end of which was connected to a pressure gage for monitoring the chamber pressure. The other end was connected in series to a plug valve and a male quick connector to provide a clean, quick connection and disconnection to a charging cylinder. The charging cylinder contained anhydrous ammonia for the test sample preparation.

2.4.3.2 Glass window. The rectangular glass windows used as transmission windows, had dimensions of 25.4x101.6 mm and were both about 12.7 mm thick. The glass was specially ordered from Optics for Research, Inc. These research quality windows were made from BK-7 glass plates and polished to achieve the following specifications:

Surface quality : 10/5

Flatness : 1/10 -1/20 of λ

Parallelism : 1 - 2 seconds of arc

The properties of BK-7 glass material are given in Appendix D.

2.4.3.3 Window retainer. The window retainer secured the glass window to the body by the use of eight screws. Neoprene flat gaskets were placed between the retainer and the glass window, and between the body and the windows. Those gaskets provided tight seals as well as allowing slight alignment of the windows (position/orientation). Details and physical dimensions of the aluminun retainer are shown in Fig. 2.8.

2.4.3.4 Test chamber base. The base was in the form of a cylindrical vessel with an outside diameter of 75 mm, a height of 100 mm, and a wall

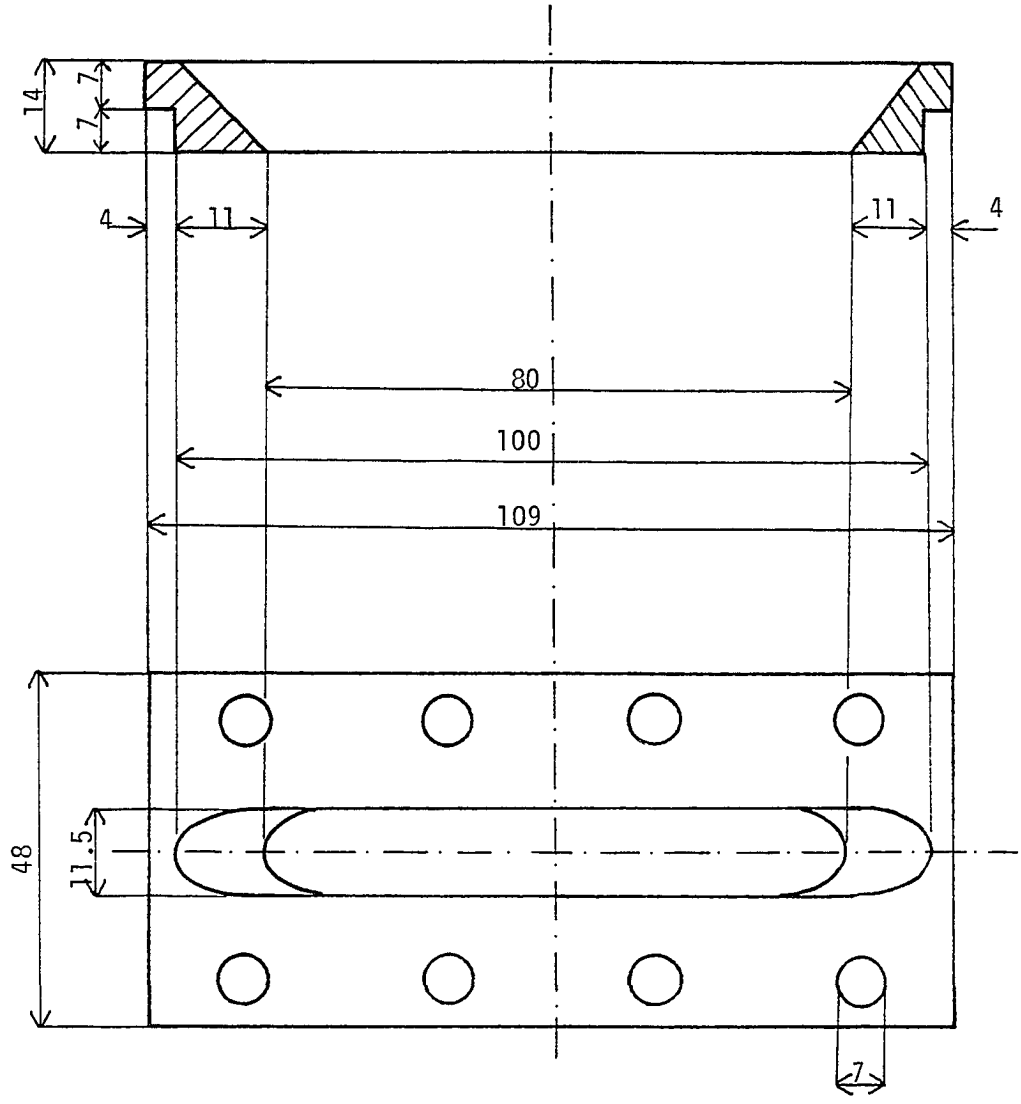

Fig. 2.8 Details and physical dimension of the window retainer.

thickness of 10 mm. Initially, it was designed to function as a pressure vessel to pressurize the test sample. However, due to unexpected problems which arose when the test chamber was pressurized (shifting of the glass window) the experiment was conducted only at near atmospheric pressure. The base was connected through a cylindrical column with threaded ends to the body. The base was equipped with three bolts which served as adjustable legs for levelling the base.

The entire test chamber was attached to another base that provided a smooth swivel for the test chamber (to form the tilted angle ϕ for example).

2.4.4 Scale

The scale used to measure the magnified displacement, shown in Fig. 2.9, consisted of a steel block, a vernier caliper, and a mounting device to accommodate the detector for the laser power meter. The steel block had a size of 12.5 x 25 x 552 mm, and it was secured to the mini type bench of the laser light source with its longest dimension perpendicular to the laser beam. The vernier caliper was a Craftsman, hardened stainless steel, metric, dial caliper which had a measurement range of 0 - 150 mm with a resolution of 0.05 mm. A specially designed and built mounting device for the detector was attached (with a slight tilted angle) to the moveable jaw of the caliper. The angle was chosen in order for the detector to be nominally perpendicular to the reflected beam. The mounting device was capable of vertical adjustment to provide scanning capability for the detector. The horizontal scanning operation was performed by moving the moveable jaw using the knurled thumb wheel. By taking into account the effective length of the steel block

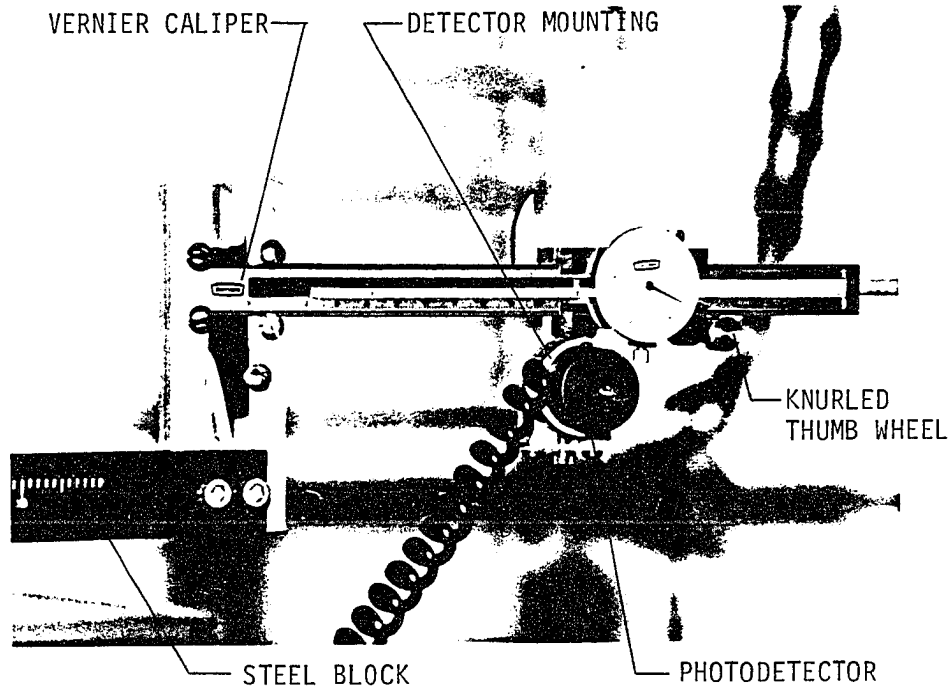

Fig. 2.9 Photograph of the scale.

and the relative position of the detector (with respect to the measuring edge of the moveable jaw), the observed magnified displacement, b, was related to the caliper reading by the following equation:

$$b = \text{caliper reading} + 198.7 \text{ mm} \tag{2.17}$$

2.4.5 Laser Power Meter

A Metrologic digital laser power meter, Model 45-540 has been used to scan the center of the reflected beam on the scale. It featured an LCD display and had four ranges with full scale readings from 20 μw to 20 mw . Calibration was within 2% of standard for the helium-neon laser light. An analog signal, available from a BNC output terminal, was available for use as a drive signal for strip chart recorders, oscilloscopes, and other devices.

The detector, a silicon photosensor, had a 7 mm aperture, 30 degree acceptance angle, and 100 mm^2 active area. The detector was mounted in a 25.4 mm diameter cell on a 50 mm coiled cable. This detector assembly was then attached to the scale by mounting it on the moveable jaw of the caliper.

Chapter 3

TEST SAMPLE PREPARATION

Since a very limited number of ammonia-water concentrations are available commercially, it was decided to mix each test sample in situ (at a specified concentration) prior to each experiment. The sample was mixed by forcing high pressure anhydrous ammonia into distilled water contained in the mixing chamber (at low pressure). The purity of the anhydrous ammonia supplied by Refrigeration Supply, Inc. was about 99.5%. The contaminant was mainly water. The distilled water was obtained from the ODU Civil Engineering Environmental Laboratory.

The mixing chamber employed in sample preparation was the test chamber described in the previous chapter. In addition, a 50 cc straight glass buret and a stainless steel charging cylinder were used in metering the amounts of distilled water and anhydrous ammonia respectively. The charging cylinder, shown in Fig. 3.1, was equipped with a pressure gage and two quick connectors (male and female) at both ends. To fill up the cylinder, the male quick connector was connected through a counterpart female connector to the anhydrous ammonia tank. In the charging process, the female connector of the cylinder was connected to the male quick connector of the mixing chamber.

3.1 Amounts of Distilled Water and Anhydrous Ammonia

To produce an ammonia-water solution at a specified concentration

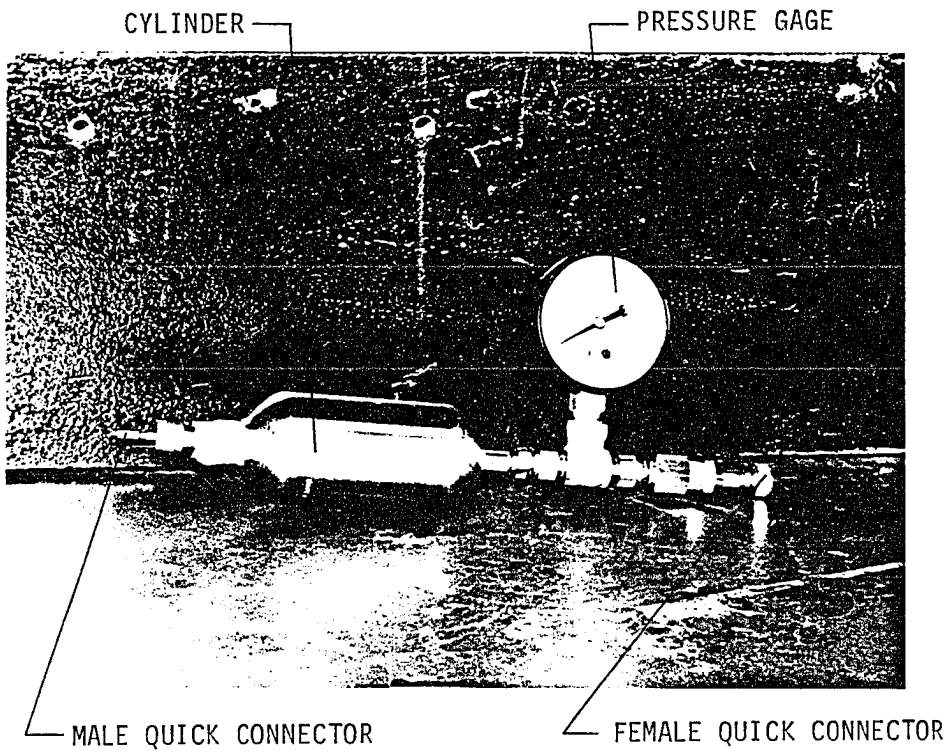

Fig. 3.1 Photograph of the charging cylinder.

(with the correct volume) in the mixing chamber, the amounts of distilled water and anhydrous ammonia were estimated based on the corresponding solution density and the volume capacity of the mixing chamber (65 cc). The density data could be obtained from literature [4,21,22].

Let the solution with 5% ammonia by weight concentration be used as an example for estimation. According to Ref. 4 the corresponding density at ambient pressure is 0.9780 gram/cc. Therefore, the total mass of the solution in the mixing chamber is equal to 63.57 grams. The masses of anhydrous ammonia, m_1, and water, m_2, are given as

$$m_1 = 0.05 \times 63.57 \text{ grams} = 3.18 \text{ grams}$$

$$m_2 = 0.95 \times 63.57 \text{ grams} = 60.39 \text{ grams}$$

These are the nominal amounts of ammonia and water that should be mixed together to produce a 5% ammonia (by weight) concentration ammonia-water solution. For the other solutions, similar methods were used to determine the amounts of the constituents.

3.2 Mixing Procedure

A schematic arrangement of the test sample preparation set-up is shown in Fig. 3.2. Prior to setting up the assembly; the burets, the charging cylinder, and the mixing chamber were cleaned thoroughly to eliminate possible contamination. For the mixing chamber, cleaning was followed by realignment of the glass windows (for parallelism and orientation) and included a careful measurement of the (inside) distance between the two glass windows. This distance was known as the liquid (or test sample) thickness in the previous chapter. The following steps were necessary in preparing an ammonia-water test sample solution:

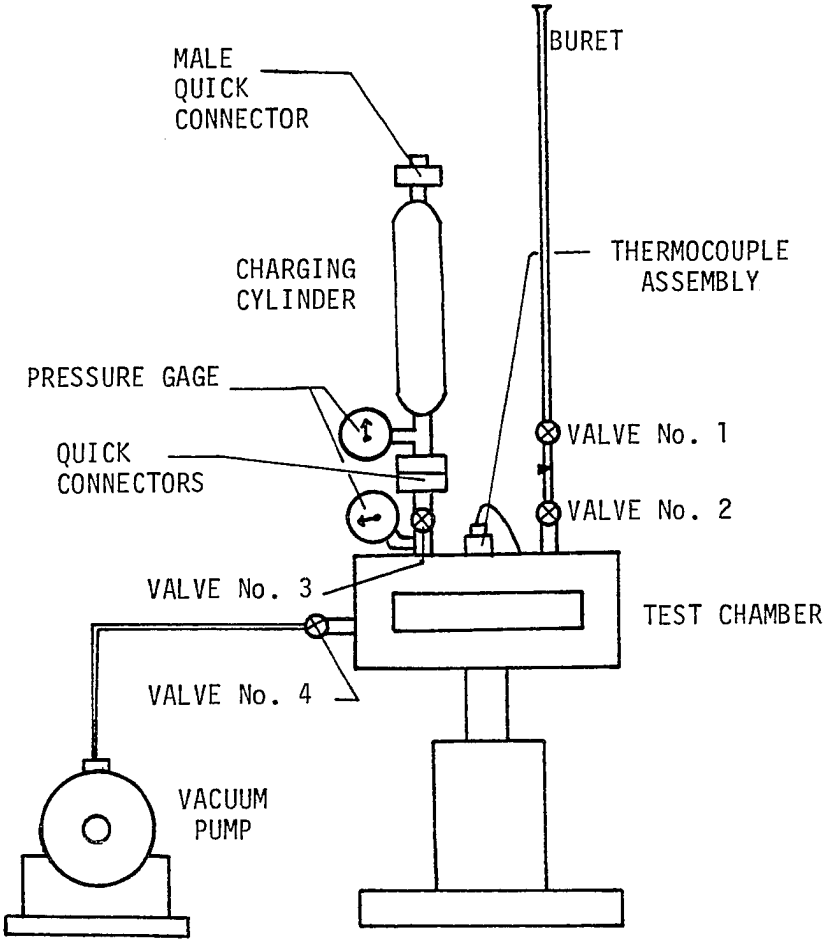

Fig. 3.2 Schematic arrangement of the test sample preparation set-up.

1. Close valve No. 1 and open valves No. 2, 3, and 4.

2. Turn on the vacuum pump to evacuate the system. This step eliminated air and other contaminants in the solution, and later would ease the injection of distilled water from the buret into the mixing chamber.

3. Turn off the vacuum pump if the pressure in the system has dropped to around -140 kPa (-20 psi).

4. Close valves No. 3 and 4, and disconnect the vacuum pump and the charging cylinder from the system.

5. Chill the charging cylinder by placing it in a freezer.

6. Fill up the buret with distilled water (50 cc).

7. Open valve No. 1 to allow the water to enter the mixing chamber.

8. Close valve No. 1 once the predetermined amount of water has been injected into the mixing chamber.

9. Remove the chilled charging cylinder from the freezer and connect it to the anhydrous ammonia tank. By opening the tank valve and regulating the delivery pressure (maximum 690 kPa), the anhydrous ammonia would fill up the charging cyliner. Obviously, the amount of transferred ammonia increased with the set delivery pressure.

10. Disconnect the cylinder from the tank, and thoroughly wipe-clean the water condensate on the cylinder surface.

11. Weigh the mass of the cylinder containing anhydrous ammonia, and call it initial mass. The difference in mass with the empty cylinder was identical to the mass of ammonia in the cylinder. The cooling process in step 5 significantly increased the amount of

ammonia transferred into the cylinder. For example, without cooling (cylinder at the room temperature) the maximum amount of ammonia transferred was only about 0.75 gram. With a sufficient chilling, this amount could be increased to about 10 grams. The amount of ammonia in the cylinder should be about 0.5 to 1.5 grams more than the predetermined amount needed for a certain concentration. Excess ammonia should be released from the cylinder until the desired amount was achieved. If the amount was less than the requirement, steps 5, and 9 through 11 should be repeated until the correct amount of ammonia was obtained.

12. Connect the charging cylinder containing a correct amount of ammonia to the mixing chamber. At this time the cylinder pressure might go up to 1.03 MPa (150 psi) due to warming effect. In contrast the water pressure in the chamber was still very low (close to -140 kPa).

13. Charge the mixing chamber with anhydrous ammonia by opening valve No. 3. At the same time observe the chamber pressure. If the pressure reached 206 kPa (30 psi), quickly close valve No. 3. Higher pressure was likely to distort the parallelism and orientation of the glass windows of the chamber.

14. Wait until the chamber pressure drops below the ambient pressure before charging (step 13) is resumed and repeated as necessary until the solution reached equilibrium state (steady chamber pressure).

15. Obtain a final equilibrium pressure that is nominally equal to ambient pressure (±34.5 kPa). The pressure in this range was desirable since the experimental measurements were intended to be

performed around ambient pressure.

16. Close valve No. 3 and disconnect the charging cylinder from the mixing chamber.

17. Finally, weigh the mass of the charging cylinder and call it the final mass. The difference between the initial and the final mass was identical to the amount of ammonia that had been mixed with water to form an ammonia-water solution. If the concentration thus obtained was satisfactory, the experiment was continued. Otherwise, the entire procedure was repeated with some necessary adjustment in the amount of water or ammonia.

Nine samples at different concentrations have been successfully mixed and used in the measurements, the weight percentage concentrations tested were: 2.54, 5.98, 7.59, 10.21, 14.41, 18.59, 20.99, 25.23, and 27.68. However, there were many samples that had been successfully mixed but could not be used to produce results due to some failures in the equipment and other problems.

Chapter 4

EXPERIMENTAL PROCEDURE

4.1 Alignment

Alignment of the experimental equipment is an important procedure that should be performed before a calibration and a data collection can be done. Results of high precision and repeatability can only be produced by a combination of appropriate equipment and accurate alignment. For the present work, alignment was performed on the laser light source, mirror orientation, and parallelism of the glass windows of the test chamber.

4.1.1 Alignment of the Laser Light Source

The objective of this alignment was twofold: To produce an imaginary horizontal plane on which the light-path shown in Fig. 2.2 laid horizontally (such a logical and desirable condition would be useful as a reference for the other alignment and later in data collection); The other objective was to make sure that the laser beam passed through the center of the test fluid (in the test chamber) with beam displacement occuring only on the horizontal plane.

The first objective was achieved by taking advantage of the fact that the laser tubes (and also the beams) are carefully centered within the steel housings so that the beams are pre-aligned and parallel to the housings. Thus, by aligning the housing mechanically, the laser beams

are aligned optically. In the present case, the housing (and the beam) was aligned horizontally by employing a precision bench level and by manipulating the levelling screws of the laser light source.

As for the second objective, the following were the procedure:

1. Place the test chamber about 400 mm in front of the laser.
2. Turn on the laser.
3. Obtain the desired height of the test chamber by adjusting the three levelling bolts of the base. Make sure that the top surface of the swivel base (which is equipped with two bench levels) is horizontal.
4. Proceed to the next alignment.

4.1.2 Mirror Orientation

The objective was to align the spherical mirror in such a way that the incoming laser beam struck the mirror surface at a right angle. In other words, the mirror should reflect the beam back on itself. The only complication was such a reflection diverged from the focal point of the mirror; and subsequently made the alignment more difficult. To overcome this difficulty an additional device was employed. This specially designed and built device, shown in Fig. 4.1, was machined from an aluminum block to form two parallel plates that were connected to each other on their upper parts. The plates were pierced with centered coincided pinholes about 1 mm in diameter. This device was then attached to an aluminum column equipped with rack and pinion gears and brake to enable controlled positioning in the vertical direction. The alignment proceeded as follow:

1. Position the parallel plates between the laser light source and the mirror.

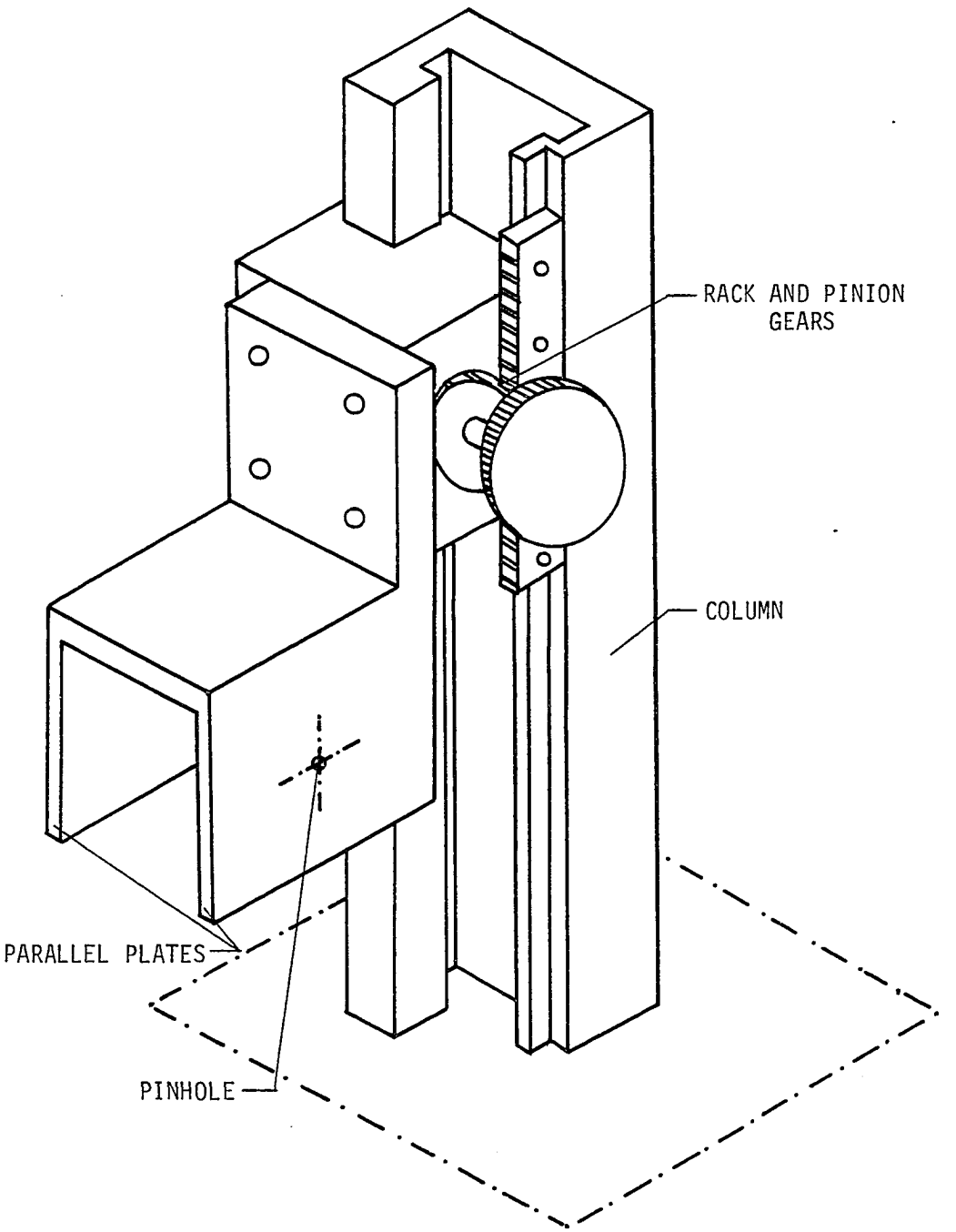

Fig. 4.1 Mirror alignment device.

2. Adjust the height and orientation of the plates so the laser beam can safely pass through both pinholes.

3. Manipulate the mirror height and orientation to reflect the beam back on itself. This can only happen if the reflected beam passes back through the pinholes (see Fig. 4.2).

4. Remove the parallel plate from the bench and proceed with the next alignment as needed.

4.1.3 Glass Windows Parallelism

To obtain appropriate displacement of the test sample, the test chamber was required to have glass windows that were highly parallel to each other. Consequently, it was also pre-required that both surfaces of each glass window should be optically flat and parallel. The glass windows employed in this work satisfied both requirements.

The alignment commenced with the glass windows, the electric heater, and the styrofoam insulation missing from the test chamber body. Initially, the test chamber was not on the bench. Next were the necessary steps:

1. Place a screen about 1000 mm in front of the laser light source.
2. Turn on the laser and mark the laser light spot on the screen.
3. Place the test chamber about 400 mm in front of the laser light source.
4. Place a precision bench level on the top surface of the test chamber body.
5. Make the surface (and the whole test chamber) horizontal by adjusting slightly the levelling bolts of the test chamber base.

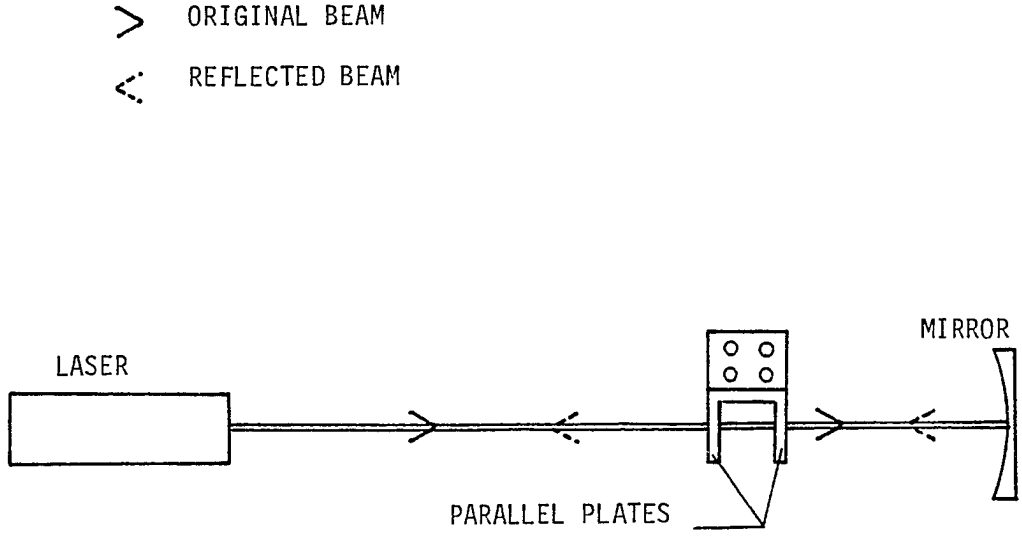

Fig. 4.2 Behavior of the laser beam that is perpendicular to the mirror.

6. Install the front glass window and its neoprene flat gaskets on the test chamber body.

7. Tighten the screws evenly on the retainer to hold the glass window in place and to prevent warping.

8. Orient the test chamber so that the reflected beam (from the glass window) falls on an imaginary vertical line that passes through the aperture of the laser light source.

9. Center the reflected beam exactly on the aperture of the laser by manipulating the retainer screws. When this occurs, the transmitted beam strikes the screen on the marked spot since the glass windows are perpendicular to the beam (no refraction).

10. Perform steps 6 and 7 for the back glass window.

11. Fill up the test chamber with distilled water. Water, which has a larger refractive index than air, would better indicate any problems with parallelism of the glass windows. That problem was detected by behavior of the two reflected beams (by the front and back glass windows) that fell back on the area around the aperture of the laser light source. Reflections produced by parallel glass windows would behave as follows:

- If the front glass window was perpendicular to the beam, both reflected beams would coincide and fall back exactly on the aperture. And the transmitted beam would strike the screen on the marked spot (see Fig. 4.3).
- If the test chamber was slightly rotated (in the clockwise direction) so the normal of the windows formed a small angle, Ψ, with the incoming beam, the reflected beam due to the back glass window would reside to the right of that one due to the front glass

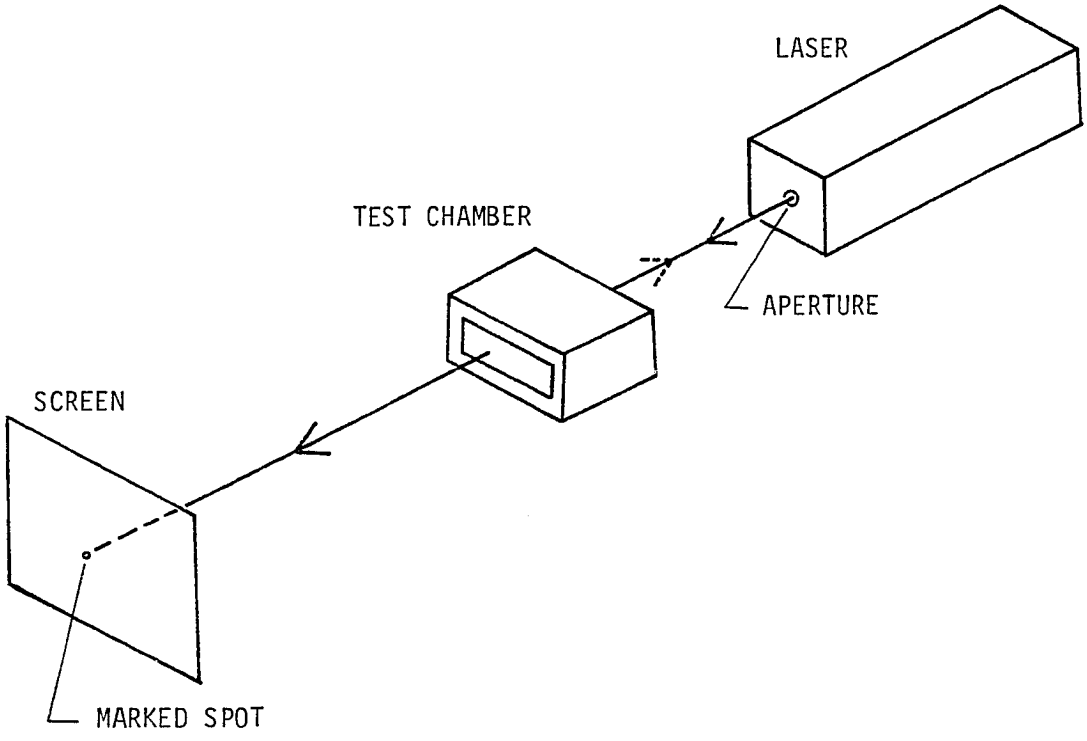

Fig. 4.3 Laser beam behavior (the test chamber is perpendicular to the beam).

window as shown in Fig. 4.4. And the transmitted beam, due to refraction, would strike the screen slightly to the left of the marked spot. The distance, l, between the two reflections increased with the angle Ψ and eventually became zero as Ψ went to zero.

- A similar but opposite trend would happen if the test chamber was rotated in the counter clockwise direction, and the distance, l, for any pair of $\pm\Psi$ would be identical.

Any deviation from the aforementioned behavior indicated that the glass windows were not parallel. Therefore, the orientation of the back glass window required further adjustment.

12. Obtain the correct orientation of the back glass window as necessary by carefully manipulating the cover screws. If the appropriate behavior described in step 11 was achieved, the glass windows alignment was completed.

13. Measure the outside distance between the two glass windows, t_{tot}, by employing a large micrometer screw and a standard block gage of 12.7 mm (0.5 inch) thickness. The inside distance or the liquid thickness, t_2, was given as:

$$t_2 = t_{tot} - t_1 - t_3 - 12.7 \text{ mm}$$

where t_1 and t_3 were the thickness of the front and back glass windows respectively.

14. Install the electric heater and the styrofoam insulation on the test chamber body. The equipment then was ready for scale observation.

During the course of the experimental measurements, each component's condition and alignment was checked from time to time,

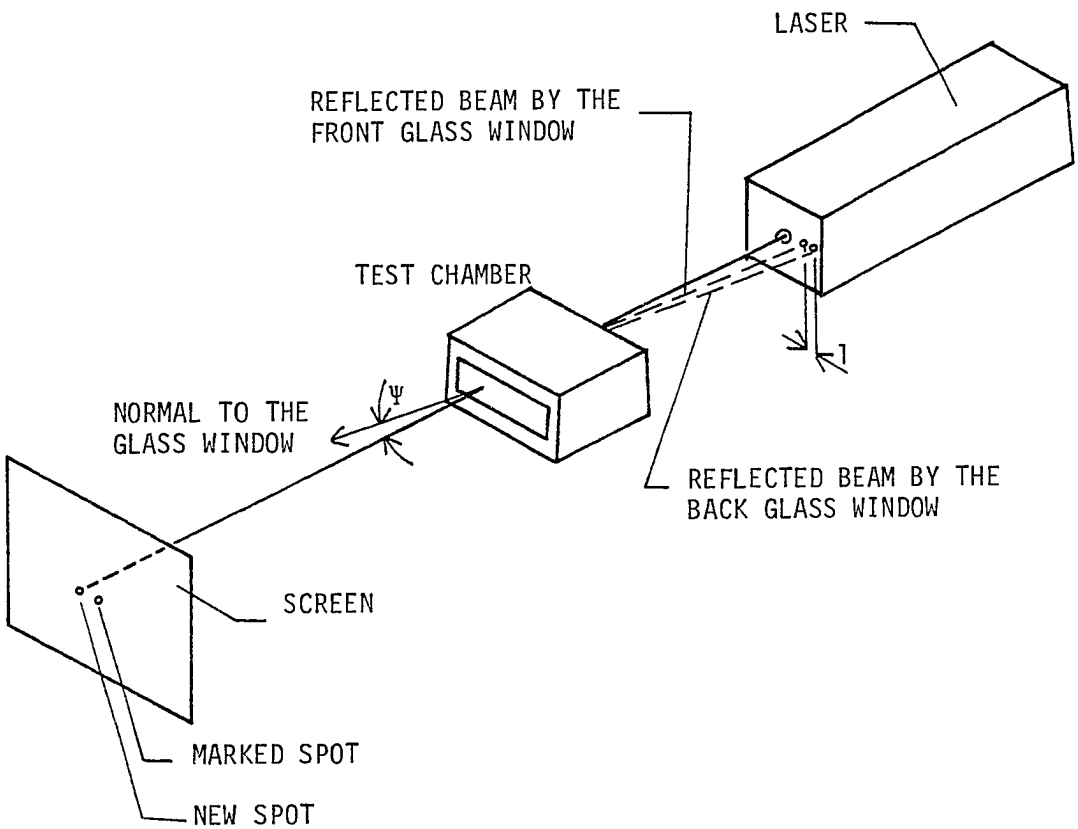

Fig. 4.4 Laser beam behavior (the test chamber is slightly tilted).

especially prior to a new test sample preparation. If any deviation was detected, necessary service or realignment was performed.

4.2 Scale Observation

As has been mentioned earlier, the magnified displacement, b, was the measured quantity in this experiment. This quantity was obtained from the scale after alignment and test sample preparation had been completed. Observation procedures for calibration using a liquid with known refractive indices and for actual data collection (of a test sample) were identical.

An important requirement of the observation was to position the test chamber (and the glass windows) at a tilted angle, ϕ, of exactly 45 degrees. The simplest and the best method to accomplish such a requirement employed a right angle (45-90-45 degrees) prism and a standard block gage of 25.4 mm thickness. The observation procedure could be described as follows;

1. Firmly hold the block gage so one of its parallel (measuring) sides is in contact with the front glass window.
2. Attach the long side of the prism against the other parallel side of the block gage. If the height of the test chamber tunnel were large enough to accommodate the thickness of the prism, the long side of the prism could have been directly attached to the front glass window.
3. Turn on the laser.
4. Rotate the swivel base of the test chamber (in the clockwise direction) to the position at which one of the 45-degree facets of the prism reflects the beam back on the laser aperture. The glass windows now make a 45-degree angle with the beam (see the illustration in Fig. 4.5).

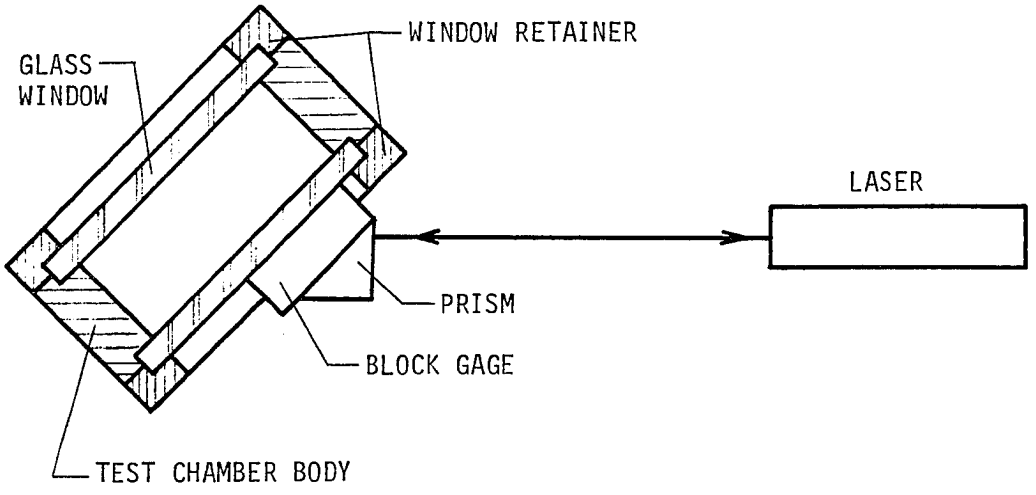

Fig. 4.5 Prism arrangement for setting the 45 degrees tilted angle.

5. Remove the standard block gage and the prism from the test chamber. The light path now is similar to the one shown in Fig. 2.2.

6. Turn on the laser power meter.

7. Move the power detector (on the scale) to intercept the incident reflected beam.

8. Adjust the vertical position of the detector to obtain maximum reading on the laser power meter.

9. Scan the center of the beam horizontally by slowly moving the detector step by step. The position that gives a maximum intensity reading is assumed to be the center of the beam.

10. Observe the caliper reading.

11. Obtain the magnified displacement, b, according to Eq. (2.17).

The procedure described above was employed for measurements of test samples at room temperatures. For higher temperature measurements, the test sample was heated before steps 1 to 10 could be performed. Control of the test sample temperature inside the test chamber has been described in Sec. 2.4.

4.3 Calibration

Various systematic errors in the equipment were compensated by calibrating the scale with a series of measurements of a liquid standard of known refractive indices. Among standard liquids, distilled water has been used in this work for calibration purposes. The refractive indices of distilled water are presented by Tilton and Taylor [23] for every one-half degree from 0 to 60°C covering 14 different wavelengths in the visible radiation spectrum. However, there are no data for Helium-Neon laser light (λ = 632.8 mm) included in that literature.

Therefore, these missing refractive index data have been computed by simply interpolating the available data. The interpolation results for every one degree from 20 to 60°C are presented in Appendix E. To justify the interpolation, refractive indices of water are plotted versus wavelength in Fig. E.1 of Appendix E.

The scale has been calibrated three times during the experimental measurements of the nine different solutions mentioned in the last part of Chap. 3. Each calibration was performed over temperature intervals of eight to ten degrees, starting from room temperature, to about 60°C. In general, the calibration discrepancies, εb, between the observed magnified, b_o, and the exact value obtained by calculation from the interpolated reference data, b_{data}, were found consistently in a range of 0.20 to 0.25 mm. The higher discrepancies (0.25 mm) were most likely to occur for the calibrations done at 45°C or higher. These calibration discrepancies have been used to correct the observed magnified displacement, b_o, of the actual testing of the test sample. The corrected displacement, b_{cor}, was obtained as:

$$b_{cor} = b_o + \varepsilon b \tag{4.1}$$

and it has been used to calculate the displacement, δ, and ultimately the corresponding refractive index. To avoid tedious and repeated individual calculations, a computer program for this calculation has been developed to provide a correlation list between the magnified displacement and the refractive index.

Chapter 5

EXPERIMENTAL RESULTS

Nine ammonia-water solutions at different concentrations have been tested in this investigation, their ammonia-weight percentage concentrations were: 2.54, 5.98, 7.59, 10.21, 14.41, 18.59, 20.99, 25.23, and 27.68. The range of the testing temperature was from room temperature to 60°C or lower depending on the concentration of the tested solution. The upper temperature limit for each solution was set not to exceed the corresponding solubility limit as given in Ref. 19. In all tests the following constant quantities have been used:

a = 1210.00 mm

f = 103.90 mm

t_1 = 12.751 mm

t_2 = 65.830 mm for $W_1 \leqslant 14.41\%$

65.730 mm for $W_1 \geqslant 18.59\%$

t_3 = 12.377 mm

n_G = 1.515

ϕ = 45° = 0.78540 radian

A summary of the experimental results are presented in Appendix E which includes the liquid thickness, the concentration and temperature of the tested solution, the observed and the corrected displacements (b_o and b_{cor}), and the calculated refractive index.

Having obtained the refractive index results, the next question was

quality of the measurements. Because no measurement is free from error, steps were taken to evaluate the accuracy and the precision of the measurements. Such an analysis is presented in the next section.

5.1 Error Analysis

To predict the magnitude of error in the final result, it is necessary to understand the nature of error, the sources, types, magnitude of errors made at various stages of the measurement process, and the interrelationship of errors. Before discussing this aspect of errors further, there are several important basic definitions that will be clarified in the next paragraph.

It is important to realize that the so-called "true-value" of any measurement is unknown and unachievable (even though it does exist). That value which can be attained by refined measurements and by techniques of multiple measurements is termed a best available value. Then error is the difference between the measured value and the corresponding true value. It follows that a true error can never be discovered since the true value is unknown. Therefore, errors in measurement are always vague and carry some amount of uncertainty which is defined as the "possible value" the error may have.

There are three types of errors that may cause uncertainty in an experimental measurement:

1. Fixed or systematic errors which will be repeated consistently in successive measurements.
2. Random errors which are produced by a large number of unpredictable and unknown variations in the experimental situation.

3. Gross blunders which are not errors at all and can always be eliminated completely by careful work.

The terms accuracy and precision are often used to distinguish between systematic and random errors. If a measurement has small systematic errors, then it has high accuracy. If a measurement has small random errors, then it has high precision.

In practice systematic errors may be reduced by calibrating the instruments. For the current experimental work, systematic errors of various components were reduced by calibrating the scale as discussed in the previous chapter. Based on the testing of water (as the media for calibration) at various temperatures, it was found that there was consistent discrepancy between the supposedly obtained measurement and the corresponding observation on the scale. This consistent offset resulted from the overall systematic errors of various components (for example: spherical aberrations of the mirror, slight imperfections of the windows parallelism, errors on the scale, etc.). It was neither possible nor the objective of this discussion to determine individual contributions of each component to the overall systematic error. Incorporating this discrepancy (overall systematic error) as a correction in the actual observation on the scale was a sufficient reason for assuming that the systematic errors had been taken care. Therefore, from here on the random errors and corresponding uncertainties will be of primary interest.

In order to go about obtaining values of the uncertainty, measurements must be distinguished first between single-sample and multisample data. Single-sample data are those in which uncertainties may not be discovered by repetition because they are prohibited by cost,

time, and other limitations. Multisample data are obtained in those instances where enough observations are performed so that the reliability of the results can be assured by statistics.

For single-sample data, the best available value of the measurement must simply be taken as the observed value. The uncertainty in that value then must be estimated using good engineering judgment based on instrument accuracy, the least count on the measuring scale (resolution), observable fluctuations in instrument readings, and the experimenter's overall experience in performing the experiment. The only single-sample observation in this work was for the scale observation to determine the magnified displacement, b. The enormous amount of time consumed for observation and considerations on the small fluctuations of the readings of the laser power meter and the digital miltimeter (for temperature measurement) had influenced significantly the decision to perform single-sample observation and the estimation of the uncertainty. The uncertainty of this quantity was estimated to be 0.05 mm which was equal to the least count (resolution) of the scale. This was twice as large as is usually chosen for single sample observation (one-half of the least count).

For multisample data it is necessary to make the following two points:

1. The arithmetic mean may be considered to be the best available value from any set of direct measurements. The mean can be considered as the nearest approximation of the true value.
2. The most important and most commonly used measure of uncertainty in statistical analyses is the standard deviation. It is defined as:

$$\sigma(x) = \left[\frac{1}{k-1}\sum_{t=1}^{k}(x_i - \bar{x})^2\right]^{1/2} \qquad (5.1)$$

where k is the number of observations (less than 20), x_i is an individual measurement and $\bar{x}$ is the arithmetic mean value. For the current analysis the uncertainty in measurement is assumed to be equal to the standard deviation.

For this work the uncertainties of the basic dimensions/quantities, which were obtained by applying the techniques discussed in the preceeding paragraphs, can be summarized as follow:

$$\Delta a = 1.0 \text{ mm}$$

$$\Delta b = 0.05 \text{ mm}$$

$$\Delta f = 0.1 \text{ mm}$$

$$\Delta t_1 = 3.17 \times 10^{-3} \text{ mm}$$

$$\Delta t_3 = 3.35 \times 10^{-3} \text{ mm}$$

$$\Delta t_{tot} = 5.08 \times 10^{-3} \text{ mm}$$

$$\Delta\phi = 0.1 \text{ degree} = 1.75 \times 10^{-3} \text{radian}$$

Eventually, the arithmentic means of the basic dimension/quantities and their uncertainties must be combined to calculate the uncertainty of the resulting refractive index. The standard method used in such calculation is described below.

Consider a quantity Q which is to be calculated from several observed quantities a,b,c,....., then in mathematical form

$$Q = Q(a,b,c,.....) \qquad (5.2)$$

If Δa, Δb, Δc,..... are the corresponding uncertainties of a, b, c, ..., the uncertainty of Q, ΔQ, can be calculated using the following formula based on Taylor series expansion

$$\Delta Q = \left[\left(\frac{\partial Q}{\partial a}\Delta a\right)^2 + \left(\frac{\partial Q}{\partial b}\Delta b\right)^2 + \left(\frac{\partial Q}{\partial c}\Delta c\right)^2 + \ldots\ldots\right]^{1/2} \qquad (5.3)$$

Alternatively, the analysis can also be performed in terms of the variance of the quantity defined as the square of the standard deviation which is, in this case, equal to the uncertainty of the quantity.

The uncertainty calculation of the refractive index should proceed in the similar succession as the calculation of the refractive index described in Sec. 2.2. For the sake of simplicity, Eq. (2.16) has been used to derive the uncertainty of the path displacement, $\Delta\delta$, as

$$(\Delta\delta)^2 = \left(\frac{f}{a}\Delta b\right)^2 + \left(\frac{b}{a}\Delta f\right)^2 + \left(-\frac{bf}{a^2}\Delta a\right)^2 \qquad (5.4)$$

The uncertainty of the displacement due to the glass window has been derived based on Eq. (2.8) as

$$(\Delta\delta_G)^2 = \left[\sin\phi\left(1 - \frac{\cos\phi}{G^{1/2}}\right)\Delta t_G\right]^2 + \left[t_G\left(\cos\phi - \frac{\sin^2\phi\cos^2\phi}{G^{3/2}}\right)\Delta\phi\right]^2 \qquad (5.5)$$

where: $G = (n_G^2 - \sin^2\phi)$

For the displacement in the test sample, its uncertainty was obtained as

$$(\Delta\delta_2)^2 = (\Delta\delta)^2 + (-\Delta\delta_1)^2 + (-\Delta\delta_3)^2 \qquad (5.6)$$

The uncertainty of the square of the refractive index has been derived based on the square of Eq. (2.15) as

$$(\Delta n_{mix}^2)^2 = \left[2\left(\sin\phi\cos\phi - \frac{t_2^3\sin^2\phi\cos^3\phi}{z}\right)\Delta\phi\right]^2 + \left[\frac{2t_2^2\sin^2\phi\cos^2\phi}{z}\Delta\delta_2\right]^2 + \left[\frac{2t_2\delta_2\sin^2\phi\cos^2\phi}{z}\Delta t_2\right]^2 \qquad (5.7)$$

where: $z = (t_2\sin\phi - \delta_2)^3$

$$(\Delta t_2)^2 = (\Delta t_{tot})^2 + (-\Delta t_1)^2 + (-\Delta t_3)^2$$

And finally, the uncertainty of the refractive index has been derived as

$$(\Delta n_{mix})^2 = \frac{(\Delta n_{mix}{}^2)^2}{\Delta n_{mix}{}^2} \tag{5.8}$$

The aforementioned formulas [Eqs. (5.4) to (5.8)] have been used to calculate the uncertainty of the experimentally obtained refractive index of ammonia-water solutions. The results of this calculation are presented in Appendix F. It was determined that the uncertainties obtained in n_{mix} vary very little and are in the range from 3.553×10^{-4} to 3.582×10^{-4}. For simplicity without overestimation, it is reasonable to round-off the values of the uncertainty to 4.0×10^{-4}.

5.2 Empirical Correlation

The refractive index data are graphically shown in Figs. 5.1 and 5.2. The first figure displays data for concentrations of 2.54, 7.59, 14.41, 20.99, and 27.68%; and data for the other concentrations are displayed in the second figure. By displaying these data in two figures, the graphical presentation becomes clearer and more distinct than if the entire data were displayed in a single figure. Both figures show that the refractive indices of ammonia-water solutions decrease with temperature but increase with concentration. The figures also indicate that it would be reasonable to assume that the actual relationship between the refractive index and the temperature is a linear one. At this point, however, it is not that easy to determine the actual increasing behavior of the refractive index with respect to the concentration. Therefore, it would be very useful if some sort of

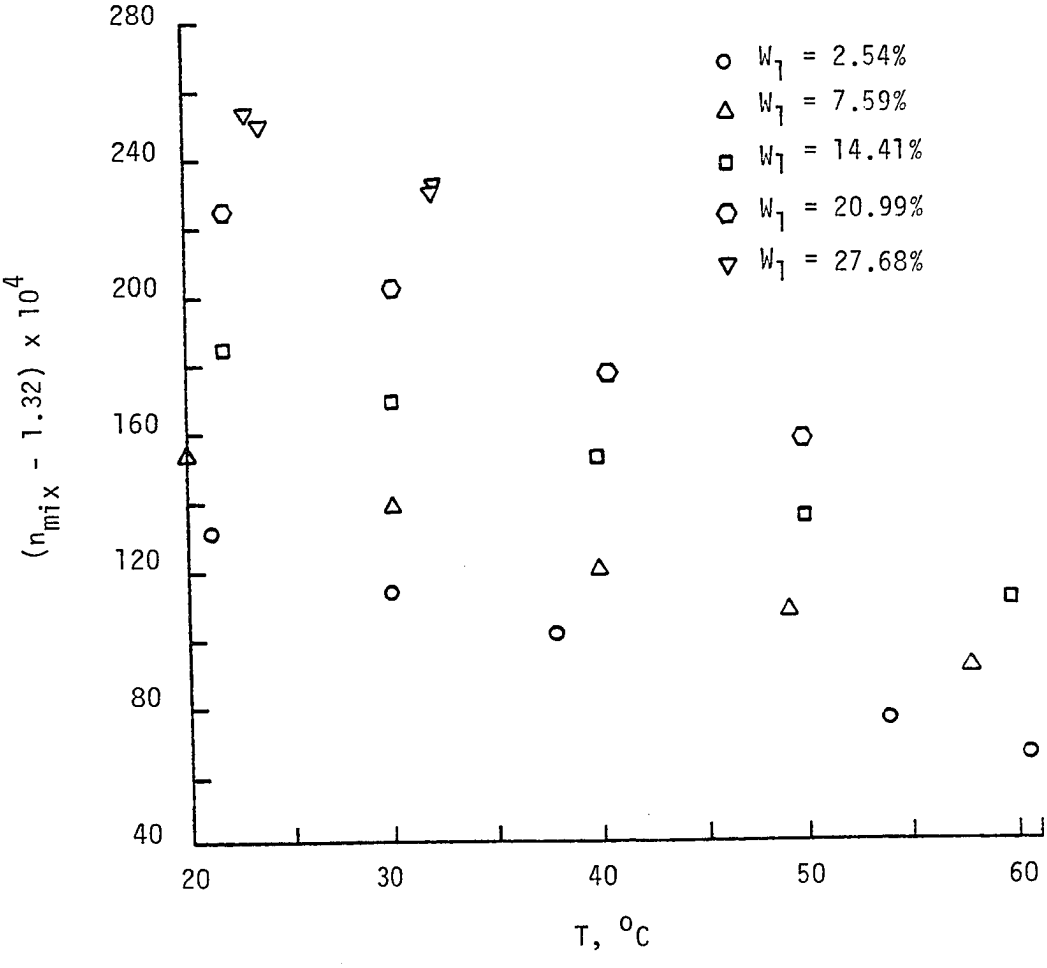

Fig. 5.1 Experimental refractive index data of ammonia-water solutions.

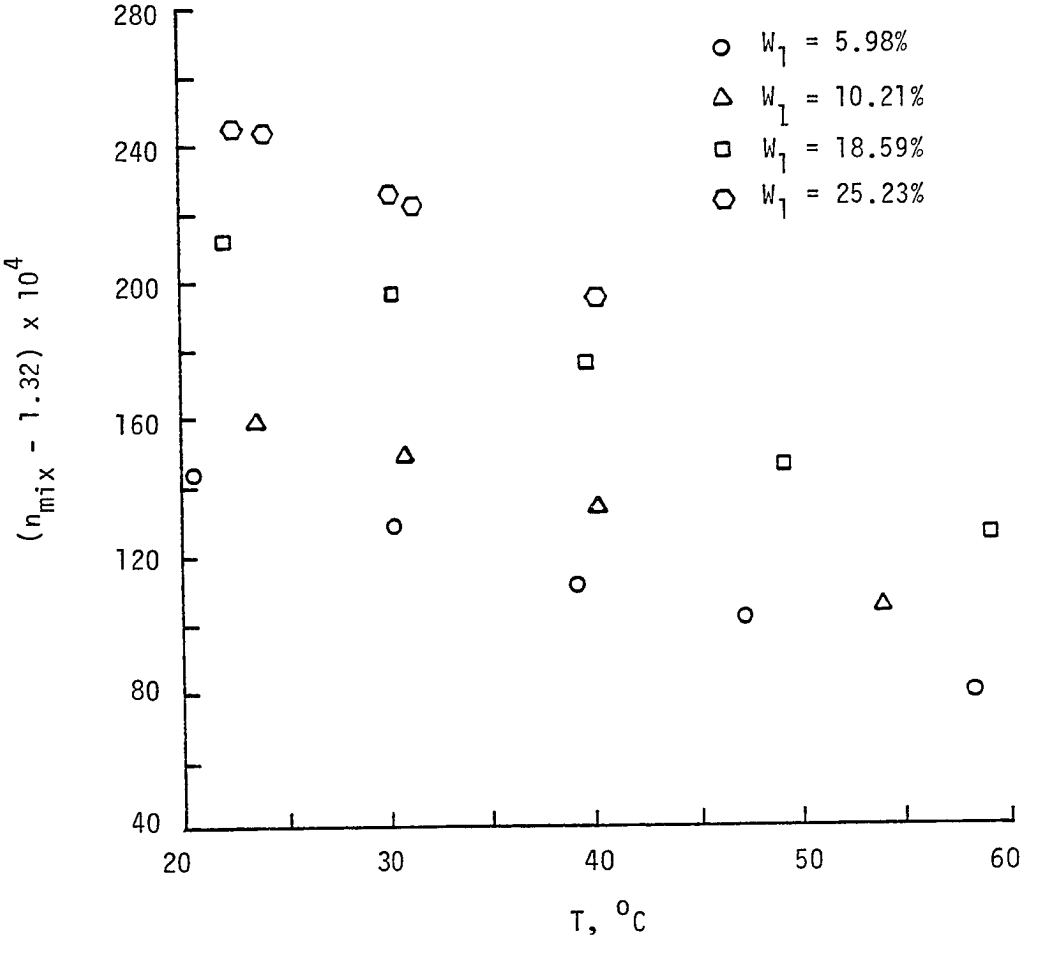

Fig. 5.2 Experimental refractive index data of ammonia-water solutions.

regression model were developed to smoothen the data and to provide a general correlation between the three variables: refractive index, temperature, and concentration.

Among others, the least-square regression model with multiple variables has been employed for this case. Basically, the least-square empirical model can provide the best approximating function that gives minimum value of the sum of the squares of the differences (errors) between the values of the original and the corresponding approximate data. For the sake of simplicity, it is assumed that the refractive index increases quadratically with the concentration. This assumption will be checked later for validation. Hence, the least squares approximation model can be written as

$$n_{mix}(T,W_1) = (B_1T + B_2)\ (B_3W_1^{\,2} + B_4W_1 + B_5) \tag{5.9}$$

or, after performing the multiplication and dropping the subscripts, mix and 1, for convenience, as

$$n(T,W) = C_1W^2T + C_2WT + C_3W^2 + C_4W + C_5T + C_6 \tag{5.10}$$

where C_1, C_2, ..., C_6 are unknown constants to be determined. Let n_i, and $(C_1W_i^{\,2}T_i + C_2W_iT_i + C_3W_i^{\,2} + C_4W_i + C_5T_i + C_6)$ denote the $\underline{i}$th values of the original and the corresponding approximate data respectively. Then, it is required to determine constants C_1, C_2, ..., C_6 which will minimize the error sum, Er, defined as

$$Er = \sum_{i=1}^{k} [n_i - (C_iW_1^{\,2}T_1 + C_2W_iT_1 + C_3W_i^{\,2} + C_4W_i + C_5T_i + C_6)]^2 \tag{5.12}$$

where k (equal to 42) is the number of data points. For a minimum error

to occur at C_1 C_2, ..., C_6 it is necessary for

$$\frac{\partial Er}{\partial C_j} = 0, \text{ for } j = 1, 2, \ldots\ldots, 6 \tag{5.12}$$

or in matrix form

$$\sum_{i=1}^{k} \begin{bmatrix} W_i^4 T_i^2 & W_i^3 T_i^2 & W_i^4 T_i & W_i^3 T & W_i^2 T_i^2 & W_i^2 T_i \\ W_i^3 T_i^2 & W_i^2 T_i^2 & W_i^3 T_i & W_i^2 T & W_i T_i^2 & W_i T_i^2 \\ W_i^4 T_1 & W_i^3 T_i & W_i^4 & W_i^3 & W_i^2 T_i & W_i^2 \\ W_i^3 T_i & W_i^2 T_i & W_i^3 & W_i^2 & W_i T_i & W_i \\ W_i^2 T_i^2 & W_i T_i^2 & W_i^2 T_i & W_i T_i & T_i^2 & T_i \\ W_i^2 T_i & W_i T_i & W_i^2 & W_i & T_i & 1 \end{bmatrix} \begin{bmatrix} C_1 \\ C_2 \\ C_3 \\ C_4 \\ C_5 \\ C_6 \end{bmatrix} = \sum_{i=1}^{k} \begin{bmatrix} W_i^2 T_i n_i \\ W_i T_i n_i \\ W_i^2 n_i \\ W_i n_i \\ T_i n_i \\ n_i \end{bmatrix}$$

This set of simultaneous equations is then solved for C_1, C_2, ..., C_6 using a numerical scheme of Gaussian elimination with maximal column pivoting. The solution to the system of equations is found to be

$$C_1 = -1.20748 \times 10^{-7}$$

$$C_2 = -1.68261 \times 10^{-6}$$

$$C_3 = 3.29814 \times 10^{-6}$$

$$C_4 = 5.45100 \times 10^{-4}$$

$$C_5 = -1.51344 \times 10^{-4}$$

$$C_6 = 1.33454$$

Hence Eq. (5.10) can be rewritten as

$$n(T,W) = -1.20748 \times 10^{-7} W^2 T - 1.68261 \times 10^{-6} WT + 3.29814 \times 10^{-6} W^2 + 5.45100 \times 10^{-4} W - 1.51344 \times 10^{-4} T + 1.33454 \tag{5.13}$$

To check the accuracy of the approximation model, Eq. (5.13) has been used to calculate the approximate refractive indices at the concentrations and temperatures which are identical to those for the experiments. The calculated results are presented in Appendix G together with their absolute discrepancies from the original experimental results. It is found that the approximate data are in agreement, to four significant digits, with the original data. The largest discrepancy is equal to 0.00052, and occurs at a concentration of 18.59% and a temperature of 39.50°C. The average discrepancy is found to be 0.000195. The largest and the average discrepancies as percentages are equal to 0.0388% and 0.0146% respectively. Furthermore, except for five cases, all the discrepancies are within the uncertainty bound of the original experimental data.

5.3 Discussion of Results

The unexpectedly good least-squares model justifies the earlier assumption that the refractive index increases quadratically with concentration. It also enables further use of Eq. (5.13) to obtain the numerical correlations between the refractive index and the temperature and between the refractive index and the concentration. For example:

$$\left.\begin{aligned}
&\text{At } W_1 = \ 2.54\%,\ n_{mix}(T) = 1.335946 - 0.00015640\ T \\
&\text{At } W_1 = \ 5.98\%,\ n_{mix}(T) = 1.337918 - 0.00016572\ T \\
&\text{At } W_1 = \ 7.59\%,\ n_{mix}(T) = 1.338867 - 0.00017107\ T \\
&\text{At } W_1 = 10.21\%,\ n_{mix}(T) = 1.340449 - 0.00018111\ T \\
&\text{At } W_1 = 14.41\%,\ n_{mix}(T) = 1.343080 - 0.00020066\ T \\
&\text{At } W_1 = 18.59\%,\ n_{mix}(T) = 1.345813 - 0.00022435\ T \\
&\text{At } W_1 = 20.99\%,\ n_{mix}(T) = 1.347435 - 0.00023986\ T
\end{aligned}\right| \qquad (5.14)$$

$$\left.\begin{aligned} &\text{At } W_1 = 25.23\%,\ n_{mix}\ (T) = 1.350392 - 0.00027066\ T \\ &\text{At } W_1 = 27.68\%,\ n_{mix}\ (T) = 1.352155 - 0.00029043\ T \end{aligned}\right]$$

and

$$\left.\begin{aligned} \text{At } T = 20°C,\ n_{mix}(W_1) &= 1.331513 + 5.114475 \times 10^{-4}\ W_1 + \\ &\quad 0.883182 \times 10^{-6}\ W_1^2 \\ \text{At } T = 30°C,\ n_{mix}(W_1) &= 1.330000 + 4.946214 \times 10^{-4}\ W_1 - \\ &\quad 0.324295 \times 10^{-6}\ W_1^2 \\ \text{At } T = 40°C,\ n_{mix}(W_1) &= 1.328486 + 4.777953 \times 10^{-4}\ W_1 - \\ &\quad 0.531772 \times 10^{-6}\ W_1^2 \\ \text{At } T = 50°C,\ n_{mix}(W_1) &= 1.326973 + 4.609693 \times 10^{-4}\ W_1 + \\ &\quad 2.739249 \times 10^{-6}\ W_1^2 \\ \text{At } T = 60°C,\ n_{mix}(W_1) &= 1.325459 + 4.441432 \times 10^{-4}\ W_1 + \\ &\quad 3.946726 \times 10^{-6}\ W_1^2 \end{aligned}\right] \quad (5.15)$$

Those correlations are then employed to calculate the refractive index for various concentrations and temperatures. The results are shown graphically in Figs. 5.3 to 5.5. The first two figures present the effect of temperature on the refractive index. Concentrations in these two figures are arranged similar to those of Figs. 5.1 and 5.2. In Fig. 5.5 the refractive index is plotted as a function of concentration for the temperature range of 20 to 60°C.

The decreasing variation of the refractive index with respect to the temperature, shown in Figs. 5.3 and 5.4, confirms the expected general behavior of refractive index of most liquids as described in the introductory chapter. It is also observed in Eq. (5.14) that the temperature coefficients of the refractive index, $\frac{\partial n_{mix}}{\partial T}$, decrease from -1.564×10^{-4} to -2.904×10^{-4} as the concentration increases from

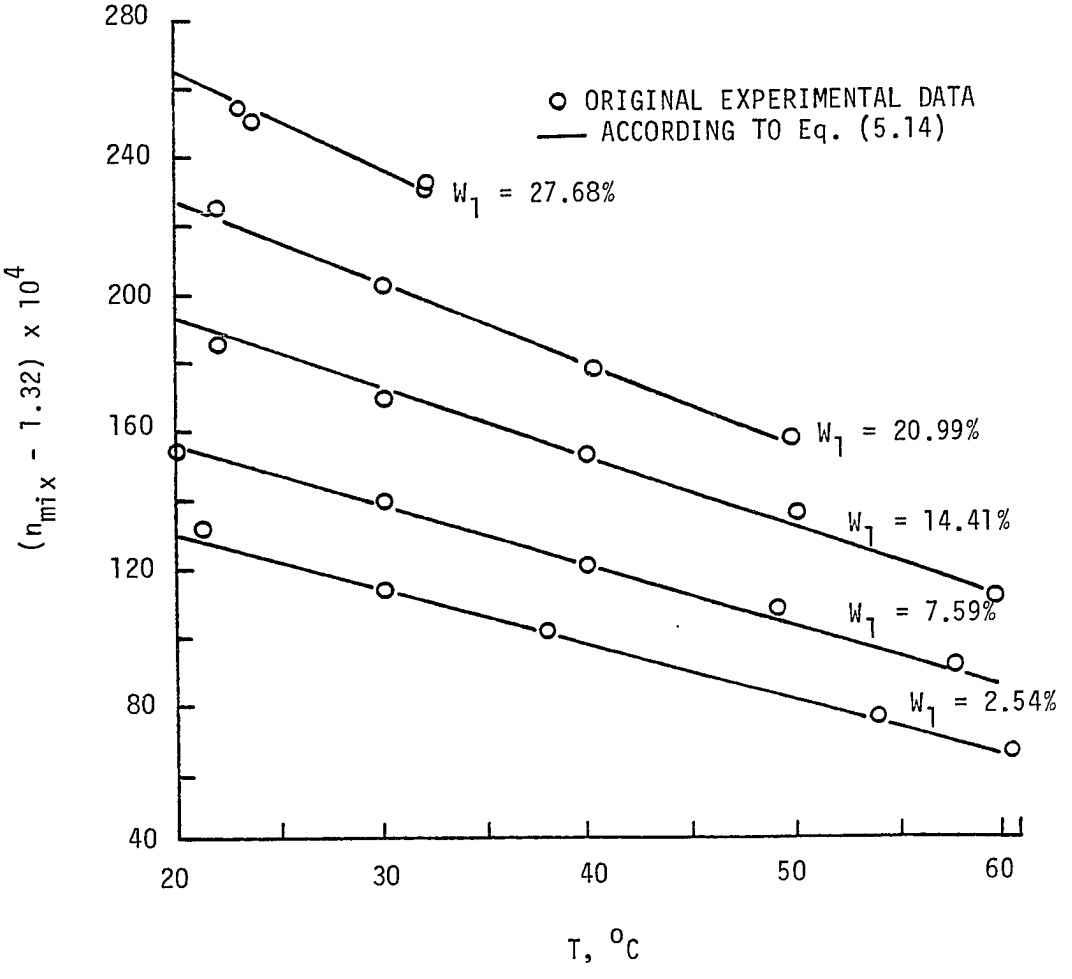

Fig. 5.3 Refractive index versus temperature.

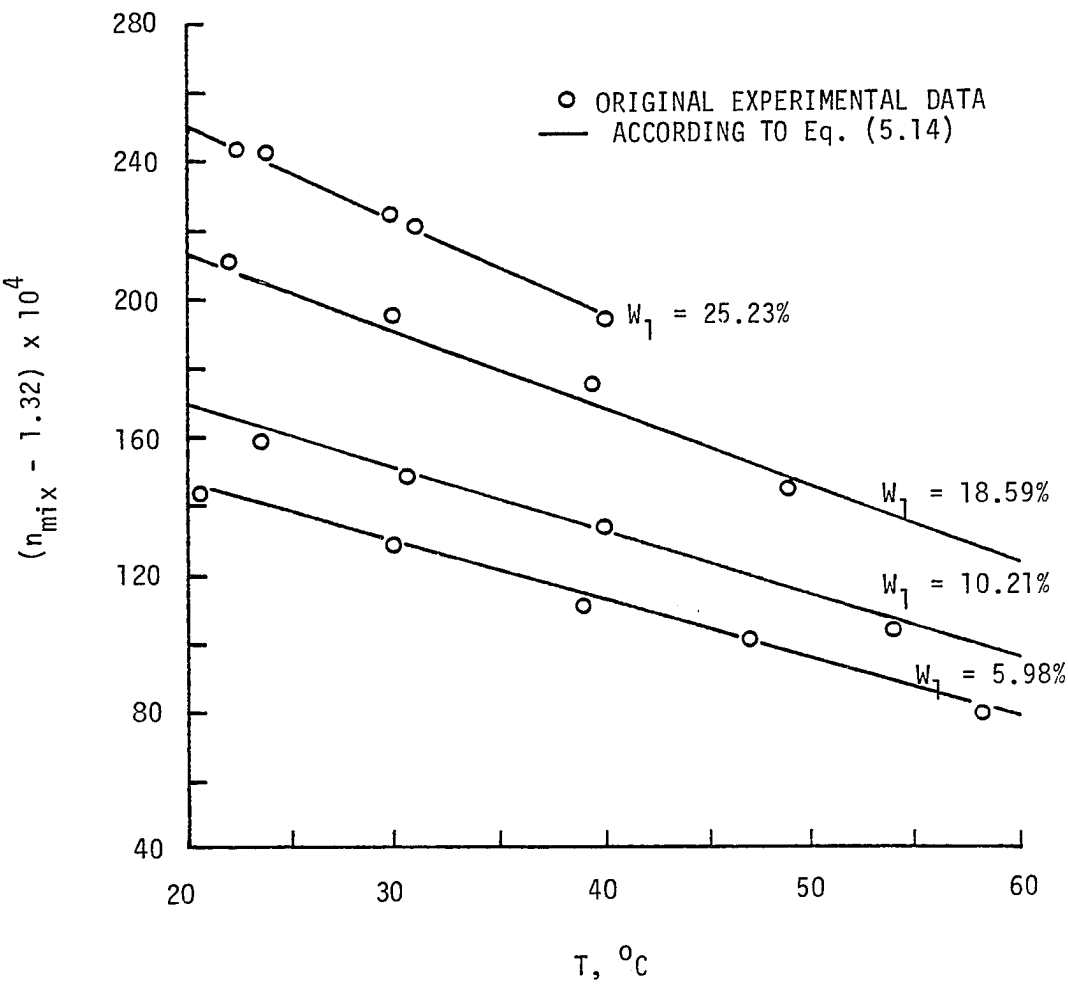

Fig. 5.4 Refractive index versus temperature.

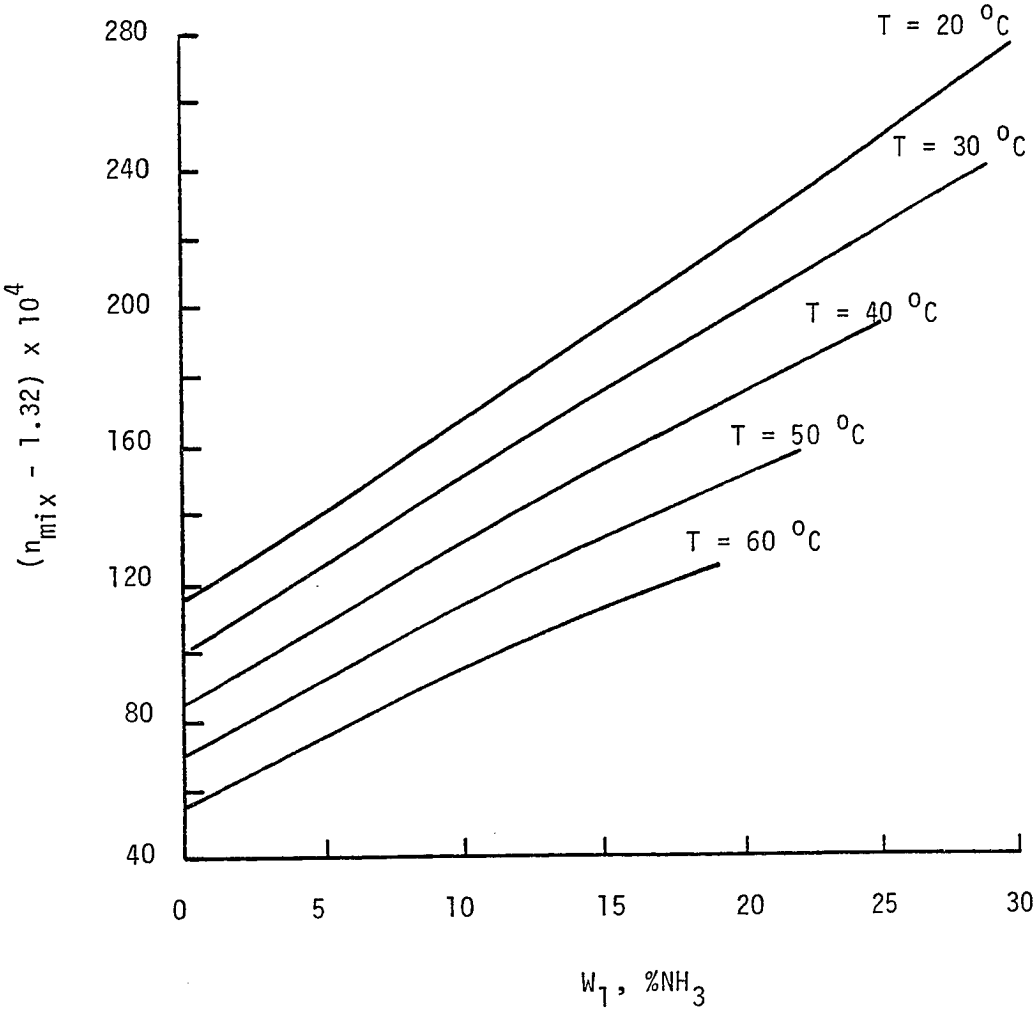

Fig. 5.5 Refractive index versus concentration.

2.54 to 27.68%. Numerous published data concerning the temperature coefficients for other liquids have reported a value as low as -4×10^{-4} [18]. Water at room temperature, as an exception, probably has the highest average temperature coefficient of -1.0×10^{-4}. Introducing ammonia in water generally shifts the property values of the solution away from those of pure water. Apparently, the presence of ammonia in water makes the temperature coefficient of the solution decrease from the highest value possessed by water. Further observation of Eq. (5.14) reveals that this coefficient does not decrease linearly with the concentration.

Equation (5.15) and Fig. 5.5 indicate that the effect of the quadratic concentration term on the refractive index is insignificant near temperatures of 30°C. This term, however, becomes more important as the temperature is increased. As for the increasing refractive index with concentration, this behavior is consistent with the previous experimental results of Ref. 17. The theoretical explanation for this behavior involves much of the molecular refractivities of the solution and its constituents (ammonia and water in this case). As will be discussed in the next chapter, ammonia has higher molecular refractivities than water. Thus, even without knowing the actual mixing rule of ammonia and water, it can be expected to a certain extent that the molecular refractivity and the refractive index of the solutions increases with ammonia concentration.

In conclusion the approximation model of Eq. (5.13) can represent the refractive index of ammonia-water solutions reasonably well--at least in the ranges of concentration and temperature considered here.

Chapter 6

SEMI-EMPIRICAL PREDICTION

6.1 Introduction

A theoretical prediction of the refractive index of a substance at various temperatures and pressures has two main purposes: To provide comparison data for experimental results and to reduce the number of required experiments.

The decision to employ the Lorentz-Lorenz equation in the theoretical part of this work has been discussed in the introductory chapter. The molecular refractivity of the solution/mixture is calculated based upon the molecular refractivities of its pure components (ammonia vapor and water in this case) and the simple additive rule of mixtures.

This chapter consists of five sections. Following this introduction the Lorentz-Lorenz equation and molecular refractivities of ammonia vapor and water are discussed. Section 6.3 deals with molecular refractivities of ammonia-water solutions and the required parameters, followed by a presentation of the predicted results and comparison with the existing experimental data in Sec. 6.4. This section also includes the correction function of the additive rule and the calculated results which incorporate this correction function. In the final section the theoretical results are compared with the experimentally obtained data of Chap. 5.

6.2 Molecular Refractivities of Ammonia Vapor and Water

According to the Lorentz-Lorenz equation the molecular refractivity, A, of a pure substance can be expressed as:

$$A = A(\lambda) = \frac{M}{\rho}\frac{n^2-1}{n^2+2} \tag{6.1}$$

or

$$A = \frac{1}{d_m}\frac{n^2-1}{n^2+2} \tag{6.2}$$

where $d_m = \rho/M$ is the molecular density that can be evaluated using the virial expansion:

$$d_m(T,P) = [RT/P + B(T) + \text{-------}]^{-1} \tag{6.3}$$

where R is the gas constant and B(T) is the second virial coefficient. Therefore depending on the available data (density or virial expansion data) the molecular refractivity can be evaluated from either of two different approaches. However, density data are preferable since they yield more accurate results.

6.2.1 Molecular Refractivity of Ammonia Vapor (A_1)

There are a number of molecular refractivity values of ammonia vapor (M_1 = 17.03) that have been reported in the literature [24-26]. However, these values are in poor agreement with each other due to the different values of density and refractive index data employed in each calculation.

Beaume's data [24] were calculated at T = 25°C, P = 0.988 atm, ρ = 0.0006353 gm/cc (vapor phase), and n_1 = 1.000335 for the sodium-D light (λ = 589.3 nm). As for the Helium-Neon laser light (λ = 632.8 nm) n_1 is equal to 1.000334. The corresponding molecular

refractivities were: A_1 = 5.4990 and 5.4716 for the sodium-D light and the Helium-Neon laser light respectively.

Based on the reported refractive index data or Frivold [25] (at 20°C, 1 atm, ρ = 0.0007067 gm/cc) the molecular refractivities of ammonia vapor were calculated to be:

A_1 = 6.0353 for n_1 = 1.0003757 (λ = 589.3 nm)

A_1 = 6.0129 for n_1 = 1.0003743 (λ = 632.8 nm)

And from the dispersion graphs or Zeiss [26] the values of A_1 were observed as:

A_1 = 5.61 for λ = 632.8 nm

A_1 = 5.58 for λ = 632.8 nm

Apparently the molecular refractivity of ammonia vapor ranges from 5.4990 to 6.0353 for λ = 589.3 nm, and from 5.4716 to 6.0129 for λ = 632.8 nm. At present, no attempt has been made to determine the optimal values of these molecular refractivities. Such an attempt will be discussed later in Sec. 6.4. The boiling point of ammonia at atmospheric pressure is -33.35°C [19], therefore, ammonia liquid does not exist in the range of temperature considered here. Consequently, molecular refractivity of ammonia liquid will not be discussed in this investigation.

6.2.2 Molecular Refractivity of Water

The molecular refractivities of water (M_2 = 18.02) were calculated at atmospheric pressure and over the temperature interval from 20 to 60°C. The density and refractive index data employed in this calculation were obtained from the ASME Steam Tables [27] and from the

NBS Research Paper No. 1085 [23]. These two references are considered the most accurate and reliable sources for these data. The density and refractive index data from these sources have been incorporated in Tables 6.1 and 6.2 at the end of this section.

In both tables it is observed that the molecular refractivities of water, A_2, are not totally independent of the temperature. It is not a surprising fact as mentioned earlier in Chap. 1, that at present there is no function available that relates density and refractive index which at the same time is absolutely independent of the temperature and the pressure. The most logical value of A_2 to be employed hereafter is the average value of A_2, which is:

$$A_2 = 3.7115 \qquad \text{for} \quad \lambda = 589.3 \text{ nm}$$

$$A_2 = 3.699 \qquad \text{for} \quad \lambda = 632.8 \text{ nm}$$

To examine the accuracy of these values in predicting the refractive index of water, calculations were performed using the Lorentz-Lorenz equation:

$$n_2(\text{cal.}) = \left[\frac{1 + 2\,A_2\rho_2/M_2}{1 - A_2\rho_2/M_2}\right]^{1/2} \tag{6.4}$$

The calculation results, together with their deviations from the original data, εn_2, are presented on Tables 6.1 and 6.2 for λ = 589.3 nm and for λ = 632.8 nm respectively. These deviations were considered small enough to allow the use of the average values of A_2 in the calculation of the molecular refractivities of the ammonia-water solution.

Table 6.1 Molecular refractivity of water for λ = 589.3 nm

T,°C	ρ,gm/cc	n_2(data)	A_2,cc/gmol	n_2(cal.)	$\varepsilon n_2 x 10^{-5}$
20	0.9983	1.33299	3.7128	1.33286	- 13
25	0.9972	1.33251	3.7121	1.33245	- 6
30	0.9957	1.33194	3.7119	1.33190	- 4
35	0.9940	1.33131	3.7118	1.33128	- 3
40	0.9923	1.33061	3.7110	1.33065	4
45	0.9901	1.32985	3.7115	1.32985	0
50	0.9882	1.32904	3.7104	1.32915	11
55	0.9855	1.32817	3.7116	1.32816	- 1
60	0.9833	1.32725	3.7104	1.32736	11

Table 6.2 Molecular refractivity of water for λ = 632.8 nm

T,°C	ρ,gm/cc	n_2(data)	A_2,cc/gmol	n_2(cal.)	$\varepsilon n_2 x 10^{-5}$
20	0.9983	1.33174	3.7002	1.33162	- 12
25	0.9972	1.33126	3.6944	1.33122	- 4
30	0.9957	1.33071	3.6994	1.33067	- 4
35	0.9940	1.33008	3.6993	1.33005	- 3
40	0.9923	1.32938	3.6985	1.32943	5
45	0.9901	1.32863	3.6990	1.32863	0
50	0.9862	1.32782	3.6978	1.32793	11
55	0.9855	1.32696	3.6991	1.32695	- 1
60	0.9833	1.32604	3.6979	1.32615	11

6.3 Molecular Refractivities of Ammonia-Water Solution

For a simple mixture of two substances, the properties of the solution can be calculated by means of the so-called additive rule.

$$k\ (Q_1 + Q_2) = k_1 Q_1 + k_2 Q_2$$

where k is the value of the property or the solution, k_1 and k_2 its values for the pure constituents, and Q_1 and Q_2 the quantities of the

constituents present in the mixture. These quantities may be expressed as mass, volume, or molecular quantities, and the correct method of representation will depend on the property under investigation. For the molecular refractivity, it is customary to represent these quantities in terms of molecular density N (number of molecules per unit volume of mixture). Thus, if two substances with molecular refractivities A_1 and A_2 are mixed, and in a unit volume of mixture there are N_1 molecules of the first substance and N_2 molecules of the second substance, then the molecular refractivity of the mixture can be calculated as:

$$A_{mix} = \frac{N_1 A_1 + N_2 A_2}{N_1 + N_2} \tag{6.5}$$

The additive rule has been used to determine the molecular refractivity of mixtures of water and sulphuric acid [28] which have similar properties and complexity due to mixing as mixtures of ammonia and water. The predicted results were found to be in reasonably good agreement with the experimental data.

Ammonia-water solutions are certainly not simple mixtures. However, the two constituents have similar chemical structures and their molecular weights are nearly equal. These similarities were the basis for using the simple additive rule in this work and it will be shown later that the results are also in reasonably good agreement with existing experimental data.

Let subscripts 1, 2, and mix denote ammonia vapor, water, and the ammonia-water solution. Then the relation between A_{mix} and n_{mix} according to the Lorentz-Lorenz equation can be expressed as:

$$A_{mix} = \frac{M_{mix}}{\rho_{mix}} \frac{n_{mix}^2 - 1}{n_{mix}^2 + 2} \tag{6.6}$$

$$n_{mix} = \left[\frac{1 + 2\, A_{mix}\rho_{mix}/M_{mix}}{1 - A_{mix}\rho_{mix}/M_{mix}} \right]^{1/2} \tag{6.7}$$

In order to evaluate Eqs. (6.6) and (6.7) the following are the required parameters: molecular density N, mixture molecular weight M_{mix}, and mixture density ρ_{mix}.

6.3.1 Molecular Densities N_1 and N_2

These quantities are related to the ammonia concentrations as:

$$\left.\begin{aligned} N_1 &= N_A\, \rho_{mix}\, W_1/M_1 \\ N_2 &= N_A\, \rho_{mix}\, W_2/M_2 \\ W_2 &= 1 - W_1 \end{aligned}\right] \tag{6.8}$$

where W_1 is the weight (mass) fraction of the ammonia in the mixture, N_A is the Avogrado's number and ρ_{mix} is the density of the mixture.

6.3.2 Molecular Weight of the Mixtures

The molecular weights of the mixtures are calculated according to a formula proposed by Bird, Stewart, and Lightfoot [29] as:

$$M_{mix} = \frac{M_1 M_2}{W_1 M_2 + W_2 M_1} \tag{6.9}$$

6.3.3 Density of the Mixture

Density of the mixture is calculated according to a method proposed by Schultz [4]. This method was intended for computer calculations of ammonia-water solution properties such as: specific volume, internal energy, enthalpy, and others. The only input data required are the ammonia concentration, temperature, and pressure. This computer scheme has the distinct advantage of being able to provide density data for

wider ranges of temperature and pressure; while most of the other published data are only available for room temperature and atmospheric pressure. However, the use of these combined input data should take into account the limit of ammonia vapor solubility into water [19]. The subroutine DENSI written for the density calculation is presented in Appendix G.

To evaluate the accuracy of this method, the densities of the solutions were calculated at 1 atm, 20°C, and at various concentrations. The results are presented in Table 6.3 together with the available experimental data [21,22]. It is observed that most of the calculated densities lie between the two data sets.

Table 6.3 Density of ammonia-water solutions

W_1,%	Expt. Data [21]	Expt. Data [22]	Calc. Data	Deviation, %, from [21]	[22]
5	0.9771	0.9804	0.9780	0.092	-0.245
10	0.9575	0.9615	0.9570	-0.052	-0.468
15	0.9396	0.9452	0.9396	0.000	-0.592
20	0.9229	0.9285	0.9245	0.173	-0.430
25	0.9071	0.9124	0.9111	0.440	-0.142
30	0.8920	0.8945	0.8985	0.729	0.447

6.4 Calculated Refractive Indices

It was found in Sec. 6.2 that the values of the molecular refractivities of ammonia vapor were between 5.4990 and 6.0353 for λ = 589.3 nm and between 5.4716 and 6.0129 for λ = 632.8 nm. Therefore

initial efforts have been focused on determining the appropriate values of these refractivities.

As noted earlier in Chap. 1 refractive index data were available for the sodium-D light at 20°C and one atmosphere for various concentrations up to 30% by weight of ammonia [17]. These data were used to compare the refractive indices calculated using Eq. (6.7). In this calculation the value of A_1 was varied from 5.48 to 5.59 (for λ= 589.3 nm) with an increment of 0.01. The value of A_1 that produced the smallest average discrepancy in the calculation would then be chosen as the appropriate value to be used in this semi-empirical investigation. The average discrepancy was calculated as:

$$\varepsilon_{AV} = \frac{1}{k} \sum_{i=1}^{k} ABS\ (n_{data_i} - n_{calc._i}) \qquad (6.10)$$

where k is the number of data included in the calculation. The average discrepancies and the corresponding values of A_1 are presented in Table 6.4.

The desired value of A_1 (which was still within the prescribed range) was selected because it is very close to the value proposed by Beaume (see Sec. 6.2). The program listing of the refractive indices calculation and the output for A_1 = 5.50 are presented in Appendix H.

Having selected the value of A_1 for λ = 589.3 nm, it was then necessary to select a value for λ = 632.8 nm. In this case the previous approach could not be used due to the lack of experimental data required for comparison purposes. It was concluded that A_1 should be set equal to 5.47 which was also the closest value to that proposed by Beaume. The reason was obvious: If Beaume's datum for λ = 589.3 nm produced estimations which were very close to the accepted data, then it should also follow for λ = 632.8 nm.

Table 6.4 A_1 and the corresponding discrepancy ε_{AV}

A_1	ε_{AV}
5.48	0.055
5.49	0.058
5.50	0.062
5.51	0.067
5.52	0.074
5.53	0.081
5.54	0.089
5.55	0.100
5.56	0.111
5.57	0.122
5.58	0.133
5.59	0.144

The index of refraction calculations were performed subsequently [using Eq. (6.7)] at pressure of one atmosphere, over the temperature range from 20 to 60°C, and at the concentrations up to 30% with the upper limit (at a given temperature) depending on the solubility limit of ammonia in water. Calculations at other pressures and/or at other temperatures can be done by merely changing the temperature and pressure input data for the computer program. This program is similar to the one presented in Appendix H.

The entire calculation was divided into two groups according to the wavelength and the molecular refractivity of ammonia vapor:

Group 1: for λ= 589.3 nm A_1 = 5.50 A_2 = 3.7115

Group 2: for λ= 632.8 nm A_1 = 5.47 A_2 = 3.699

The tabulated results are presented in Appendix I for the two groups. At this point, the existing experimental data from Ref. 17 (λ = 589.3 nm, T = 20°C, and P = 1 atm) was employed to check the calculated results. Comparison of these experimental data with the

calculated results at the same ρ, T, and P revealed that very good agreement between the two occurred for the solutions with ammonia concentrations between 5 and 20%. Outside this range the deviations became more significant--both above and below the concentration interval. However, the maximum deviation of 0.17% for the solution with 30% concentration can still be considered fair. These deviations are attributable to the imperfection of the additive rule.

Consequently, a corrective measure was desired in order to improve this mixing rule, as well as to minimize these deviations. The idea was to develop a correction function, F, which was a function of concentration only, to correct the molecular refractivity of the solutions. This function was related to the molecular refractivities (which were also concentration dependent) as

$$A_{mix}\ (\text{corrected}) = F(W_1)\ A_{mix}\ (\text{additive rule}) \tag{6.11}$$

The function $F(W_1)$ was obtained by curve-fitting the ratios of A_{mix} (data) and A_{mix} (additive rule). According to the Lorentz-Lorenz equation, A_{mix} (data) can be written as:

$$A_{mix}\ (\text{data}) = \frac{M_{mix}}{\rho_{mix}} \frac{n_{data}^2 - 1}{n_{data}^2 + 2} \tag{6.12}$$

and A_{mix} (additive rule) was calculated according to Eq.(6.5). The curve-fitting process was done by utilizing standard regression analysis programs (IMSL subroutines RLFOTH and RLDOPM). The program listing and the output are presented in Appendix J. For a fifth degree polynomial model the optimum correction function was:

$$F(W_1) = 0.9950372 + 0.1165953\ W_1 - 0.5882163\ W_1^2 + 0.08025509\ W_1^3 + 3.098517\ W_1^4 - 4.326903\ W_1^5$$

A higher order model was not required since the A_{mix} (corrected) with the present correction function model and the A_{mix} (data) are in agreement to four significant digits (see Appendices J and K).

Incorporating the correction function in the molecular refractivities of the mixtures, the refractive indices can be calculated using the following formula:

$$\frac{M_{mix}}{\rho_{mix}} \frac{n_{mix}^2 - 1}{n_{mix}^2 + 2} = \frac{N_1 A_1 + N_2 A_2}{N_1 + N_2} F(W_1) \qquad (6.14)$$

Calculations have been performed for the two groups mentioned earlier. The tabulated results are presented in Appendix K. These results, together with the uncorrected results of Appendix I, are shown graphically in Figs. 6.1 to 6.4. The first two figures are for sodium-D light and the rest are for the helium-neon laser light (λ = 632.8 nm).

The corrected refractive index data obtained using the corrected molecular refractivities are larger than the uncorrected refractive index data for the cases with medium concentrations (6% < W_1 < 16%), however, outside this range of concentration the corrected data were smaller than the uncorrected ones. This behavior was consistent with the deviation characteristic between the available experimental data [17] and the corresponding calculated data at 20°C for λ = 589.3 nm. Overall comparison of the figures reveals that the results of the first group (λ = 589.3 nm) are respectively larger than those of the second group (λ = 632.8 nm). This characteristic is consistent with the general refractive index behavior of all other substances that refractive index decreases with increasing wavelength, λ. It is also observed that the refractive index increases with the concentration and

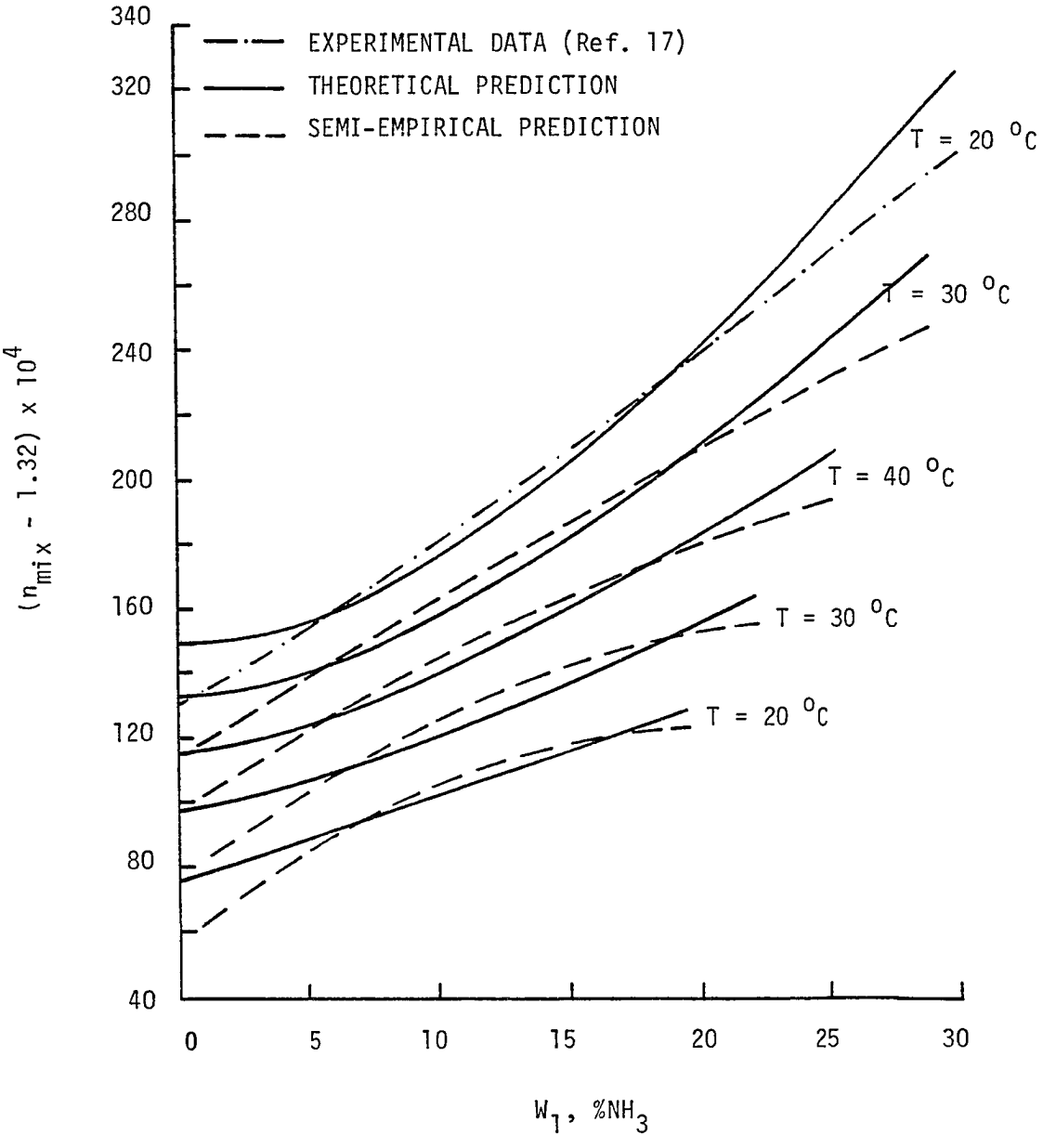

Fig. 6.1 Refractive index versus concentration (λ = 589.3 nm, A_1 = 5.50, A_2 = 3.7115).

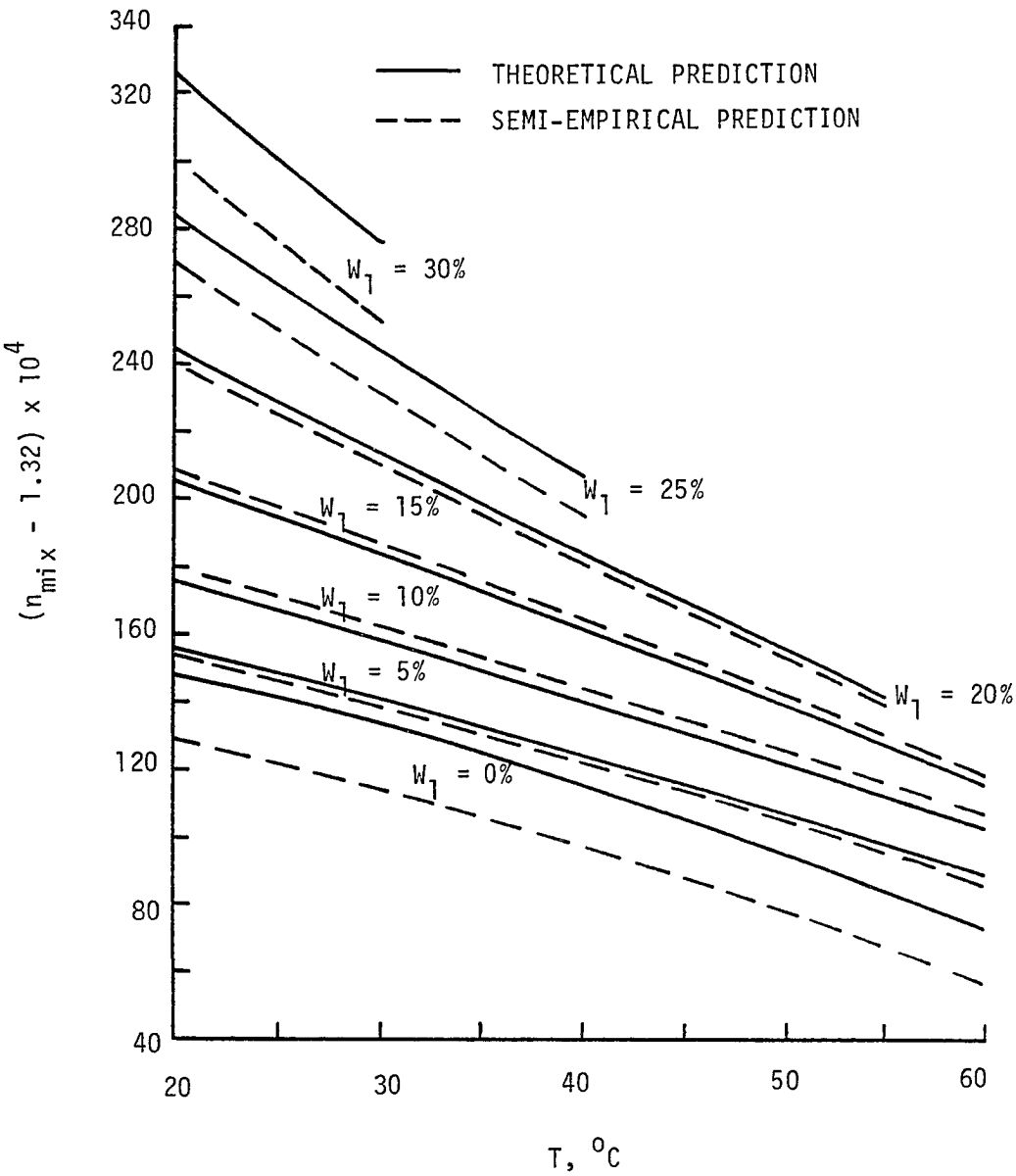

Fig. 6.2 Refractive index versus temperature (λ = 589.3 nm, A_1 = 5.50, A_2 = 3.7115)

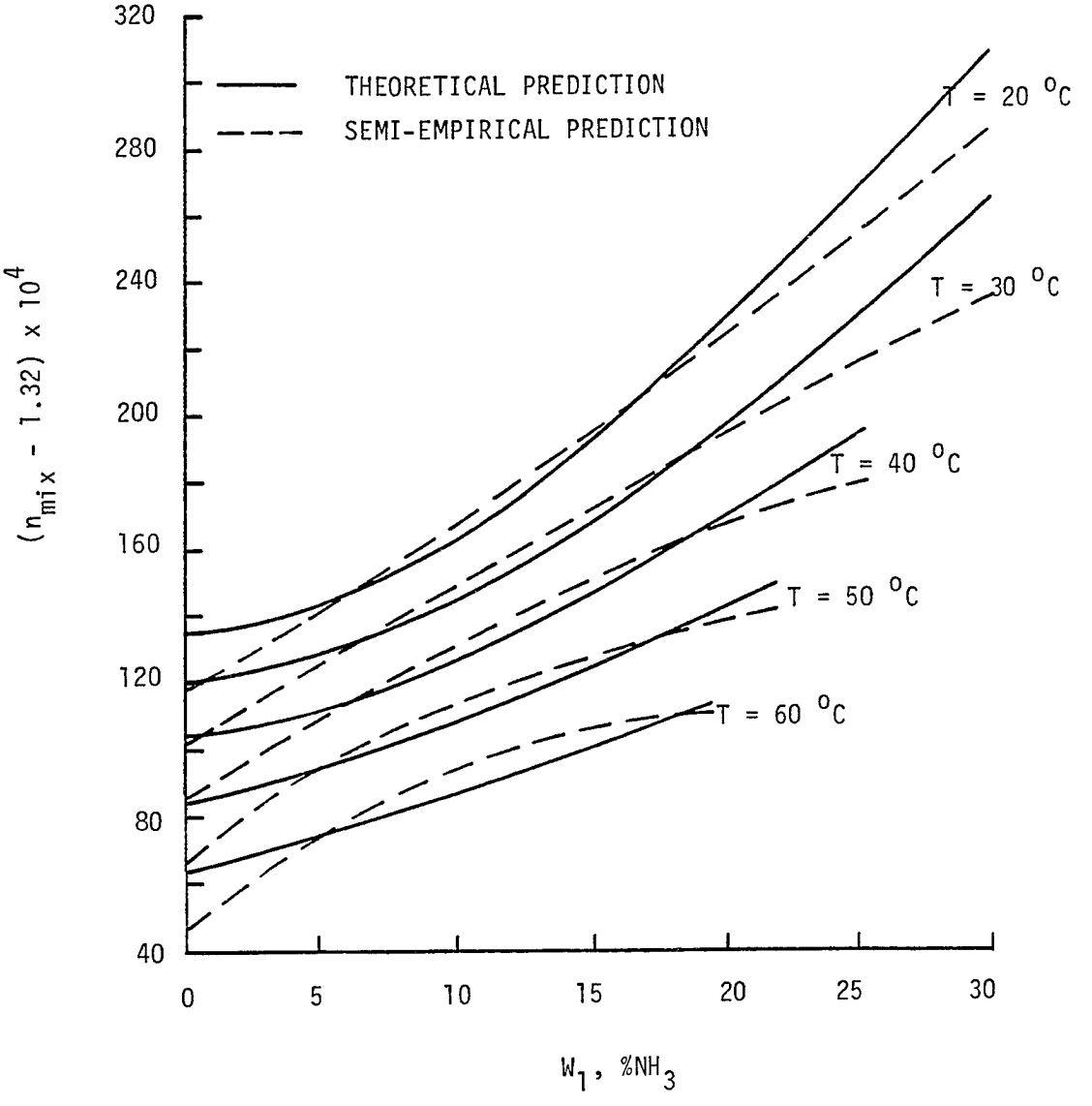

Fig. 6.3 Refractive index versus concentration (λ = 632.8 nm, A_1 = 5.47, A_2 = 3.699).

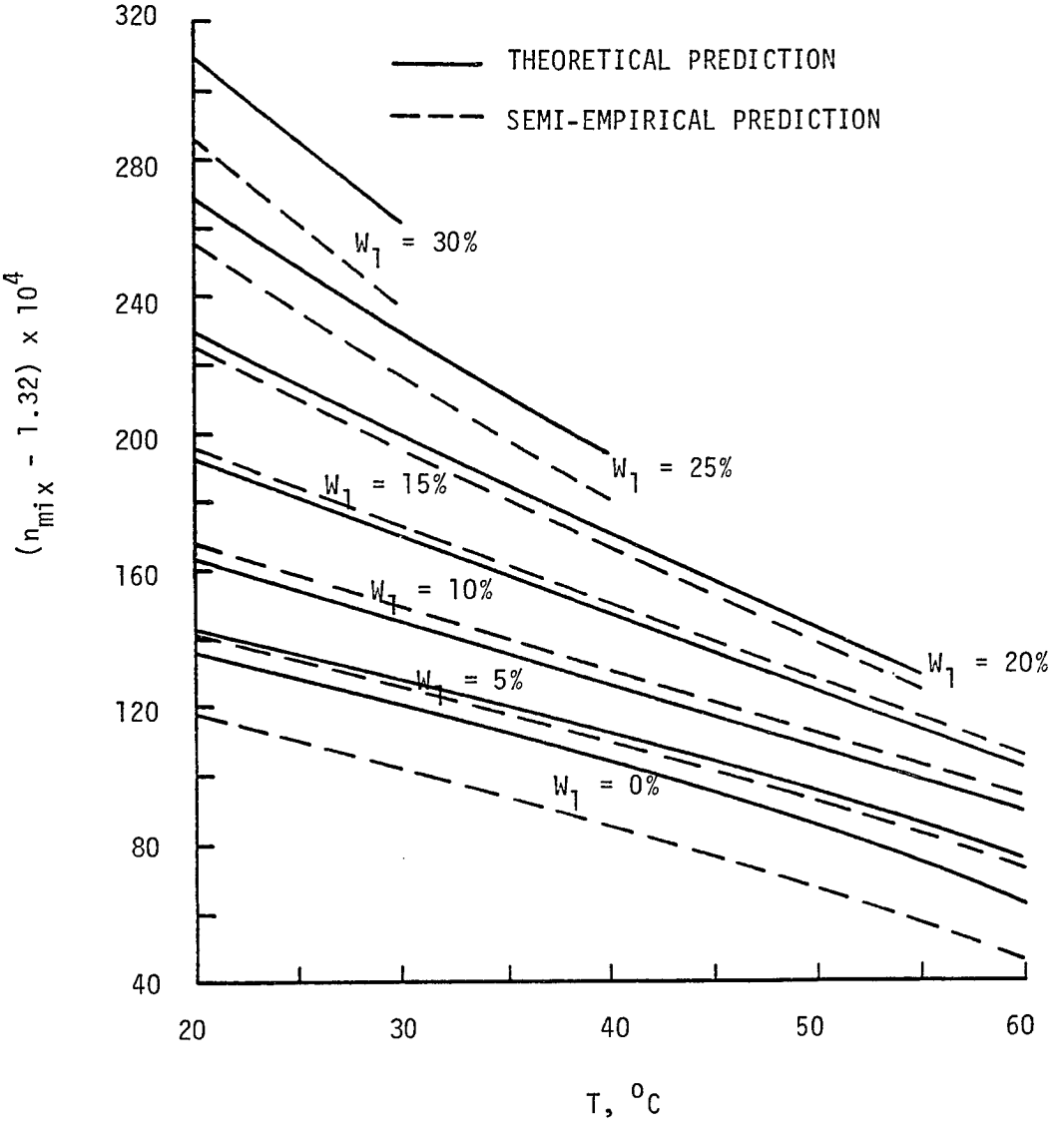

Fig. 6.4 Refractive index versus temperature (λ = 632.8 nm, A_1 = 5.47, A_2 = 3.699).

decreases with the temperature. Theoretical explanations for this behavior have been discussed in the previous chapter. Furthermore, the qualitative variations of the refractive index with respect to the concentration, for all considered temperatures, are very much alike for the two groups. The same trend applies to the decreasing variations of the refractive index with respect to the temperature for all considered concentrations.

6.5 Comparison with the Experimental Results

The semi-empirical prediction results (for λ = 632.8 nm) are compared with the current experimental results in two ways: direct and indirect. For direct comparison the experimental data are directly compared to the prediction results which have been calculated at the same temperatures and concentrations as those used in the experiment. This comparison is shown in Appendix L which presents two sets of data: experimental data and semi-empirical prediction data calculated according to Eq. 6.14. It also includes discrepancies of the prediction data from the experimental data, εn_{pred}. For the cases with concentrations up to 14.41%, it is observed that the discrepancies are small. Most of the εn_{pred} are within the uncertainty bound of the experimental data of 4.0×10^{-4}. The arithmetic mean of the absolute discrepancies in this range of concentrations ($\leq$14.41%) is calculated to be 2.63×10^{-4}. For the higher concentrations ($\geq$18.59%), the discrepancies are generally higher and there are several cases where the discrepancies are about three times the uncertainty bound. The overall arithmetic means are found to be 4.40×10^{-4}.

Despite the large discrepancies for a few cases, overall direct

comparison has proven that the results of the semi-empirical prediction adequately matched the original experimental data.

For indirect comparison, the semi-empirical results are compared to the empirically calculated refractive index over a temperature range of 20 to 60°C and a concentration range of 0 to 30%. Theses calculations have been performed in Chap. 5 and earlier in this chapter. The calculated results have also been shown in Figs. 5.3 - 5.5 and in Figs. 6.2 and 6.3. The indirect comparison is performed graphically by superimposing Fig. 5.5 and the semi-empirical part of Fig. 6.3 as shown in Fig. 6.5. In general Fig. 6.5 confirms the finding of the earlier comparison that the discrepancies are small for the cases with concentrations under 15% and they become more significant for the higher concentrations. In addition, the significant discrepancies for the higher concentration cases are more pronounced as the temperature increases. However, overall observation of Fig. 6.5 indicates that the semi-empirical results are in reasonably good agreement with empirical results which have been obtained by curve-fitting the experimental data.

Essentially, application of the semi-empirical prediction to obtain refractive index of ammonia-water solutions can be extended beyond the ranges that have been covered by the experimental investigation. It is especially promising for the cases with low concentrations (under 15%) with pressures much different from atmospheric pressure.

Some efforts have also been made to investigate whether there are some connections between the terms of the equations used in the empirical calculation, Eq. (5.13), and in the semi-empirical calculation, Eq. (6.14). Among other efforts, all terms of Eq. (6.14)

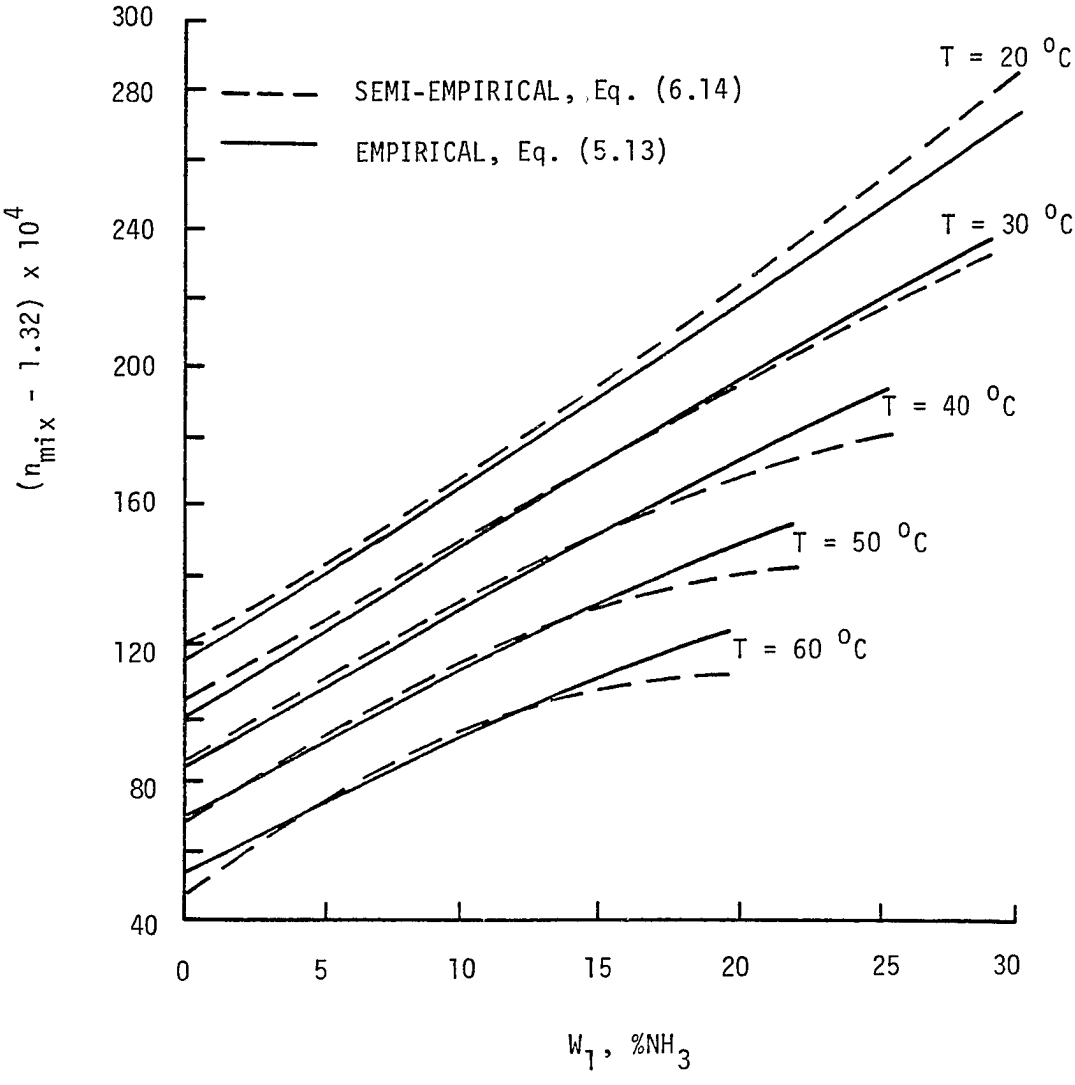

Fig. 6.5 Refractive index versus concentration.

have been converted in terms of temperature and concentration. It was hoped that the modified equation turned out to be very complicated to analyze. It is unfortunate that this effort, as well as many other efforts, has failed to accomplish such a challenging goal.

In concluding this chapter it is important to present the probable reasons that may cause the discrepancies between the semi-empirical and the experimental data, they are as follows:

1. The Lorentz-Lorenz equation used in the prediction is not prefectly valid for both ammonia vapor and water.
2. The additive rule (even with a correction function) employed in the molecular refractivity of the solutions is not exactly equivalent to the actual mixing rule or ammonia and water.
3. The uncertainties (errors) of the empirically calculated density of the solutions are unaccounted in the prediction.
4. The uncertainties (errors) of the current experimental results certainly contributes to the overall discrepancies.

Chapter 7

CONCLUSIONS

The refractive index of ammonia-water solutions at various concentrations and temperatures has been investigated. The investigation has been carried out experimentally as well as theoretically at atmospheric pressure, in the concentration range up to 30%, and in the temperature range of 20 to 60°C. Two light sources have been considered in the theoretical part: Sodium-D light and Helium-Neon laser light. However, only laser light has been employed in the experimental part.

A simple refractometer has been designed and built to perform the experimental measurements which can be categorized as an absolute method of refractive index measurement. The refractive index was deduced from measurement of light beam displacement, due to refraction in the test chamber of the refractometer, by the sample ammonia-water solution. Each test sample solution was prepared in the test chamber prior to each measurement. Nine different concentrations were tested to produce a total of 42 data points. Based on those data, an empirical correlation has been developed to correlate the refractive index with the concentration, and the temperature. Most of the discrepancies between the original refractive index data and the empirically calculated refractive index are within the uncertainty bound of the experimental data. This enabled the utilization of the empirical correlation to

estimate the refractive index continuously over the experimental interval. It was found that the experimentally obtained refractive index decreased linearly with temperature and increased quadratically with concentration.

A theoretical approach has been formulated based on the classical Lorentz-Lorenz equation and the additive rule of mixtures. To improve the additive rule and the results, it was found necessary to include a correction function that was obtained by employing experimental data of another investigator. The semi-empirical results thus obtained were in good agreement with the theoretical results over the concentration range of 5 to 20%.

The possibility of extending the application of the theoretical investigation has been examined by comparing the semi-empirical results with the experimental results. Both the experimentally and the empirically obtained refractive indices were qualitatively consistent with the general behavior of refractive index of liquids, i.e: they decreased with increases in either temperature or wavelength of the light. The results indicated that the refractive index of ammonia-water solutions increased with the ammonia concentration in the ranges investigated. It was observed that the two sets of results were in good agreement for the cases with concentrations up to 15% and most of the discrepancies were within the uncertainty bound of the experimental data. Therefore, extended application of the semi-empirical techniques is recommended primarily to obtain the refractive index of moderate concentrations (up to 15%) of ammonia-water solutions at pressures above atmospheric pressure. As for the refractive index in the investigated ranges, the use of the empirical correlation is the obvious and reliable choice.

REFERENCES

1. Ervin, G., "Solar Heat Storage Based on Inorganic Chemical Reaction, "Proceedings of the Workshop on Solar Energy Storage Subsystems for the Heating & Cooling of Buildings, Charlottesville, Va., June 1975, pp. 91-95.

2. Grassie, S.L. and Sheridan, N.R., "Modelling of a Solar Operated Absorption Air Conditioner System with Refrigerant Storage," Solar Energy, Vol. 19, No. 6, 1977, pp. 691-700.

3. Macriss, R.A., Eakin, B.E., Ellington, R.T., and Huebler, J., "Physical and Thermodynamic Properties of Ammonia Water Mixtures," Institute of Gas Technology Research Bulletin, No. 34, September 1964.

4. Schultz, S.C.G., "Equations of State for the System Ammonia-Water for Use with Computers," Proceedings of the International Congress of Refrigeration, 12th, 1971, pp. 431-436.

5. Scheffer, J.D.R., "Untersungen uber die Diffusion Wasseriger Losungen," Zeitschrift fur Physikalische Chemie (Leipzig), Vol. 2, 1888, pp. 390-404.

6. Arrhenius, S., "Untersungen uber Diffusion von in Wasser Gelosten Stoffen," Zeitschrift fur Physikalische Chemie (Leipzig), Vol. 10, 1893 pp. 51-95.

7. Huffner, G., "Ueber die Diffusion von in Wasser und durch Agargallerte," Zeitschrift fur Physikalische Chemie (Leipzig), Vol. 27, 1898, pp. 227-249.

8. Haselden, G.G., and Malaty, S.A., "Heat and Mass Transfer Accompanying the Absorption of Ammonia in Water," Transactions of the Institution of Chemical Engineers, Vol. 37, 1959, pp. 137-146.

9. Vignes, A., "Variation of Diffusion Coefficients with Composition," Industrial & Engineering Chemistry Fundamentals, Vol. 5, May 1966, pp. 189-199.

10. Darken, L.S., Transactions of the American Institute of Mining and Metallurgical Engineers, Vol. 175, 1948, p. 184.

11. Leffler, J. and Cullinan, H.T., "Variation of Liquid Diffusion Coefficients with Composition, "Industrial & Engineering Chemistry Fundamentals, Vol. 9, February 1970, pp. 84-88.

12. Himmelblau, D.M., "Diffusion of Dissolved Gases in Liquids," Chemical Review, Vol. 64, October 1964, pp. 527-550.

13. Vest, C.M., Holographic Interferometry, John Wiley & Sons, New York, 1979.

14. Kegeles, G. and Gosting, L.J., "The Theory of an Interference Method for the Study of Diffusion," Journal of the American Chemical Society, Vol. 69, October 1947, pp. 2516-2523.

15. Gabor, D., "Miscroscopy by Reconstructed Wavefront," Proceedings of the Royal Society, Series A, Vol. 197. July 1949, pp. 454-487.

16. Mayinger, F. and Panknin, W., "Holography in Heat and Mass Transfer," Proceedings of the Fifth International Heat Transfer Conference, Vol. IV, Tokyo, September 1974, pp. 28-43.

17. American Optical, "Tables of Properties of Aqueous Solutions Related to Index of Refraction, Catalog 10403," Buffalo, New York, 1974, p. 3.

18. Tilton, L.W. and Taylor, J.K., "Refractive Index Measurement" Physical Methods in Chemical Analysis, Vol. I, Academic Press, New York, 1960, pp. 412-462.

19. Scheirer, D.E., Theuner, K., and Nelson, E.L., "Ammonia," Encyclopedia of Industrial Chemical Analysis, Vol. 5, 1967, pp. 290-324.

20. Stong, C.L., "Making a Refractometer for the Identification of Liquids," Scientific American, Vol. 232, May 1975, pp. 109-115.

21. Washburn, E.W. (editor), International Critical Table, Vol. 3, McGraw Hill, New York, 1926, p. 59.

22. Jennings, B.H., "Liquid Phase P, V, T, x Properties of Ammonia-Water," Proceedings of the International Congress of Refrigeration, 12th, Madrid, 1967, pp. 329-334.

23. Tilton, L.W. and Taylor, J.K., "Refractive Index and Dispersion of Distilled Water for Visible Radiation, at Temperature 0 to 60°C, "National Bureau of Standards Research Paper 1085, Journal of Research of the National Bureau of Standards, Vol. 20, April 1938.

24. Beaume, R., "Indice de Refraction et Relation de Lorentz-Lorenz pour le Gaz Ammoniac," Comptes Rendus Hebdomadaires des Seances de L'Academie des Sciences, Serie B, Vol. 265, 1967, pp. 309-311.

25. Frivold, D.E., Hassel, O., and Rustad, S., "Refractive Indexes of Ordinary and Heavy Ammonia," Nature, Vol. 138, August 1936, p. 138.

26. Zeiss, G.D. and Meath, W.J., "Dispersion Energy Constants C_6 (A, B) Dipole Oscillator Strength Sums and Refractivities for Li, N. O, H_2, O_2, NH_3, H_2O, NO, and NO_2," Molecular Physics, Vol. 33, No. 4, April 1977, pp. 1155-1176.

27. The American Society of Mechanical Engineers, 1967 ASME Steam Tables, 2nd ed., New York, 1968.

28. Born, M., Principles of Optics, 4th ed., Pergamon Press, Oxford, 1970, p. 89.

29. Bird, R.B., Stewart, W.E., and Lightfoot, E.N., Transport Phenomena, John Willey & Sons, New York, 1969, p. 498.

30. Threlkeld, J.L., Thermal Environmental Engineering, 2nd ed., Prentice-Hall, Inc., 1970, pp. 106-110.

31. Waxler, R.M. and Weir, C.E., "Effect of Pressure and Temperature on the Refractive Indices of Benzenes, Carbon Tetrachloride, and Water," Journal of Research of the National Bureau of Standards, Vol. 67A, No. 2, March 1963, pp. 163-171.

32. Waxler, R.M., Weir, C.E., and Schamp, H.W., "Effect of Pressure and Temperature upon the Optical Dispersion of Benzene, Carbon Tetrachloride, and Water," Journal of Research of the National Bureau of Standards, Vol. 68A, No. 5, September 1964, pp. 489-498.

33. Newton, I., Opticks, Book II, 1704, p. 245.

34. Gladstone, T. and Dale, T., Philosophical Transactions of the Royal Society of London, Vol. 153, 1863, p. 317.

35. Lorentz, H.A., Weid. Ann. Phys., Vol. 9, 1880, p. 641 (as refer in Ref. 37).

36. Lorenz, L.V., Weid. Ann. Phys., Vol. 11, 1880, p. 70 (as refer in Ref. 37).

37. Batsanov, S.S., Refractometry and Chemical Structure, Consultants Bureau, New York, 1961, pp. 6-7.

38. Johst, W., Wied. Ann. Phys., Vol. 20, 1883, p. 47 (as refer in Ref. 37).

39. Eykman, J.F., Recueil des Travaux Chimiques des Pays-Bas, Vol. 14, 1895, p. 185 (as refer in Ref. 37).

40. Bottcher, C.J.F., Theory of Electric Polarization, Elsevier, Amsterdam, 1952, pp. 201-202.

41. Omini, M., "A Theory of Electric Polarization in Liquids," Physics A, Vol. 83, No. 3, 1976, pp. 431-453.

42. Spectra-Physics, "Model 155, 155A, and 15C Helium-Neon Lasers," Instruction Manual, Mountain View, California.

43. Mells Griot, Optics Guide 2 - A Service to the Industry, Irvine, California, 1982, pp. 66-68 and 203.

APPENDICES

APPENDIX A

SCHEMATIC AND THERMODYNAMIC ANALYSIS OF A POSSIBLE ABSORPTION CYCLE MODIFICATION

Figure A.1 shows a schematic arrangement of a possible absorption cycle modification to recover heat and utilize low grade thermal energy. The major components of the modified cycle are similar to the ones used in the conventional absorption cycle, except for an additional heat exchanger where the useful heat is recovered. In the conventional system the absorber is placed in the low pressure side of the system. Here, the absorber is located in the high pressure side of the modified system.

In the generator the strong concentration ammonia-water solution is separated into ammonia vapor and a weak concentration ammonia-water liquid solution. Through the use of the rectifying column of the dephlegmator, the concentration of the ammonia vapor entering the condenser can be made almost equal to unity. The liquid ammonia leaving the condenser and the weak liquid solution are then pumped to a higher pressure. The temperature of the liquid ammonia is raised using the low grade thermal energy in the heat exchanger. At this point the liquid ammonia and the weak liquid solution can be used as energy storage media. That is, they are separated and can be stored at ambient conditions. At any time, energy can be recovered by recombining the liquid ammonia and the weak liquid solution. The recombination (absorption) process takes place in the absorber, and, due to the heat

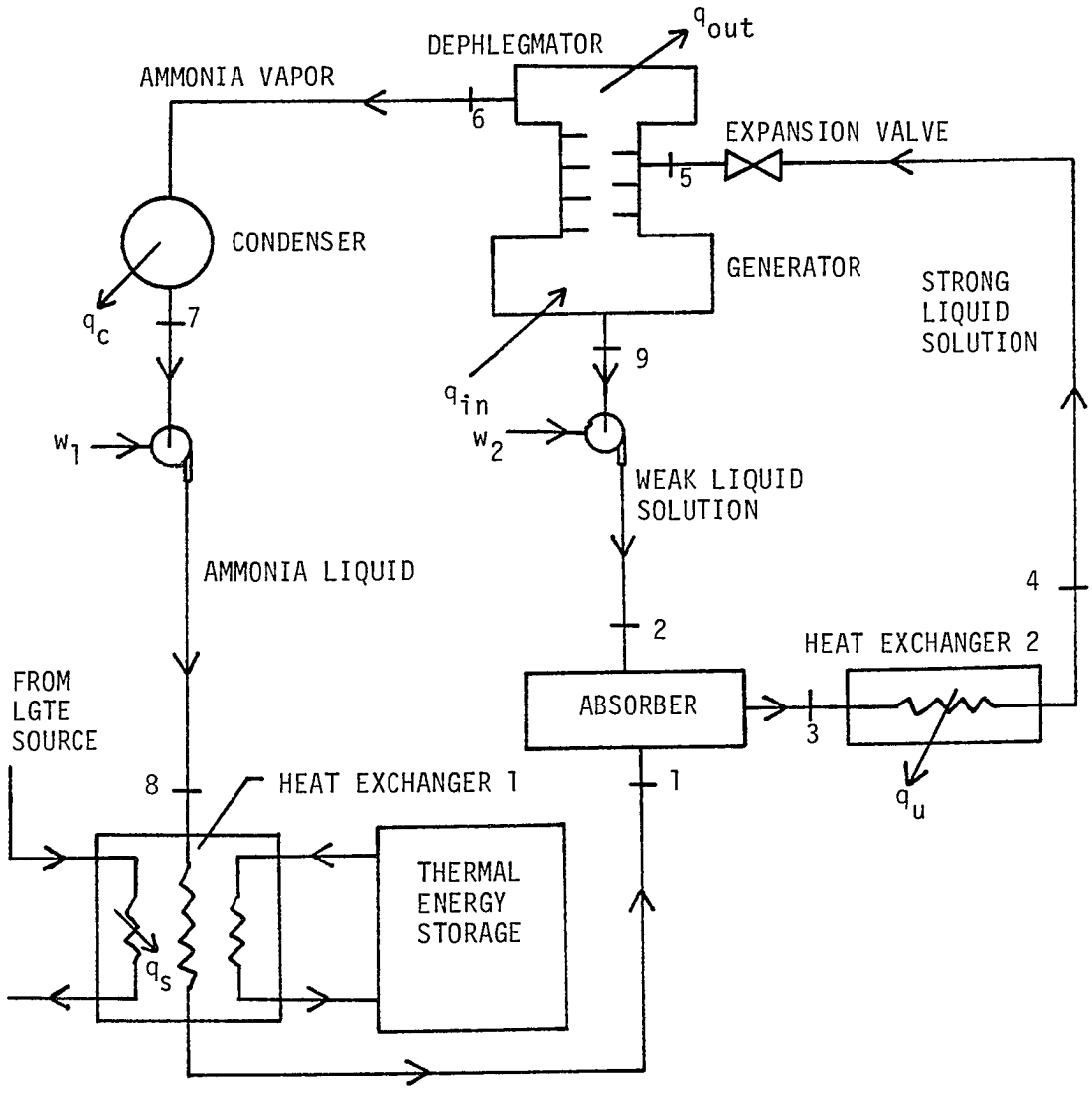

Fig. A.1 A schematic of a possible absorption cycle modification to recover heat and utilize low grade thermal energy.

of formation, the resulting strong concentration ammonia-water solution has a higher temperature. After releasing energy in the heat exchanger, the strong liquid solution will be subjected to a throttling process before entering the generator for the next cycle. To ensure continuous operation of the system (as an alternative to intermittent operation using chemical separation storage), it may also be necessary to store thermal energy conventionally to provide back up heating capacity.

To illustrate the significance of the modified cycle, a thermodynamic analysis for a space heating application has been developed. The following conditions were selected:

Condensing (low) pressure: 0.6147 MPa

Absorber (high) pressure : 2.0684 MPa

Assumptions: - No pressure drops and heat losses in the pipes

- State points 1, 3, 5, 7, and 9 are in equilibrium (saturated) conditions.

The thermodynamic properties for the equilibrium state points can be located directly on the ammonia-water solution Mollier chart developed by Macriss [3]. Then, by performing energy and mass balances, the properties of the other state points and the mass flow rates in terms of the condenser flow rate can be calculated. Table A.1 shows a tabulation of the thermodynamic properties and the mass flow rates for all state points.

Having determined the properties of the state points, the energy transfer per unit mass (in terms of the condenser mass flow rate, $\dot{m}_1$) can be calculated for each component:

Table A.1 Thermodynamic properties and mass flow rates

State Point	Pressure P MPa	Temperature T °C	Concentration W_1 kg NH_3/kg mix	Enthalpy h kj/kg	Flow Rate $\dot{m}$ kg/s	Condition
1	2.0684	50.6	1.000	1293.53	$\dot{m}_1$	sat.vapor
2	2.0684	50.6	0.465	- 21.43	6.576 $\dot{m}_1$	subcooled
3	2.0684	86.7	0.536	152.16	7.576 $\dot{m}_1$	sat.liquid
4	2.0684	41.7	0.536	- 65.08	7.576 $\dot{m}_1$	subcooled
5	0.6147	41.7	0.536	- 65.08	7.576 $\dot{m}_1$	sat.liquid
6	0.6147	10.0	1.000	1273.07	$\dot{m}_1$	sat.vapor
7	0.6147	10.0	1.000	47.42	$\dot{m}_1$	sat.liquid
8	2.0684	10.0	1.000	49.74	$\dot{m}_1$	subcooled
9	0.6147	50.6	0.465	23.24	6.576 $\dot{m}_1$	sat.liquid

1. In the generator and the dephlegmator

Using the graphical method presented by Threlkeld [30] it can be shown that:

q_{in} = 1734.93 kJ/kg (of $\dot{m}_1$)

q_{out} = 121.57 kJ/kg (of $\dot{m}_1$)

2. In the condenser

$q_c = h_6 - h_7$ = 1225.65 kJ/kg (of $\dot{m}_1$)

3. In the heat exchanger 1

$q_s = h_1 - h_8$ = 1243.79 kj/kg (of $\dot{m}_1$)

4. In the heat exchanger 2

$q_u = (h_3 - h_4)\ \dot{m}_3/\dot{m}_1$ = 1645.81 kJ/kg (of $\dot{m}_1$)

5. In the pumps

$w_1 = h_8 - h_7$ = 2.32 kJ/kg (of $\dot{m}_1$)

$w_2 = (h_2 - h_9)\ \dot{m}_2/\dot{m}_1$ = 12.02 kJ/kg (of $\dot{m}_1$)

Since the sum of), $(q_{in} + q_s + w_1 + w_2)$ is equal to the sum of $(q_{out} + q_c + q_u)$, thermodynamically the calculations are correct. The fraction of the energy recovery is calculated as:

$$\frac{q_u}{q_{in} + q_s + w_1 + w_2} = 0.55$$

In summary, the analysis has shown that for every unit energy input into the system, about 55% can be recovered at higher temperature (87°C) and availability. The energy input required to drive the pumps, which is a high grade energy (electric energy), is very small. It is only 0.5% of the total energy input.

APPENDIX B

THEORETICAL BACKGROUND OF REFRACTIVE INDEX PREDICTIONS

The refractive index of a substance is affected by temperature and pressure in two ways-density changes and resonance frequency changes associated with certain molecular vibrations in the substance. For most liquids and gases, the temperature variation changes mainly the densities and consequently the refractive indices according to the relation

$$\frac{\partial n}{\partial T} = f(n) \frac{\partial \rho}{\partial T} \tag{B.1}$$

where f(n) is a positive function. Since all liquids and gases expand when heated, their refractive indices decrease with increasing temperature. The changes in refractive indices due to temperature variation are assumed to be independent of wavelength [18]. Experimental results for many liquids [31,32] have shown that the refractive indices increase with pressure, however, the effects are negligible for moderate pressure changes. For example the refractive index of water (for λ = 643.85 nm) at 24.8°C changes from 1.33136 to 1.33499 if the pressure is increased from 100 kPa to 25.960 MPa.

As both the density, ρ, and the refractive index, n, of a substance depend on temperature and pressure, a great deal of earlier work has been devoted to developing empirical relationships between ρ and n which are independent of temperature and pressure. Such a function, which is

constant for a specified substance (at a specified wavelength), has been defined as the Specific Refractivity, SR. It has been used primarily as a basis for theoretical predictions of refractive indices of substances at various temperatures. Alternatively, the molecular refractivity, A, has been defined as the product of the specific refractivity and the molecular weight, M, of the investigated substance.

A number of important specific refractivity relationships (theoretical and empirical) has been developed in the last three centuries and is summarized here. The first functional representation for specific refractivity was developed by Newton in the early eighteenth century [33] as

$$SR(\text{Newton}) = \frac{n^2 - 1}{\rho} \tag{B.2}$$

It was found, however, that for liquids this function was not sufficiently insensitive to temperature variations. More than a century and a half later, Gladstone and Dale [34] proposed, for empirical reasons, the function

$$SR(\text{Gladstone - Dale}) = \frac{n - 1}{\rho} \tag{B.3}$$

This relation has proven to be reliable for gases and established the invariance of specific refractivity with temperature.

By a remarkable coincidence in 1880, the well-known Lorentz-Lorenz equation was discovered independently by two scientists of almost identical names, Lorentz and Lorenz.

$$SR(\text{Lorentz - Lorenz}) = \frac{1}{\rho}\frac{n^2 - 1}{n^2 + 2} \tag{B.4}$$

This equation was derived by Lorentz [35] from the electromagnetic

theory and by Lorenz based on Maxwell's theory for propagation of light [36]. A compact derivation according to Lorentz is presented by Batsanov [37]. With gases at moderate pressures, n differs only slightly from unity and so the Lorentz-Lorenz equation leads in this case to the Gladstone-Dale equation. The Lorentz-Lorenz equation is indeed an improvement upon the Gladstone-Dale equation especially for liquids and solids.

At this point it should be noted that the Lorentz-Lorenz equation is not accurate for all substances at all conditions. Continuing attempts to develop new functions is an indication of this fact. Among many, the following relationships represent such attempts:

- The Johst equation [38]

$$SR(Johst) = \frac{1}{\rho}\frac{n - 1}{n + 2} \tag{B.5}$$

This empirical relation was developed in 1883 and it was found particularly good for five different mixtures of aniline and ethyl alcohol.

- The Eykman equation [39]

$$SR(Eykman) = \frac{1}{\rho}\frac{n^2 - 1}{n + 0.4} \tag{B.6}$$

The only experimental justification for this empirical relation was found in the data for some organic liquids.

- The Onsager-Bottcher equation [40]

$$SR(Onsager) = \frac{9n^2}{(n^2 - 1)(2n^2 + 1)} + \frac{2(n^2 - 1)}{(2n^2 + 1)}\frac{1}{\xi} \tag{B.7}$$

where $\xi = \frac{4\pi N r^3}{3}$

N: number of molecules perunit volume

r: effective radius of the molecule

This modification of the Lorentz-Lorenz equation was developed by improving the internal field formulation of the dielectric polarization theory.

- The Omini equation [41]

$$3SR\,\frac{1 + 3SR\,[3 + F(SR)]}{(1 + 3SR)\,(1 - \gamma SR) + \gamma SRF(SR)} = \frac{n^2 - 1}{\rho} \qquad (B.8)$$

where $F(SR) = 1 + 0.1756\ 3SR/(1 + 3SR)$

$\gamma = (1 - N_o\ \beta k_B T)^{-1}$

β : isothermal compressibility

k_B : Boltzmann's constant

This most recent relationship was derived by representing the pair distribution function and the dipole-dipole interaction as a finite set of Fourier transforms. For many polar and nonpolar liquids, this relationship was found good to correlate the refractive index, the density, and the temperature.

Unfortunately, each of these functions [Eqs. (B.5) to (B.8)] has been applied successfully for only a specific condition and/or specific substance. In other words, each function has failed to be independent of temperature and pressure for all substances. They are also by no means superior to the classical Lorentz-Lorenz equation.

APPENDIX C

SPECIFICATIONS LIST OF THE SPECTRA-PHYSICS, MODEL 155 HELIUM-NEON LASER [42]

Output Power	0.4 mw - 0.76 mw
Wavelength	623.8 nm, Visible red
Plasma Tube	060-4
Spatial Mode	TEM_{00}
Polarization	random
Longitudinal Mode Spacing (c/2L)	550 MHz
Beam Diameter, at $1/e^2$ points	0.9 mm
Beam Divergence	1.0 mrad full angle
Amplitude Noise (1 KHz to 100 KHz)	< 0.3% rms
Amplitude Ripple (10Hz to 1 KHz)	< 0.5% rms
Long Term Power Drift (12 hours)	< ± 2.5%
Input Voltage	100/115/220 ± 10% Vac 50/60 Hz
Power at Turn-on	> 0.35 mW
Warm-up Time to Full Power	15 minutes
Operating Temperature	10°C to 40°C
Storage Temperature	-20°C to 60°C
Power Requirement	22 W
Weight - Laser	1.8 Kg
Size	67 x 88 x 253 mm
BRH Class	II

APPENDIX D

PROPERTIES LIST OF THE BK-7 GLASS [43]

Max. recommended service temperature	350°C
Young modulus	8.1×10^{11} dynes/cm^2
Poisson's ratio	0.208
Moh hardness	5
Thermal conductivity at 20°C	26.6×10^{-3} cal/sec cm^3 °C
Coef. of linear thermal expansion	8.3×10^{-6} °C^{-1}
Mean refractive index (λ = 632.8nm)	1.51509
Density	2.51gm/cm^3

APPENDIX E

REFRACTIVE INDEX OF DISTILLED WATER

FOR λ = 632.8 nm

T, °C	n	T, °C	n
20	1.33174	41	1.32924
21	165	42	909
22	156	43	894
23	147	44	878
24	137	45	863
25	126	46	847
26	115	47	832
27	105	48	815
28	093	49	798
29	082	50	782
30	071	51	765
31	058	52	748
32	046	53	731
33	037	54	713
34	021	55	695
35	008	56	678
36	1.32994	57	660
37	980	58	641
38	967	59	623
39	953	60	604
40	938		

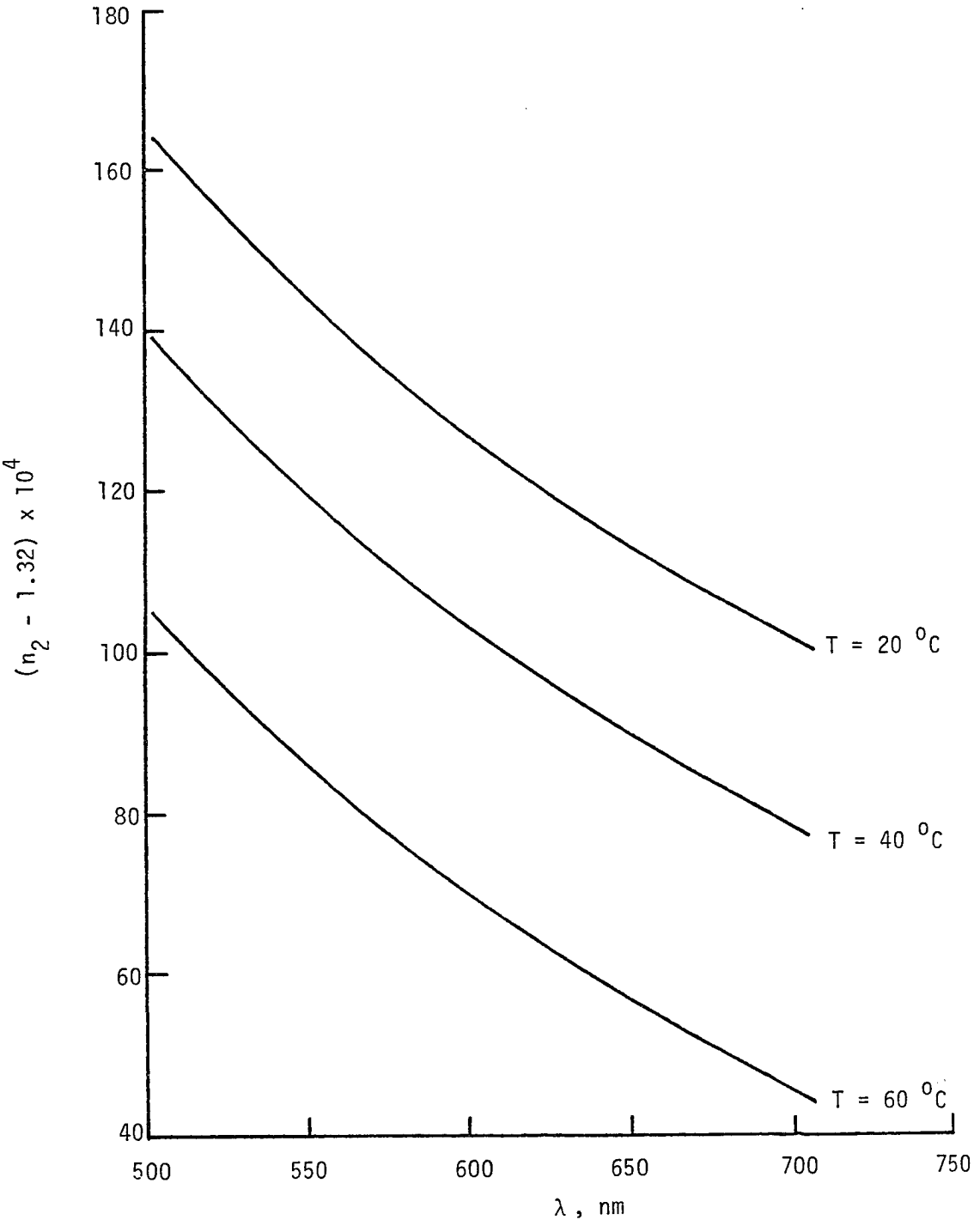

Fig. E.1 Refractive index of water versus wavelength (Ref. 23).

APPENDIX F

SUMMARY OF THE EXPERIMENTAL RESULTS

t_2,mm	W_1,%	T,^oC	b_o,mm	b_{cor},mm	n_{mix}	$\Delta n_{mix} x10^4$
65.830	2.54	21.15	305.15	305.35	1.33307	3.563
65.830	2.54	29.90	304.50	304.70	1.33132	3.560
65.830	2.54	38.00	304.05	304.25	1.33011	3.558
65.830	2.54	54.00	303.05	303.30	1.32758	3.555
65.830	2.54	60.75	302.65	302.90	1.32652	3.553
65.830	5.98	20.50	305.60	305.80	1.33428	3.564
65.830	5.98	29.90	305.05	305.25	1.33280	3.562
65.830	5.98	39.00	304.40	304.60	1.33105	3.560
65.830	5.98	47.10	304.00	304.25	1.33011	3.558
65.830	5.98	58.20	303.20	303.45	1.32798	3.555
65.830	7.59	20.00	306.00	306.20	1.33537	3.566
65.830	7.59	30.00	305.45	305.65	1.33388	3.564
65.830	7.59	40.00	304.75	304.95	1.33199	3.561
65.830	7.59	49.10	304.25	304.50	1.33078	3.559
65.830	7.59	57.90	303.60	303.85	1.32904	3.557
65.830	10.21	23.50	306.15	306.35	1.33577	3.566
65.830	10.21	30.60	305.80	306.00	1.33482	3.565
65.830	10.21	40.00	305.25	305.45	1.33333	3.563
65.830	10.21	54.00	304.10	304.35	1.33038	3.559
65.830	14.41	21.90	307.15	307.35	1.33849	3.570
65.830	14.41	30.00	306.55	306.75	1.33686	3.568
65.830	14.41	40.00	305.95	306.15	1.33523	3.566
65.830	14.41	49.80	305.25	305.50	1.33347	3.563
65.830	14.41	59.90	304.35	304.60	1.33105	3.560
65.730	18.59	21.90	307.75	307.95	1.34103	3.576
65.730	18.59	29.90	307.20	307.40	1.33952	3.574
65.730	18.59	39.50	306.45	306.65	1.33747	3.571
65.730	18.59	49.00	305.30	305.55	1.33448	3.567
65.730	18.59	59.10	304.55	304.80	1.33246	3.564
65.730	20.99	22.25	308.25	308.45	1.34241	3.578
65.730	20.99	30.10	307.40	307.60	1.34007	3.575
65.730	20.99	40.30	306.45	306.65	1.33750	3.571
65.730	20.99	49.20	305.75	306.00	1.33570	3.569
65.730	25.23	22.40	308.95	309.15	1.34434	3.581
65.730	25.23	23.85	308.90	309.10	1.34420	3.580
65.730	25.23	29.80	308.25	308.45	1.34241	3.578
65.730	25.23	31.00	308.15	308.35	1.34213	3.576
65.730	25.23	40.00	307.15	307.35	1.33939	3.574
65.730	27.68	22.80	309.30	309.50	1.34531	3.582
65.730	27.68	23.50	309.15	309.35	1.34490	3.581
65.730	27.68	31.60	308.45	308.65	1.34296	3.579
65.730	27.68	31.90	308.50	308.70	1.34310	3.579

APPENDIX G

EMPIRICALLY CALCULATED REFRACTIVE INDEX AND ITS DISCREPANCY

W_1,%	T,^oC	n_{mix}	$\varepsilon n_{mix} \times 10^4$	εn_{mix},%
2.54	21.15	1.33264	4.3	3.242E-02
2.54	29.90	1.33127	0.5	3.806E-03
2.54	38.00	1.33000	1.1	8.081E-03
2.54	54.00	1.32750	0.8	6.013E-03
2.54	60.75	1.32645	0.7	5.691E-03
5.98	20.50	1.33452	2.4	1.799E-02
5.98	29.90	1.33296	1.6	1.217E-02
5.98	39.00	1.33145	4.0	3.037E-02
5.98	47.10	1.33011	0.0	1.367E-04
5.98	58.20	1.32827	2.9	2.200E-02
7.59	20.00	1.33545	0.8	5.664E-03
7.59	30.00	1.33374	1.4	1.088E-02
7.59	40.00	1.33202	0.3	2.570E-03
7.59	49.10	1.33047	3.1	2.348E-02
7.59	57.90	1.32896	0.8	5.864E-03
10.21	23.50	1.33619	4.2	3.166E-02
10.21	30.60	1.33491	0.9	6.522E-03
10.21	40.00	1.33321	1.2	9.403E-03
10.21	54.00	1.33067	2.9	2.173E-02
14.41	21.90	1.33869	2.0	1.457E-02
14.41	30.00	1.33706	2.0	1.493E-02
14.41	40.00	1.33505	1.8	1.326E-02
14.41	49.80	1.33309	3.8	2.876E-02
14.41	59.90	1.33107	0.2	7.355E-04
18.59	21.90	1.34090	1.3	9.721E-03
18.59	29.90	1.33911	4.1	3.100E-02
18.59	39.50	1.33695	5.2	3.880E-02
18.59	49.00	1.33482	3.4	2.545E-02
18.59	59.10	1.33255	0.9	7.034E-03
20.99	22.25	1.34210	3.1	2.327E-02
20.99	30.10	1.34022	1.5	1.080E-02
20.99	40.30	1.33777	2.7	2.004E-02
20.99	49.20	1.33563	0.7	4.990E-03
25.23	22.40	1.34433	0.1	7.947E-04
25.23	23.85	1.34394	2.6	1.958E-02
25.23	29.80	1.34233	0.8	6.224E-03
25.23	31.00	1.34200	1.3	9.563E-03
25.23	40.00	1.33957	1.8	1.312E-02
27.68	22.80	1.34553	2.2	1.659E-02
27.68	31.60	1.34298	0.2	1.296E-03
27.68	31.90	1.34280	2.1	1.561E-02

APPENDIX H

PROGRAM LISTING OF THE REFRACTIVE INDEX CALCULATION TO OBTAIN THE APPROPRIATE VALUES OF A_1

Parameters

W1	:	Ammonia weight concentration
X	:	Ammonia molecular concentration
MMIX	:	Molecular weight of the solution
NMIX	:	Calculated refractive index of the solution
AMIX	:	Molecular refractivity of the solution
NDATA	:	Refractive index of the solution (Ref. 17)
DELN	:	$\frac{\text{NMIX - NDATA}}{\text{NDATA}} \times 100\%$
ROMIX	:	Density of the solution
VGR	:	Specific volume of the solution

Program and output: see page 111 and 112.

```
00100            REAL N1,N2,M1,M2,MMIX,MMIX,NDATA(16)
00150            OPEN(UNIT =21, FILE='A1.DAT')
00200            A1=5.48
00300            A2=3.7115
00400            M1=17.03
00500            M2=18.02
00600            T=293.15
00700            P=1.013
00800            DATA NDATA/1.3330,1.3339,1.3349,1.3359,1.3370,1.3381,
00900           +  1.3393,1.3404,1.3416,1.3428,1.3440,1.3453,1.3465,
01000           +  1.3477,1.3490,1.3502/
01100            DO 5 J=1,12
01200            W1=0.
01300            WRITE(21,6)A1,A2,T,P
01400    6       FORMAT('1','A1=',F5.2,5X,'A2=',F7.4,5X,'T=',F6.2,1X,
01500           +  'K',5X,'P=',F5.3,1X,'BARS')
01600            WRITE(21,11)
01700    11      FORMAT(' ',2(/),2X,'W1',5X,'X',4X,'MMIX',4X,'AMIX',2X,
01800           +  'ROMIX',3X,'NMIX',2X,'NDATA',3X,'DELN',3X,'VGR')
01900            SUM=0.
02000            DO 10 I=1,16
02100            W2=1-W1
02200            N1=W1/M1
02300            N2=W2/M2
02400            X=N1/(N1+N2)
02500            MMIX=M1*M2/(W1*M2+W2*M1)
02600            AMIX=(N1*A1+N2*A2)/(N1+N2)
02700            CALL DENSI(T,P,X,MMIX,ROMIX,VGR)
02800            FMIX=AMIX*ROMIX/MMIX
02900            SNMIX=(1+2*FMIX)/(1-FMIX)
03000            NMIX=SQRT(SNMIX)
03100            DELN=(NMIX-NDATA(I))*100/NDATA(I)
03200            WRITE(21,22)W1,X,MMIX,AMIX,ROMIX,NMIX,NDATA(I),DELN,VGR
03300    22      FORMAT('0',F5.3,F7.4,F6.2,F7.4,F7.4,F8.5,F7.4,F6.3,F8.5)
03400            SUM=SUM+ABS(DELN)
03500    10      W1=W1+0.02
03600            AVER=SUM/16.
03700            WRITE(21,33) AVER
03800    33      FORMAT(' ',4(/),' AVERAGE ERROR IS ',F7.3)
03900    5       A1=A1+0.01
04000            STOP
04100            END
04200    C
04300            SUBROUTINE DENSI(T,P,X,MMIX,ROMIX,VGR)
04400            REAL CWA(4),CAM(4),F(5),MMIX
04500            DATA CWA/0.0242044,-0.00000458,-0.00263238,0.00059429/
04600            DATA CAM/0.0386536,-0.00011033,-0.0125573,0.00371324/
04700            DATA F/-0.121603,0.672809,-1.02601,0.026458,-0.106125/
04800            TETA=T/100
04900            PHI=P/10
05000            CMIX=0.
05100            COWA=CWA(1)+CWA(2)*PHI+CWA(3)*TETA+CWA(4)*TETA**2
05200            COAM=CAM(1)+CAM(2)*PHI+CAM(3)*TETA+CAM(4)*TETA**2
05300            CMIX=F(1)+F(2)/TETA+F(3)/TETA**2
05400            CMIX=CMIX+(F(4)+F(5)/TETA)*(2*X-1)
05500            VMOL=831.43*((1-X)*COWA+X*COAM+(X-X**2)*CMIX)
05600            ROMIX=MMIX/VMOL
05700            VGR=1/ROMIX
05800            RETURN
05900            END
```

A1= 5.50 A2= 3.7115 T=293.15 K P=1.013 BARS

W1	X	MMIX	AMIX	ROMIX	NMIX	NDATA	DELN	VGR
.000	0.0000	18.02	3.7115	1.0037	1.33483	1.3330	0.137	0.99634
.020	0.0211	18.00	3.7493	0.9927	1.33496	1.3339	0.080	1.00731
.040	0.0422	17.98	3.7870	0.9827	1.33534	1.3349	0.033	1.01759
.060	0.0633	17.96	3.8247	0.9735	1.33593	1.3359	0.002	1.02724
.080	0.0843	17.94	3.8622	0.9650	1.33672	1.3370	-0.021	1.03632
.100	0.1052	17.92	3.8997	0.9570	1.33768	1.3381	-0.031	1.04488
.120	0.1261	17.90	3.9370	0.9497	1.33879	1.3393	-0.038	1.05297
.140	0.1469	17.87	3.9743	0.9428	1.34004	1.3404	-0.027	1.06063
.160	0.1677	17.85	4.0115	0.9364	1.34140	1.3416	-0.015	1.06793
.180	0.1885	17.83	4.0486	0.9303	1.34286	1.3428	0.004	1.07491
.200	0.2092	17.81	4.0856	0.9245	1.34439	1.3440	0.029	1.08162
.220	0.2298	17.79	4.1226	0.9190	1.34598	1.3453	0.051	1.08811
.240	0.2505	17.77	4.1594	0.9137	1.34762	1.3465	0.083	1.09442
.260	0.2710	17.75	4.1962	0.9086	1.34928	1.3477	0.117	1.10062
.280	0.2915	17.73	4.2329	0.9036	1.35095	1.3490	0.145	1.10673
.300	0.3120	17.71	4.2695	0.8986	1.35262	1.3502	0.179	1.11283

AVERAGE ERROR IS 0.062

APPENDIX I

THEORETICALLY CALCULATED REFRACTIVE INDEX

(see Appendix H for parameters)

PARAMETERS: A1= 5.50 A2= 3.7115 T= 293.15 K

W1	X	MMIX	AMIX	RUMIX	NMIX	VGR
.000	0.0000	18.02	3.7115	1.0037	1.33483	0.9963
.020	0.0211	18.00	3.7493	0.9927	1.33496	1.0073
.040	0.0422	17.98	3.7870	0.9827	1.33534	1.0176
.060	0.0633	17.96	3.8247	0.9735	1.33593	1.0272
.080	0.0843	17.94	3.8622	0.9650	1.33672	1.0363
.100	0.1052	17.92	3.8997	0.9570	1.33768	1.0449
.120	0.1261	17.90	3.9370	0.9497	1.33879	1.0530
.140	0.1469	17.87	3.9743	0.9428	1.34004	1.0606
.160	0.1677	17.85	4.0115	0.9364	1.34140	1.0679
.180	0.1885	17.83	4.0486	0.9303	1.34286	1.0749
.200	0.2092	17.81	4.0856	0.9245	1.34439	1.0816
.220	0.2298	17.79	4.1226	0.9190	1.34598	1.0881
.240	0.2505	17.77	4.1594	0.9137	1.34762	1.0944
.260	0.2710	17.75	4.1962	0.9086	1.34928	1.1006
.280	0.2915	17.73	4.2329	0.9036	1.35095	1.1067
.300	0.3120	17.71	4.2695	0.8986	1.35262	1.1128

PARAMETERS: A1= 5.50 A2= 3.7115 T= 303.15 K

W1	X	MMIX	AMIX	RUMIX	NMIX	VGR
.000	0.0000	18.02	3.7115	0.9995	1.33328	1.0005
.020	0.0211	18.00	3.7493	0.9887	1.33345	1.0114
.040	0.0422	17.98	3.7870	0.9787	1.33382	1.0218
.060	0.0633	17.96	3.8247	0.9693	1.33436	1.0316
.080	0.0843	17.94	3.8622	0.9606	1.33505	1.0410
.100	0.1052	17.92	3.8997	0.9524	1.33587	1.0500
.120	0.1261	17.90	3.9370	0.9446	1.33680	1.0586
.140	0.1469	17.87	3.9743	0.9373	1.33783	1.0669
.160	0.1677	17.85	4.0115	0.9303	1.33894	1.0749
.180	0.1885	17.83	4.0486	0.9236	1.34012	1.0827
.200	0.2092	17.81	4.0856	0.9171	1.34134	1.0903
.220	0.2298	17.79	4.1226	0.9109	1.34260	1.0978
.240	0.2505	17.77	4.1594	0.9048	1.34388	1.1052
.260	0.2710	17.75	4.1962	0.8989	1.34516	1.1125
.280	0.2915	17.73	4.2329	0.8931	1.34643	1.1197
.300	0.3120	17.71	4.2695	0.8873	1.34768	1.1271

PARAMETERS: A1= 5.50 A2= 3.7115 T= 313.15 K

W1	X	MMIX	AMIX	ROMIX	NMIX	VGR
.000	0.0000	18.02	3.7115	0.9947	1.33154	1.0053
.020	0.0211	18.00	3.7493	0.9842	1.33180	1.0160
.040	0.0422	17.98	3.7870	0.9744	1.33220	1.0263
.060	0.0633	17.96	3.8247	0.9650	1.33272	1.0362
.080	0.0843	17.94	3.8622	0.9562	1.33334	1.0458
.100	0.1052	17.92	3.8997	0.9477	1.33406	1.0551
.120	0.1261	17.90	3.9370	0.9397	1.33485	1.0642
.140	0.1469	17.87	3.9743	0.9319	1.33570	1.0730
.160	0.1677	17.85	4.0115	0.9245	1.33660	1.0817
.180	0.1885	17.83	4.0486	0.9172	1.33754	1.0902
.200	0.2092	17.81	4.0856	0.9102	1.33849	1.0987
.220	0.2298	17.79	4.1226	0.9033	1.33945	1.1070
.240	0.2505	17.77	4.1594	0.8966	1.34041	1.1154
.260	0.2710	17.75	4.1962	0.8899	1.34135	1.1237

PARAMETERS: A1= 5.50 A2= 3.7115 T= 323.15 K

W1	X	MMIX	AMIX	ROMIX	NMIX	VGP
.000	0.0000	18.02	3.7115	0.9895	1.32963	1.0106
.020	0.0211	18.00	3.7493	0.9794	1.32999	1.0211
.040	0.0422	17.98	3.7870	0.9697	1.33044	1.0313
.060	0.0633	17.96	3.8247	0.9604	1.33097	1.0412
.080	0.0843	17.94	3.8622	0.9515	1.33156	1.0509
.100	0.1052	17.92	3.8997	0.9429	1.33220	1.0605
.120	0.1261	17.90	3.9370	0.9346	1.33287	1.0699
.140	0.1469	17.87	3.9743	0.9266	1.33357	1.0793
.160	0.1677	17.85	4.0115	0.9187	1.33429	1.0885
.180	0.1885	17.83	4.0486	0.9110	1.33500	1.0977
.200	0.2092	17.81	4.0856	0.9034	1.33571	1.1069
.220	0.2298	17.79	4.1226	0.8960	1.33641	1.1161
.240	0.2505	17.77	4.1594	0.8886	1.33707	1.1254

PARAMETERS: A1= 5.50 A2= 3.7115 T= 333.15 K

W1	X	MMIX	AMIX	ROMIX	NMIX	VGP
.000	0.0000	18.02	3.7115	0.9838	1.32754	1.0165
.020	0.0211	18.00	3.7493	0.9741	1.32803	1.0266
.040	0.0422	17.98	3.7870	0.9646	1.32855	1.0367
.060	0.0633	17.96	3.8247	0.9555	1.32909	1.0466
.080	0.0843	17.94	3.8622	0.9466	1.32966	1.0564
.100	0.1052	17.92	3.8997	0.9379	1.33024	1.0662
.120	0.1261	17.90	3.9370	0.9294	1.33081	1.0760
.140	0.1469	17.87	3.9743	0.9210	1.33138	1.0857
.160	0.1677	17.85	4.0115	0.9128	1.33193	1.0955
.180	0.1885	17.83	4.0486	0.9047	1.33245	1.1054
.200	0.2092	17.81	4.0856	0.8966	1.33293	1.1153

PARAMETERS: A1= 5.47 A2= 3.6990 T= 293.15 K

W1	X	MMIX	AMIX	ROMIX	NMIX	VGR
.000	0.0000	18.02	3.6990	1.0037	1.33359	0.9963
.020	0.0211	18.00	3.7364	0.9927	1.33369	1.0073
.040	0.0422	17.98	3.7738	0.9827	1.33404	1.0176
.060	0.0633	17.96	3.8110	0.9735	1.33461	1.0272
.080	0.0843	17.94	3.8482	0.9650	1.33538	1.0363
.100	0.1052	17.92	3.8853	0.9570	1.33631	1.0449
.120	0.1261	17.90	3.9223	0.9497	1.33740	1.0530
.140	0.1469	17.87	3.9592	0.9428	1.33862	1.0606
.160	0.1677	17.85	3.9961	0.9364	1.33995	1.0679
.180	0.1885	17.83	4.0328	0.9303	1.34138	1.0749
.200	0.2092	17.81	4.0695	0.9245	1.34288	1.0816
.220	0.2298	17.79	4.1061	0.9190	1.34445	1.0881
.240	0.2505	17.77	4.1426	0.9137	1.34606	1.0944
.260	0.2710	17.75	4.1790	0.9086	1.34769	1.1006
.280	0.2915	17.73	4.2153	0.9036	1.34933	1.1067
.300	0.3120	17.71	4.2515	0.8986	1.35097	1.1128

PARAMETERS: A1= 5.47 A2= 3.6990 T= 303.15 K

W1	X	MMIX	AMIX	ROMIX	NMIX	VGR
.000	0.0000	18.02	3.6990	0.9995	1.33204	1.0005
.020	0.0211	18.00	3.7364	0.9887	1.33219	1.0114
.040	0.0422	17.98	3.7738	0.9787	1.33253	1.0218
.060	0.0633	17.96	3.8110	0.9693	1.33305	1.0316
.080	0.0843	17.94	3.8482	0.9606	1.33371	1.0410
.100	0.1052	17.92	3.8853	0.9524	1.33451	1.0500
.120	0.1261	17.90	3.9223	0.9446	1.33541	1.0586
.140	0.1469	17.87	3.9592	0.9373	1.33642	1.0669
.160	0.1677	17.85	3.9961	0.9303	1.33750	1.0749
.180	0.1885	17.83	4.0328	0.9236	1.33865	1.0827
.200	0.2092	17.81	4.0695	0.9171	1.33985	1.0903
.220	0.2298	17.79	4.1061	0.9109	1.34109	1.0978
.240	0.2505	17.77	4.1426	0.9048	1.34234	1.1052
.260	0.2710	17.75	4.1790	0.8989	1.34359	1.1125
.280	0.2915	17.73	4.2153	0.8931	1.34484	1.1197
.300	0.3120	17.71	4.2515	0.8873	1.34606	1.1271

PARAMETERS: A1= 5.47 A2= 3.6990 T= 313.15 K

W1	X	MMIX	AMIX	ROMIX	NMIX	VGR
.000	0.0000	18.02	3.6990	0.9947	1.33032	1.0053
.020	0.0211	18.00	3.7364	0.9842	1.33055	1.0160
.040	0.0422	17.98	3.7738	0.9744	1.33092	1.0263
.060	0.0633	17.96	3.8110	0.9650	1.33141	1.0362
.080	0.0843	17.94	3.8482	0.9562	1.33201	1.0458
.100	0.1052	17.92	3.8853	0.9477	1.33270	1.0551
.120	0.1261	17.90	3.9223	0.9397	1.33347	1.0642
.140	0.1469	17.87	3.9592	0.9319	1.33430	1.0730
.160	0.1677	17.85	3.9961	0.9245	1.33518	1.0817
.180	0.1885	17.83	4.0328	0.9172	1.33608	1.0902
.200	0.2092	17.81	4.0695	0.9102	1.33701	1.0987
.220	0.2298	17.79	4.1061	0.9033	1.33795	1.1070
.240	0.2505	17.77	4.1426	0.8966	1.33888	1.1154
.260	0.2710	17.75	4.1790	0.8899	1.33980	1.1237

PARAMETERS: A1= 5.47 A2= 3.6990 T= 323.15 K

W1	X	MMIX	AMIX	ROMIX	NMIX	VGR
.000	0.0000	18.02	3.6990	0.9895	1.32841	1.0106
.020	0.0211	18.00	3.7364	0.9794	1.32875	1.0211
.040	0.0422	17.98	3.7738	0.9697	1.32917	1.0313
.060	0.0633	17.96	3.8110	0.9604	1.32967	1.0412
.080	0.0843	17.94	3.8482	0.9515	1.33024	1.0509
.100	0.1052	17.92	3.8853	0.9429	1.33085	1.0605
.120	0.1261	17.90	3.9223	0.9346	1.33150	1.0699
.140	0.1469	17.87	3.9592	0.9266	1.33218	1.0793
.160	0.1677	17.85	3.9961	0.9187	1.33287	1.0885
.180	0.1885	17.83	4.0328	0.9110	1.33356	1.0977
.200	0.2092	17.81	4.0695	0.9034	1.33425	1.1069
.220	0.2298	17.79	4.1061	0.8960	1.33492	1.1161
.240	0.2505	17.77	4.1426	0.8886	1.33556	1.1254

PARAMETERS: A1= 5.47 A2= 3.6990 T= 333.15 K

W1	X	MMIX	AMIX	ROMIX	NMIX	VGR
.000	0.0000	18.02	3.6990	0.9838	1.32633	1.0165
.020	0.0211	18.00	3.7364	0.9741	1.32679	1.0266
.040	0.0422	17.98	3.7738	0.9646	1.32728	1.0367
.060	0.0633	17.96	3.8110	0.9555	1.32781	1.0466
.080	0.0843	17.94	3.8482	0.9466	1.32835	1.0564
.100	0.1052	17.92	3.8853	0.9379	1.32890	1.0662
.120	0.1261	17.90	3.9223	0.9294	1.32945	1.0760
.140	0.1469	17.87	3.9592	0.9210	1.33000	1.0857
.160	0.1677	17.85	3.9961	0.9128	1.33052	1.0955
.180	0.1885	17.83	4.0328	0.9047	1.33102	1.1054
.200	0.2092	17.81	4.0695	0.8966	1.33148	1.1153

APPENDIX J

PROGRAM LISTING AND OUTPUT OF DATA

REGRESSION TO OBTAIN THE CORRECTION FUNCTION, $F(W_1)$

Parameters

W1	:	Ammonia weight concentration
X	:	Ammonia molecular concentration
MMIX	:	Molecular weight of the solution
NDATA	:	Refractive index of the solution (Ref. 17)
ROMIX	:	Density of the solution
MIXA	:	Molecular refractivity of the solution (obtained by additive rule)
DMIXA	:	Molecular refractivity of the solution (calculated using data of Ref. 17)

Program and output: see page 124 and 125.

```
00100           REAL N1,N2,M1,M2,NMIX,MMIX,NDATA(16),MIXA(16),DMIXA(16)
00200           REAL W1(16),Y(16),C(8),S(8),A(5),B(5),Z(16)
00300           REAL*8 P(30),T(24)
00400           OPEN (UNIT=21, FILE='A3.DAT')
00500           A1=5.5
00600           A2=3.7115
00700           M1=17.03
00800           M2=18.02
00900           TM=293.15
01000           PR=1.013
01100           DATA NDATA/1.3330,1.3339,1.3349,1.3359,1.3370,1.3381,1.3393,
01200         + 1.3404,1.3416,1.3428,1.3440,1.3453,1.3465,1.3477,1.3490,1.3502/
01300           W1(1)=0.
01400           WRITE(21,9)
01500    9      FORMAT('0',2X,'W1',2X,'MMIX',3X,'NDATA',2X,'ROMIX',2X,'MIXA',
01600         + 2X,'DMIXA',8X,'Y')
01700           DO 5 I=1,16
01800           IF(I.GT.1)W1(I)=W1(I-1)+0.02
01900           Z(I)=W1(I)
02000           W2=1-W1(I)
02100           N1=W1(I)/M1
02200           N2=W2/M2
02300           X=N1/(N1+N2)
02400           MMIX=M1*M2/(W1(I)*M2+W2*M1)
02500           MIXA(I)=(N1*A1+N2*A2)/(N1+N2)
02600           CALL DENSI(TM,PR,X,MMIX,ROMIX)
02700           DMIXA(I)=MMIX*(NDATA(I)**2-1)/(ROMIX*(NDATA(I)**2+2))
02800           Y(I)=DMIXA(I)/MIXA(I)
02900           WRITE(21,11) W1(I),MMIX,NDATA(I),ROMIX,MIXA(I),DMIXA(I),Y(I)
03000    11     FORMAT('0',F5.2,F6.2,4(F7.4),F12.8)
03100    5      CONTINUE
03200           N=16
03300           RSQ=100.
03400           MD=5
03500           CALL RLFOTH(W1,Y,N,RSQ,MD,ID,P,C,S,A,B,IER)
03600           CALL RLDOPM(C,ID,A,B,T)
03700           WRITE(21,22)
03800    22     FORMAT(' ',4(/),' THE COEFFICIENTS OF THE DEGREE 5 REGRESSION:
03900           WRITE(21,*)(C(I),I=1,6)
04000           STOP
04100           END
04200    C
04300           SUBROUTINE DENSI(TM,PR,X,MMIX,ROMIX)
04400    C
04500           REAL CWA(4),CAM(4),F(5),MMIX
04600           DATA CWA/0.0242044,-0.00000458,-0.00263238,0.00059429/
04700           DATA CAM/0.0386536,-0.00011033,-0.0125573,0.00371324/
04800           DATA F/-0.121603,0.672809,-1.02601,0.026458,-0.106125/
04900           TETA=TM/100.
05000           PHI=PR/10.
05100           CMIX=0.
05200           COWA=CWA(1)+CWA(2)*PHI+CWA(3)*TETA+CWA(4)*TETA**2
05300           CCAM=CAM(1)+CAM(2)*PHI+CAM(3)*TETA+CAM(4)*TETA**2
05400           CMIX=F(1)+F(2)/TETA+F(3)/TETA**2
05500           CMIX=CMIX+(F(4)+F(5)/TETA)*(2*X-1)
05600           VMOL=831.43*((1-X)*COWA+X*CCAM+(X-X**2)*CMIX)
05700           ROMIX=MMIX/VMOL
05800           RETURN
05900           END
```

W1	MMIX	NDATA	KOMIX	MIXA	DMIXA	Y
0.00	18.02	1.3330	1.0037	3.7115	3.6931	0.99503715
0.02	18.00	1.3339	0.9927	3.7493	3.7385	0.99712396
0.04	17.98	1.3349	0.9827	3.7870	3.7825	0.99881867
0.06	17.96	1.3359	0.9735	3.8247	3.8243	0.99991801
0.08	17.94	1.3370	0.9650	3.8622	3.8651	1.00075632
0.10	17.92	1.3381	0.9570	3.8997	3.9040	1.00112510
0.12	17.90	1.3393	0.9497	3.9370	3.9423	1.00135115
0.14	17.87	1.3404	0.9428	3.9743	3.9781	1.00095601
0.16	17.85	1.3416	0.9364	4.0115	4.0136	1.00052792
0.18	17.83	1.3428	0.9303	4.0486	4.0480	0.99985222
0.20	17.81	1.3440	0.9245	4.0856	4.0815	0.99897952
0.22	17.79	1.3453	0.9190	4.1226	4.1152	0.99821980
0.24	17.77	1.3465	0.9137	4.1594	4.1474	0.99709628
0.26	17.75	1.3477	0.9086	4.1962	4.1791	0.99591681
0.28	17.73	1.3490	0.9036	4.2329	4.2117	0.99498213
0.30	17.71	1.3502	0.8986	4.2695	4.2431	0.99381865

THE COEFFICIENTS OF THE DEGREE 5 REGRESSION:
0.9950372, 0.1165953, -0.5882163, 8.025509E-02, 3.098516,
-4.326903

APPENDIX K

SEMI-EMPIRICALLY CALCULATED REFRACTIVE INDEX

(see Appendix H for parameters)

PARAMETERS: A1= 5.50 A2= 3.7115 T= 293.15 K

WL	X	MMIX	AMIX	ROMIX	NMIX	VGR
.000	0.0000	18.02	3.6931	1.0037	1.33300	0.9963
.020	0.0211	18.00	3.7386	0.9927	1.33390	1.0073
.040	0.0422	17.98	3.7824	0.9827	1.33488	1.0175
.060	0.0633	17.96	3.8245	0.9735	1.33592	1.0272
.080	0.0843	17.94	3.8651	0.9650	1.33700	1.0363
.100	0.1052	17.92	3.9042	0.9570	1.33811	1.0449
.120	0.1261	17.90	3.9419	0.9497	1.33926	1.0530
.140	0.1469	17.87	3.9783	0.9428	1.34042	1.0606
.160	0.1677	17.85	4.0137	0.9364	1.34160	1.0679
.180	0.1885	17.83	4.0481	0.9303	1.34281	1.0749
.200	0.2092	17.81	4.0817	0.9245	1.34402	1.0816
.220	0.2298	17.79	4.1148	0.9190	1.34525	1.0881
.240	0.2505	17.77	4.1473	0.9137	1.34649	1.0944
.260	0.2710	17.75	4.1795	0.9086	1.34774	1.1006
.280	0.2915	17.73	4.2114	0.9036	1.34898	1.1067
.300	0.3120	17.71	4.2432	0.8986	1.35020	1.1128

PARAMETERS: A1= 5.50 A2= 3.7115 T= 303.15 K

W1	X	MMIX	AMIX	ROMIX	NMIX	VGR
.000	0.0000	18.02	3.6931	0.9995	1.33146	1.0005
.020	0.0211	18.00	3.7386	0.9887	1.33240	1.0114
.040	0.0422	17.98	3.7824	0.9787	1.33337	1.0218
.060	0.0633	17.96	3.8245	0.9693	1.33435	1.0316
.080	0.0843	17.94	3.8651	0.9606	1.33532	1.0410
.100	0.1052	17.92	3.9042	0.9524	1.33630	1.0500
.120	0.1261	17.90	3.9419	0.9446	1.33726	1.0586
.140	0.1469	17.87	3.9783	0.9373	1.33821	1.0669
.160	0.1677	17.85	4.0137	0.9303	1.33915	1.0749
.180	0.1885	17.83	4.0481	0.9236	1.34007	1.0827
.200	0.2092	17.81	4.0817	0.9171	1.34098	1.0903
.220	0.2298	17.79	4.1148	0.9109	1.34188	1.0978
.240	0.2505	17.77	4.1473	0.9048	1.34277	1.1052
.260	0.2710	17.75	4.1795	0.8989	1.34364	1.1125
.280	0.2915	17.73	4.2114	0.8931	1.34449	1.1197
.300	0.3120	17.71	4.2432	0.8873	1.34531	1.1271

PARAMETERS: A1= 5.50 A2= 3.7115 T= 313.15 K

W1	X	MMIX	AMIX	RDMIX	NMIX	VGR
.000	0.0000	18.02	3.6931	0.9947	1.32973	1.0053
.020	0.0211	18.00	3.7386	0.9842	1.33075	1.0160
.040	0.0422	17.98	3.7824	0.9744	1.33175	1.0263
.060	0.0633	17.96	3.8245	0.9650	1.33270	1.0362
.080	0.0843	17.94	3.8651	0.9562	1.33362	1.0458
.100	0.1052	17.92	3.9042	0.9477	1.33449	1.0551
.120	0.1261	17.90	3.9419	0.9397	1.33531	1.0642
.140	0.1469	17.87	3.9783	0.9319	1.33608	1.0730
.160	0.1677	17.85	4.0137	0.9245	1.33680	1.0817
.180	0.1885	17.83	4.0481	0.9172	1.33749	1.0902
.200	0.2092	17.81	4.0817	0.9102	1.33813	1.0987
.220	0.2298	17.79	4.1148	0.9033	1.33874	1.1070
.240	0.2505	17.77	4.1473	0.8966	1.33931	1.1154
.260	0.2710	17.75	4.1795	0.8899	1.33985	1.1237

PARAMETERS: A1= 5.50 A2= 3.7115 T= 323.15 K

W1	X	MMIX	AMIX	RUMIX	NMIX	VGR
.000	0.0000	18.02	3.6931	0.9895	1.32783	1.0106
.020	0.0211	18.00	3.7386	0.9794	1.32895	1.0211
.040	0.0422	17.98	3.7824	0.9697	1.33000	1.0313
.060	0.0633	17.96	3.8245	0.9604	1.33096	1.0412
.080	0.0843	17.94	3.8651	0.9515	1.33183	1.0509
.100	0.1052	17.92	3.9042	0.9429	1.33262	1.0605
.120	0.1261	17.90	3.9419	0.9346	1.33332	1.0699
.140	0.1469	17.87	3.9783	0.9266	1.33394	1.0793
.160	0.1677	17.85	4.0137	0.9187	1.33449	1.0885
.180	0.1885	17.83	4.0481	0.9110	1.33496	1.0977
.200	0.2092	17.81	4.0817	0.9034	1.33536	1.1069
.220	0.2298	17.79	4.1148	0.8960	1.33570	1.1161
.240	0.2505	17.77	4.1473	0.8886	1.33598	1.1254

PARAMETERS: A1= 5.50 A2= 3.7115 T= 333.15 K

W1	X	MMIX	AMIX	ROMIX	NMIX	VGR
.000	0.0000	18.02	3.6931	0.9838	1.32576	1.0165
.020	0.0211	18.00	3.7386	0.9741	1.32699	1.0266
.040	0.0422	17.98	3.7824	0.9646	1.32810	1.0367
.060	0.0633	17.96	3.8245	0.9555	1.32908	1.0466
.080	0.0843	17.94	3.8651	0.9466	1.32994	1.0564
.100	0.1052	17.92	3.9042	0.9379	1.33066	1.0662
.120	0.1261	17.90	3.9419	0.9294	1.33126	1.0760
.140	0.1469	17.87	3.9783	0.9210	1.33175	1.0857
.160	0.1677	17.85	4.0137	0.9128	1.33212	1.0955
.180	0.1885	17.83	4.0481	0.9047	1.33240	1.1054
.200	0.2092	17.81	4.0817	0.8966	1.33258	1.1153

PARAMETERS: A1= 5.47 A2= 3.6990 T= 293.15 K

W1	X	MMIX	AMIX	ROMIX	NMIX	VGR
.000	0.0000	18.02	3.6806	1.0037	1.33176	0.9963
.020	0.0211	18.00	3.7257	0.9927	1.33264	1.0073
.040	0.0422	17.98	3.7692	0.9827	1.33359	1.0176
.060	0.0633	17.96	3.8109	0.9735	1.33460	1.0272
.080	0.0843	17.94	3.8511	0.9650	1.33565	1.0363
.100	0.1052	17.92	3.8898	0.9570	1.33674	1.0449
.120	0.1261	17.90	3.9271	0.9497	1.33786	1.0530
.140	0.1469	17.87	3.9632	0.9428	1.33899	1.0606
.160	0.1677	17.85	3.9982	0.9364	1.34015	1.0679
.180	0.1885	17.83	4.0323	0.9303	1.34133	1.0749
.200	0.2092	17.81	4.0656	0.9245	1.34252	1.0816
.220	0.2298	17.79	4.0983	0.9190	1.34372	1.0881
.240	0.2505	17.77	4.1305	0.9137	1.34494	1.0944
.260	0.2710	17.75	4.1623	0.9086	1.34616	1.1006
.280	0.2915	17.73	4.1939	0.9036	1.34737	1.1067
.300	0.3120	17.71	4.2253	0.8986	1.34857	1.1128

PARAMETERS: A1= 5.47 A2= 3.6990 T= 303.15 K

W1	X	MMIX	AMIX	RUMIX	NMIX	VGR
.000	0.0000	18.02	3.6806	0.9995	1.33023	1.0005
.020	0.0211	18.00	3.7257	0.9887	1.33115	1.0114
.040	0.0422	17.98	3.7692	0.9787	1.33209	1.0218
.060	0.0633	17.96	3.8109	0.9693	1.33304	1.0316
.080	0.0843	17.94	3.8511	0.9606	1.33399	1.0410
.100	0.1052	17.92	3.8898	0.9524	1.33493	1.0500
.120	0.1261	17.90	3.9271	0.9446	1.33587	1.0586
.140	0.1469	17.87	3.9632	0.9373	1.33679	1.0669
.160	0.1677	17.85	3.9982	0.9303	1.33771	1.0749
.180	0.1885	17.83	4.0323	0.9236	1.33861	1.0827
.200	0.2092	17.81	4.0656	0.9171	1.33949	1.0903
.220	0.2298	17.79	4.0983	0.9109	1.34037	1.0978
.240	0.2505	17.77	4.1305	0.9048	1.34123	1.1052
.260	0.2710	17.75	4.1623	0.8989	1.34208	1.1125
.280	0.2915	17.73	4.1939	0.8931	1.34291	1.1197
.300	0.3120	17.71	4.2253	0.8873	1.34370	1.1271

PARAMETERS: A1= 5.47 A2= 3.6990 T= 313.15 K

W1	X	MMIX	AMIX	ROMIX	NMIX	VGR
.000	0.0000	18.02	3.6806	0.9947	1.32851	1.0053
.020	0.0211	18.00	3.7257	0.9842	1.32950	1.0160
.040	0.0422	17.98	3.7692	0.9744	1.33047	1.0263
.060	0.0633	17.96	3.8109	0.9650	1.33140	1.0362
.080	0.0843	17.94	3.8511	0.9562	1.33229	1.0458
.100	0.1052	17.92	3.8898	0.9477	1.33313	1.0551
.120	0.1261	17.90	3.9271	0.9397	1.33392	1.0642
.140	0.1469	17.87	3.9632	0.9319	1.33467	1.0730
.160	0.1677	17.85	3.9982	0.9245	1.33537	1.0817
.180	0.1885	17.83	4.0323	0.9172	1.33604	1.0902
.200	0.2092	17.81	4.0656	0.9102	1.33666	1.0987
.220	0.2298	17.79	4.0983	0.9033	1.33724	1.1070
.240	0.2505	17.77	4.1305	0.8966	1.33779	1.1154
.260	0.2710	17.75	4.1623	0.8899	1.33830	1.1237

PARAMETERS: A1= 5.47 A2= 3.6990 T= 323.15 K

WL	X	MMIX	AMIX	ROMIX	NMIX	VGR
.000	0.0000	18.02	3.6806	0.9895	1.32662	1.0106
.020	0.0211	18.00	3.7257	0.9794	1.32771	1.0211
.040	0.0422	17.98	3.7692	0.9697	1.32873	1.0313
.060	0.0633	17.96	3.8109	0.9604	1.32966	1.0412
.080	0.0843	17.94	3.8511	0.9515	1.33051	1.0509
.100	0.1052	17.92	3.8898	0.9429	1.33127	1.0605
.120	0.1261	17.90	3.9271	0.9346	1.33195	1.0699
.140	0.1469	17.87	3.9632	0.9266	1.33255	1.0793
.160	0.1677	17.85	3.9982	0.9187	1.33307	1.0885
.180	0.1885	17.83	4.0323	0.9110	1.33352	1.0977
.200	0.2092	17.81	4.0656	0.9034	1.33390	1.1069
.220	0.2298	17.79	4.0983	0.8960	1.33422	1.1161
.240	0.2505	17.77	4.1305	0.8886	1.33448	1.1254

PARAMETERS: A1= 5.47 A2= 3.6990 T= 333.15 K

W1	X	MMIX	AMIX	RO*IX	NMIX	VGR
.000	0.0000	18.02	3.6806	0.9838	1.32455	1.0165
.020	0.0211	18.00	3.7257	0.9741	1.32576	1.0266
.040	0.0422	17.98	3.7692	0.9646	1.32684	1.0367
.060	0.0633	17.96	3.8109	0.9555	1.32780	1.0466
.080	0.0843	17.94	3.8511	0.9466	1.32862	1.0564
.100	0.1052	17.92	3.8898	0.9379	1.32932	1.0662
.120	0.1261	17.90	3.9271	0.9294	1.32990	1.0760
.140	0.1469	17.87	3.9632	0.9210	1.33036	1.0857
.160	0.1677	17.85	3.9982	0.9128	1.33072	1.0955
.180	0.1885	17.83	4.0323	0.9047	1.33097	1.1054
.200	0.2092	17.81	4.0656	0.8966	1.33113	1.1153

APPENDIX L

COMPARISON OF REFRACTIVE INDEX DATA SETS

Parameters

n_{expt} : Experimentally obtained refractive index

n_{empi} : Empirically obtained refractive index, Eq. (5.13)

n_{pred} : Semi-empirically obtained refractive index, Eq. (6. 14)

$\varepsilon n_{pred} = n_{expt} - n_{pred}$

Tabulation of data on page 137.

W_1, %	T, °C	n_{expt}	n_{pred}	$\varepsilon n_{pred} \times 10^4$
2.54	21.15	1.33307	1.33273	3.4
2.54	29.90	1.33132	1.33141	- 0.9
2.54	38.00	1.33011	1.33011	0.0
2.54	54.00	1.32758	1.32724	3.4
2.54	60.75	1.32652	1.32591	6.1
5.98	20.50	1.33428	1.33451	- 2.3
5.98	29.90	1.33280	1.33304	- 2.4
5.98	39.00	1.33105	1.33156	- 5.1
5.98	47.10	1.33011	1.33017	- 0.6
5.98	58.20	1.32798	1.32813	- 1.5
7.59	20.00	1.33537	1.33544	- 0.7
7.59	30.00	1.33388	1.33379	0.9
7.59	40.00	1.33199	1.33211	- 1.2
7.59	49.10	1.33078	1.33051	2.7
7.59	57.90	1.32904	1.32887	1.7
10.21	23.50	1.33577	1.33621	- 4.4
10.21	30.60	1.33482	1.33492	- 1.0
10.21	40.00	1.33333	1.33322	1.1
10.21	54.00	1.33038	1.33058	- 2.0
14.41	21.90	1.33849	1.33879	- 3.0
14.41	30.00	1.33686	1.33698	- 1.2
14.41	40.00	1.33523	1.33482	4.1
14.41	49.80	1.33347	1.33271	7.6
14.41	59.90	1.33105	1.33047	5.8
18.59	21.90	1.34103	1.34113	- 1.0
18.59	29.90	1.33952	1.33890	6.2
18.59	39.50	1.33747	1.33635	11.2
18.59	49.00	1.33448	1.33389	5.9
18.59	59.10	1.33246	1.33127	11.9
20.99	22.25	1.34241	1.34237	0.4
20.99	30.10	1.34007	1.33990	1.7
20.99	40.30	1.33750	1.33686	6.4
20.99	49.20	1.33570	1.33429	14.1
25.23	22.40	1.34434	1.34471	- 3.7
25.23	23.85	1.34420	1.34413	0.7
25.23	29.80	1.34241	1.34183	5.8
25.23	31.00	1.34213	1.34138	7.5
25.23	40.00	1.33939	1.33811	12.8
27.68	22.80	1.34531	1.34590	- 5.9
27.68	23.50	1.34490	1.34559	- 6.9
27.68	31.60	1.34296	1.34211	8.5
27.68	31.90	1.34310	1.34198	11.2